SPYROS ANTONOPOULOS

SDPO.20.014.m

# Long-Term Feedback Enabled Energy Management Control Framework for Ships with Hybrid Power Supply

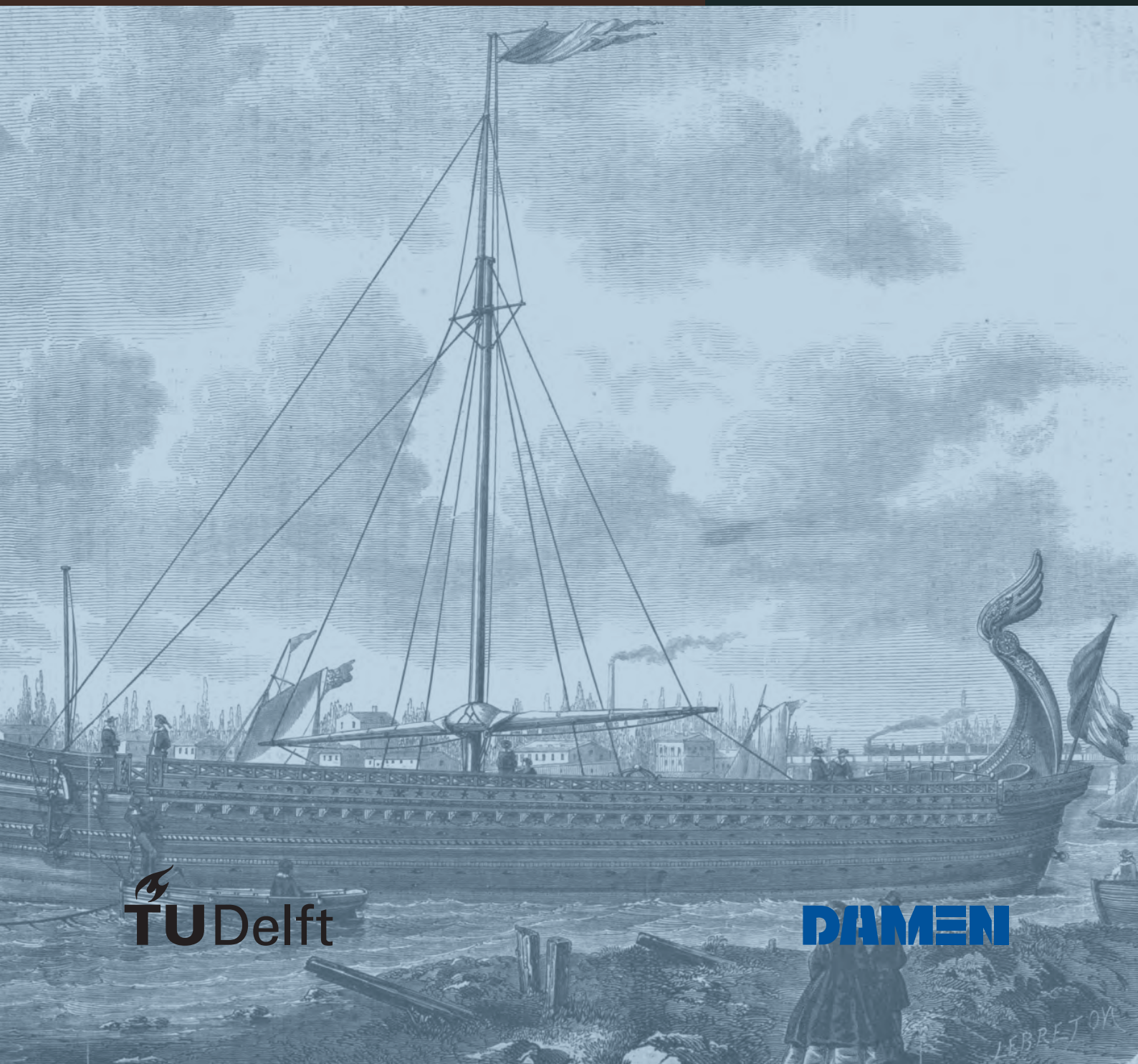

TU Delft

DAMEN

Thesis for the degree of Master of Science in Marine Technology
at the Delft University of Technology,
Faculty of Mechanical, Maritime, and Materials Engineering

# Long-Term Feedback Enabled Energy Management Control Framework for Ships with Hybrid Power Supply

By

Spyridon Antonopoulos

Performed at

Damen Schelde Naval Shipbuilding BV

This thesis (SDPO.20.014.m) is classified as confidential in accordance with the general conditions for projects performed by the TUDelft.

Monday, July 13th, 2020

**Company supervisor**
Responsible supervisor: Ir. M. Kalikatzarakis
Daily supervisor: Ir. M. Kalikatzarakis

**Thesis exam committee**
Chair/Responsible Professor: Ir. K. Visser
Staff Member: Prof. dr. ir. C.A. Ramírez
Staff Member: Dr. V. Reppa
Staff Member: Dr. ir. L. van Biert
Company Member: Ir. M. Kalikatzarakis

**Author Details**
Student number: 4805135

# Long-Term Feedback Enabled Energy Management Control Framework for Ships with Hybrid Power Supply

by

**Spyridon Antonopoulos**

**Abstract**

In the present study, a Model Predictive Control (MPC) - based, Energy Management Strategy (EMS) is proposed, aiming at the minimisation of the fuel consumption of vessels with hybrid propulsion and power supply. This approach is capable of utilising online information regarding realistic future predictions of the propulsive power demand, addressing the current gap in the literature regarding the implementation of MPC EMSs onboard ships, and pragmatic future mission information utilisation. To the author's best knowledge, MPC for fuel consumption minimisation has not yet been implemented at this timescale in maritime propulsion plants with hybrid power supply. Furthermore, online mission information from the Integrated Bridge Systems (IBSs) and the governor's human input cannot be utilised by EMSs onboard ships, due to the lack of a mathematical pathway to enable such an information feedback flow. Increasingly powerful processing units in ship controllers and a wider application of batteries in marine powertrains motivated such a computationally heavy and, simultaneously, highly fuel-efficient control approach. The proposed controller framework has been tested and verified in a case study using a Mean Value First Principle (MVFP) propulsion plant model of a hybrid naval vessel with batteries in Simulink®, provided by DAMEN® SNS. By using provided mission data, realistic mission profiles were generated, in which the proposed controller is validated against perfectly and piecewise, non-perfectly informed Dynamic Programming (DP) solutions in an information barrier scheme, yielding close to optimal performance, and a fuel consumption reduction of up to 3.5% when compared to any non-long-term feedback enabled controller.

*To my parents, for their loving support*

*To the people close to me in Delft, for making me feel like home away from home*

*To everyone who helped me from TU Delft and DAMEN Schelde, for their guidance and support*

# Contents

# List of Figures

# List of Tables

# Nomenclature

**Abbreviations**

$A-ECMS$ Adaptive ECMS

$BEV$ Battery Electric Vehicle

$BM$ Blended-Mode

$CD$ Charge-Depleting

$CDG$ Controllable DG

$CS$ Charge-Sustaining

$DE$ Diesel Engine

$DER$ Distributed Engergy Resource

$DG$ Distributed Generation

$DoF$ Degree of Freedom

$DP$ Dynamic Programming, or Dynamic Positioning

$DS$ Distributed Storage

$DSM$ Demand-Side Management

$ECDISs$ Electronic Chart Display and Information Systems

$ECMS$ Equivalent Consumption Minimisation Strategy

$ED$ Economic Dispatch

$EEDI$ Energy Efficiency Design Index

$EGCS$ Exhaust Gas Cleaning System

$EM$ Electric Motor

$EMS$ Energy Management (Control) Strategy

$ESS$ Energy-Storage System

$GPS$ Global Positioning System

$HEV$ Hybrid Electric Vehicle

$HFO$ Heavy Fuel Oil

$IBSs$ Integrated Bridge Systems

$ICE$ Internal Combustion Engine

$IM$ Induction Machine

$INSs$ Intelligent Navigation Systems

$ITSs$ Intelligent Transport Systems

$LHV$ Lower Heating Value

$MGCC$ Microgrid Central Controller

$MIP$ Mixed Integer Programming

$MPC$ Model Predictive Control

$MT$ Micro Turbine

$OCP$ Optimal Control Problem

$PEMFC$ Proton-Exchange Membrane Fuel Cell

$PHEV$ Plug-In Hybrid Electric Vehicle

$PMP$ Pontryagin's Minimum Principle

$PTC$ Power-Train-Control

$PTI$ Power Take In

$PTO$ Power Take Out

$QP$ Quadratic Programming

$RB$ Rule-Based

$RDG$ Renewable DG

$RES$ Renewable Energy Sources

$SDP$ Stochastic Dynamic Programming

$SEEMP$ Ship Energy Management Plan

$SoC$ State of Charge

$T-ECMS$ Telemetry ECMS

$UC$ Ultracapacitors

$UC$ Unit Commitment

$WT$ Wind Turbine

**Roman Symbols**

$\Delta t$ Smaller Time Interval

$\dot{m}$ Mass Flow

$\eta$ Efficiency

$\mu$ Penalty Parameter

$\phi$ Final Cost Function

$\pi$ Control Policy Sequence

$a$ Well-to-Wheel (or even better propeller) Efficiency

$C$ Propulsive Coefficients

$E$ End Constraint Window Parameter

$h$ Arc Cost Function

$I$ Current

$J$ Cost Functional

$k$ Intermediate Time Step

$k_p$ number of Propellers

$K_Q$ Torque Coefficient

$K_T$ Thrust Coefficient

| | |
|---|---|
| $M$ | Torque |
| $N$ | Mission Steps |
| $N_c$ | Control Horizon |
| $N_p$ | Prediction Horizon |
| $n_p$ | Propeller Shaft Speed |
| $N_u$ | Discretisation of Control Input |
| $N_x$ | Discretisation of State |
| $NoE$ | number of active Generator Sets |
| $P$ | Power |
| $P_D$ | Pitch Ratio, or $P/D$ |
| $pf$ | Power Factor |
| $Q$ | Charge |
| $r$ | Disturbance |
| $s$ | Equivalency Factor |
| $SFOC$ | Specific Fuel Oil Consumption |
| $SoC$ | State of Charge |
| $t$ | Time |
| $Te$ | Telegraph Position |
| $u$ | Control Variable |
| $V$ | Voltage |
| $v_s$ | Ship Speed |
| $x$ | State Variable |
| $y$ | Output |

**Subscripts**

| | |
|---|---|
| $*$ | Optimal |

| | |
|---|---|
| 0 | Initial |
| $B$ | Main Engine |
| $b$ | Battery |
| $dem$ | Demand |
| $f$ | Fuel or Final when it is a subscript to time |
| $gen$ | Diesel Generator Set |
| $hot$ | Hotel |
| $m$ | Motor |
| $n$ | Normalised |
| $nom$ | Nominal |
| $prop$ | Propulsive |
| $ref$ | Reference |
| $virt$ | Virtual |

# Chapter 1

# Introduction

## 1.1 On Hybridisation in the Maritime Domain

Hybrid ships date back to ancient Mediterranean civilisations (Phoenicians and Ancient Greeks), when the triremes had three banks of oars, together with sails, as means of propulsion. Triremes were also used in the Roman era, while several such ships have been reconstructed in modern times. The very cover of this thesis is from a page of the french journal *L'Illustration* from 1864, depicting the construction of a Roman trireme, built according to the instructions of Emperor Napoleon III. In modern times, Gustave Trouvé was the first to patent an electric motor for ship propulsion, in 1880. When the battery technology emerged, submarines with electric power were first built in Russia in 1884, by a Polish engineer named Stefan Drzewiecki. Diesel-electric transmission, developed by the US Navy in 1928, was the first instance of the combination of electric and diesel propelled vessels. Since then and up until recently, submarines were almost the only vessels using electric propulsion in combination with a diesel engine.

Maritime hybrid applications have been rising in popularity over the past few decades. The potential of such applications to reduce the environmental impact of ships has been identified by researchers, international organisations, and the industry, however, the application cases are still limited to only some ship types with diverse operating profiles, such as tugboats, naval vessels and yachts [1, 2].

On the contrary, hybridisation in the automotive industry has been a subject of extensive research and has been implemented in various ways, while even commercial, large-scale, all-electric, plug-in vehicles are becoming increasingly successful. This development in the automotive industry is not just due to successful marketing strategies or sheer luck, or due to the maritime industry being too conservative in implementing new technologies. Land-based vehicles have a number of key, favourable technologies and characteristics to facilitate hybridisation, the most important of which

are [3]:

- Regenerative braking, that recovers a fraction of the otherwise dissipated potential (due to altitude alterations) and kinetic energy. This energy would have been lost by using conventional mechanical breaks. By producing negative torque (using the electric motors as generators) regenerative breaking is storing energy in an energy buffer (i.e. batteries, super-capacitors etc.).

- Diverse operating profile, especially in a city driving cycle with frequent stops and demand for different low-power operating points from the internal combustion engine (ICE). This provides a margin for efficiency improvements and consequent energy savings, if the ICE can operate on a stable, more energy efficient point. The ICE can even get shut off if the stored energy is able to cover the power and energy demand, in order to prevent frequent starts and stops, which are associated with increased fuel consumption, emissions and wear. As it will be explained later on in the chapter, the requirement for the implementation of hybridisation is that the positive effects (primarily on fuel savings) overcome the energy losses introduced in hybrid architectures due to energy conversions.

- Plug-in points and grid infrastructure can facilitate charge depleting (plug-in) vehicles with oversized, technologically advanced high-density batteries, which can support sufficiently large driving ranges.

Figure 1.1: An Electric Motor being fitted on *Opal*, a sailing vessel with a regenerative plug-in hybrid-electric propulsion, as part of the RENSEA II project, as found in [4, 5]

After providing the primary reasons behind the success of hybridisation in the automotive industry (see also Section 2.1 for a more extensive review of hybridisation advantages in the automotive industry), difficulties in the implementation of hybrid architectures in ships are becoming more evident; Firstly, the means of restoring energy in maritime applications, namely via heave compensation and crane operations, only apply to a limited number ship types [1,6]. Potential energy is not

relevant to maritime applications and apart from the RENSEA II project on vessels with sails [5], regenerative marine propulsion (i.e. using the propeller as a turbine while sailing) is not versatile enough to be implemented in ships with no sails. Secondly, diverse operating profiles are characteristic to a limited number of ship types, namely towing vessels, yachts, ferries, research, offshore and naval vessels [1]. Although the operating profile of cargo transportation vessels is changing during a trip due to various sea states, resulting in the main engine not operating optimally [7, 8], this is relatively insignificant compared to the findings in [9], where it is shown that in order for hybrid propulsion with conventional power supply to yield economic benefits, the vessel has to sail for considerable periods below 15% of its propulsive power. Moreover, size and weight limitations in maritime applications are of great importance [10]. Lastly, charge depleting hybrid ships have to rely on the grid on land, thus, the opportunities for re-charging are coarser compared to their inland counterparts, while, also, the energy storage size to cover the vessel energy demands has to be considerably larger, introducing larger CAPEX costs, space and weight requirements, and re-charging time.

Although cargo transportation vessels show limited opportunities for hybridisation, several publications support such technology. Appropriate use of a motor in hybrid powertrains, by also utilising the air-to-fuel ratio of a diesel engine as a feedback in a system-level controller, led to reduced $NOx$ and fuel consumption during acceleration in [11]. DC power systems together with energy storage yielded significant additional fuel savings (7%), due to smaller conversion losses, for vessels with load variations and extensive part load operations in [12]. By utilising batteries in slow speed deep sea vessels for load levelling of the auxiliary loads by optimal use of the installed generator sets [7], fuel savings have been demonstrated in simulated powertrains. Using a battery hybrid system for ship crane operations, due to the regenerative breaking capabilities, yielded a corresponding hybrid installation with a very short payback time in [6].

## 1.2 The Societal, Regulatory, and Techno-economical Framework for Vessel Hybridisation

Hybridisation has been a widely adopted approach to emission reduction, gaining vast popularity especially in the automotive industry. A hybrid ship can refer to both hybrid propulsion, comprised of a direct mechanical drive and an electric motor connected to the same shaft through a gearbox, and hybrid power supply, a combination of two or more different power sources able to provide electrical power [2]. Hybrid electric maritime applications of a combination of internal combustion engines (ICEs) with energy storage (batteries), has long been implemented on conventional submarines [7] as a solution for providing stored energy to propel the vessel without the need of snorkelling. However, the stringent regulatory framework around the environmental impact of ship operations and the costs

of fuel oil has pushed the industry towards applying hybrid architectures to a number of different types of vessels. The Royal Netherlands Navy and the Swedish Navy have acquired hybrid ASD tug boats built by DAMEN, prioritising environmentally friendly solutions for their fleet. British Columbia ferries, operating in Canada, has awarded DAMEN with a total of 6 new buildings of hybrid-electric ferries. BC ferries prioritised operating cost reduction and environmental impact mitigation and thus opted for hybrid technology, after an extensive tender process [13, 14].


Figure 1.2: Hybrid-electric ferry build by Damen for British Columbia ferries [13]

## Regulatory Framework

Worldwide societal and intergovernmental concerns over climate change have been firmly expressed over the past decades, with the major landmarks being the Kyoto Protocol, an international treaty signed in 1997 by the United Nations Framework Convention on Climate Change (UNFCCC)[1], and Paris Agreement, into force since November 2016, according to which all parties are obligated to set new emission targets with a specified timeline [15, 16]. The UN body, and more specifically IMO's Marine Environment Protection Committee (MEPC) has adopted a climate change strategy for shipping, following the emission goals set by the Paris Agreement [17].

According to the third IMO GHG emissions study in 2014 [18], during the period of 2007 to 2012, total shipping contributed to an average of 2.4% of total anthropogenic $CO_2$ equivalent emissions,[2] while the absolute $CO_2$ emissions amounted to 796 million tons in 2012. For the global $NO_x$ and $SO_x$ emissions, the average contribution has been 15% and 13%, correspondingly. To that end, IMO has been actively involved in, amongst others, enhancing the energy efficiency of ships, via a regulatory framework known as MARPOL Annex VI.

In more detail regarding the regulatory framework, MARPOL Annex VI mandates that a large

[1] the ratification of the Kyoto Protocol has not been followed only by the US, while Japan, Canada and Russia have withdrawn from the treaty

[2] Equivalency conversions have been done according to the Intergovernmental Panel on Climate Change, Fifth Assessment Report (IPCC AR5)

portion of merchant ship types (responsible for $\sim 85\%$ of the total $CO_2$ emissions from international shipping, the extensive list can be found in [19]) must comply with the ship-type-specific Energy Efficiency Design Index (EEDI). EEDI requires for a minimum energy efficiency per capacity mile, in order to meet a $CO_2$ ship emissions reduction requirement equal to an ultimate figure of 30% by 2025. Other requirements of this Annex (MEPC 70) include the mandatory fuel consumption data collection and Ship Energy Management Plan (SEEMP), $SO_x$ (2020 global sulphur cap) and $NO_x$ emissions (Tier II for ships constructed after 2011). The $SO_x$ 2020 sulphur cap significantly increases the fuel costs, as Heavy Fuel Oil (HFO 3.5% S) has to be substituted with Very Low Sulphur Fuel Oil[3], if no Exhaust Gas Cleaning System (EGCS) is installed. The $NOx$ emissions are important for NECA and future NECA zones (currently US coastline).

EEDI introduces a number of problems already identified in literature publications (summarised in [21]). To begin with, EEDI is calculated using a single design point, only at calm sea, and not the actual operating profile of the vessel, resulting in a trend of reduced installed power on ships rather than introduction of innovative propulsion concepts, potentially compromising safety under adverse weather conditions [22], and neglecting the potential efficiency and safety benefit of a larger engine on-board operating at a lower percentage of the rated power (slow steaming) [23].[4]. For that very reason EEDI is inaccurate in identifying the efficiency of ships that have diverse operating profiles. EEDI is also difficult to be extended to account for performance other than transport (non-merchant ships). To that end, in practice the EEDI-affected ship types (mostly merchant ships and not the types described before e.g. naval, tugs etc.) do not implement hybrid architectures, but focus more on engine efficiency, energy saving devices, waste heat recovery systems and exhaust gas treatment systems. This is because, diverse operating profiles are not a characteristic of merchant ship types, while an EEDI-based index for non-transportation ship types is difficult to be implemented. Nonetheless, as indicated in [2], measures are generally expected to be extended to other ship types, substantiating the exploration for new technologies for fuel efficiency and emission reduction

[3] VLSFO 0.5% S, +180$/ton over HFO, [20]

[4] It is noted, however, that accoding to IMO [18], slow steaming has been widely adopted in the period of 2007 to 2012

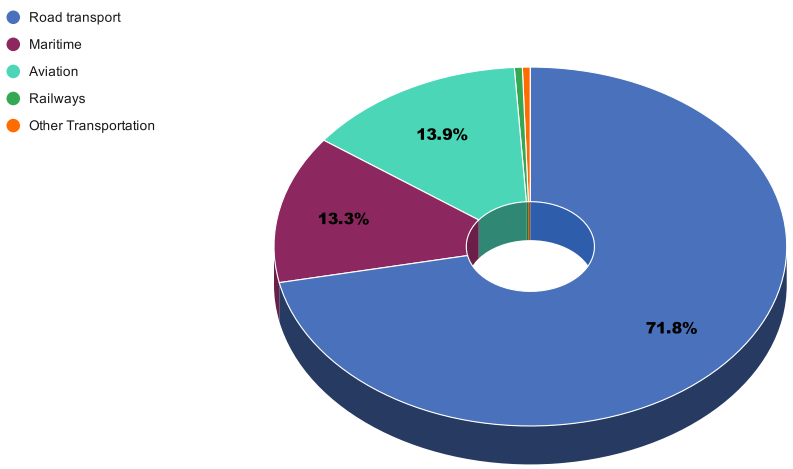


Figure 1.3: Transportation Greenhouse Gas Emissions per Sector in the EU-28, adapted from the European Environment Agency (EEA) [24]

The European Commission [25] established GHG emission targets for the transport sector, in the context of the Effort Sharing Decision, which is part of EU's "Climate and Energy Policy Framework for 2020". According to the Decision, national targets of the EU countries are set, taking into account the GDP per capita, in order to attain an EU collective reduction of -10% by 2020, compared to the 2005 figure. After 2020, correspondingly, EU's implementation of the Paris Agreement, called Effort Sharing Regulation, sets new binding emission targets to its Member States, with a collective emission reduction goal of -30% by 2030. On the basis of the data shown in 1.3, where shipping emissions showed to account for 13% of the total in the transportation sector, EU implemented data collection measures, which took effect from the beginning of 2018 and are known as Monitoring, Reporting and Verification of $CO_2$ emissions (EU MRV). These measures constitute the first phase of a three-step plan for emission reductions, the rest of which include setting reduction targets and implementing further measures [26].

## Techno-economical Framework

More importantly, the fuel savings and the subsequent economic benefits are the primary motivation behind hybrid implementations in the maritime industry. Hybrid implementations can refer to either hybrid propulsion (a combination of mechanical and electrical propulsion) or hybrid power supply (a combination of ICEs with batteries, fuel cells or super-capacitors) [2]. A set of technological advances (power electronics technology, variable speed drives, efficient power converters, high-temperature superconductors and alternate power sources) have facilitated the development and rise of hybrid ship propulsion over the last few decades [27], while the increasingly better and

safer, energy-dense and fast-charging lithium-ion batteries are radically being implemented in both automotive and maritime systems due to their advantages over the conventional Lead-Acid technology [28].

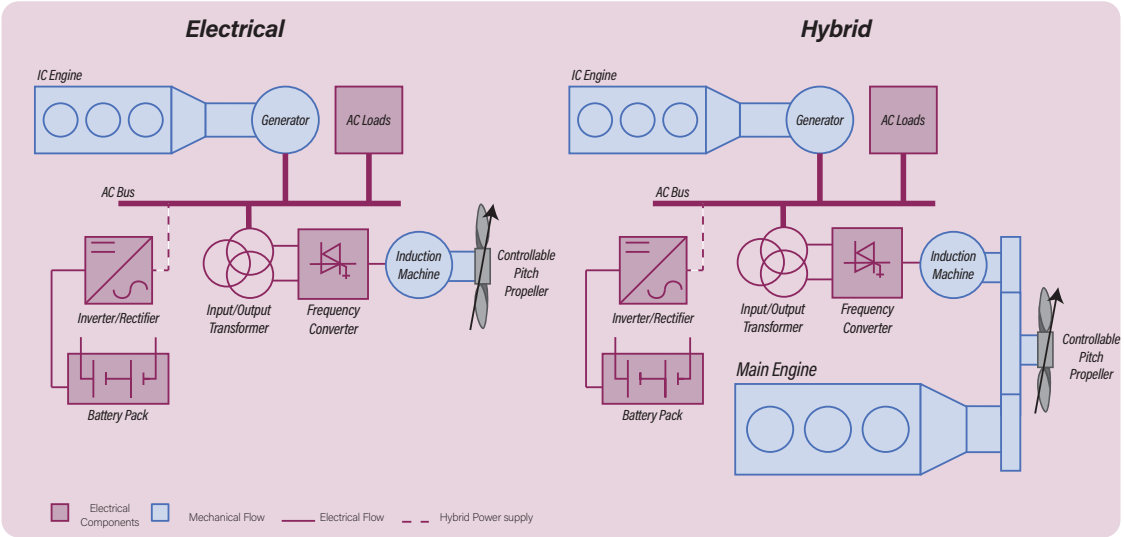


Figure 1.4: Electric and Hybrid Propulsion. With the dotted line the power train turns into a Hybrid Power Supply configuration. Adapted from [2]

In summary, in [2] it is described that typical applications of hybrid propulsion include naval frigates due to the very low efficiency of their gas turbines or main engines under part-load [29], towing vessels due to them sailing at 20% of their engines' rating for more than 90% of their operational profile [30], and offshore vessels due to the increased travelling distance to cite in combination with the stringent availability requirement during DP operation [31]. The three applications described indicate three key different reasons why hybrid propulsion can be economical:

- the part-loading of the prime mover results in significant deterioration of efficiency (i.e. gas turbines)
- the operating profile demands an extensive time period at very low loads (i.e. tug boats)
- the performance of the propulsion is crucial and associated with big risks (i.e. DP operations)

All of these reasons, if translated to costs, yield the same result; it is more economic to have a hybrid architecture, in order to:

- utilise electric propulsion when the corresponding overall energy conversion losses yield more efficient performance than part-loading the prime mover, or when propulsive availability is crucial

- utilise mechanical propulsion when the load is close to the engines' rated capacity and losses due to energy conversions in electric propulsion cannot be compensated

An extra degree of flexibility which corresponds to additional benefits is possible if the generator sets can also be used in a Power Take Out (PTO) configuration.

Regarding hybrid power supply and focusing on batteries, in [2] it is explained that in order to acquire corresponding benefits the electric load has to be spread over time. Furthermore, significant reduction in fuel consumption is possible with DC power systems [12], when the major consumers can be fed from a shared DC-link (i.e. variable speed propulsion drives, heavy pumps, heavy lifting cranes). Additionally, hybrid power supply can potentially be beneficial for added availability (providing spinning reserve so that the extra diesel engines do not need to run) and corresponding downsizing of the auxiliary engines, while noise reduction and improved maintainability can also be important benefits [2].

Studies on energy storage and the corresponding added efficiency potential provide insight into different applications, by varying the ship powertrain configurations and topologies, the engine types, and the operating modes. In [10], it is shown that using energy storage in combination with sequentially turbocharged ICEs, even in the case of hybrid transmission (or PTI/PTO) provide negligible or even adverse effects. On the other hand, there are, in most cases, efficiency gains for adding energy storage to powertrains with gas engines, where the efficiency drop at low loads is substantial, or to diesel electric powertrains, where the electrical losses happen even if there is no energy storage. In fact, in the same study it has been remarked that the shape of the specific fuel consumption map is a determining factor. Positive effects are also noticed when using energy storage to provide spinning reserve or in the case of load levelling, however, PTI applications would be more efficient by just using additional engines. The isolated benefits of energy storage are also demonstrated in an Offshore Support Vessel application in [12].

## 1.3 Hybridisation and Control System

The improved fuel efficiency and emissions reduction associated with hybridisation depends on the implemented architecture and the load cycle, while the true potential for each case can only be realised with a sophisticated control system to optimise energy flow [32], also known as Energy Management Strategy (EMS). It is due to the degrees of freedom introduced in the hybrid power-train arrangement that the EMS has the control task to determine set-points of operation for the components of this power-train (i.e. ICE, EM), aiming at minimising an objective function (typically fuel consumption) [33]. Although EMSs have been a field of control research for two decades [1,33], a number of challenges continue to be unresolved, especially for maritime implementations. Namely, it is of urgent importance for research to be conducted into extending the objective function in order to

include the optimisation of various performance criteria [2], to benchmark EMSs using standardised load cycles and cycle information for an on-line solution and to test their robustness, and to utilise predictive approaches, aiming to real-time EMSs parameter adaptation [1].

The comparison between automotive and maritime applications is useful in order to identify the key differences between these implementations. To that end, the significant architectural complexity (compared to their automotive counterparts) of the hybrid power-trains typically found in maritime vessels, and the consequent additional degrees of freedom (i.e. several generators, added flexibility), pose significant challenges for the control strategy [34]. Another challenge in hybrid maritime propulsion applications arises due to the more complicated connection between the shaft speed and the power demand: unlike cars which mostly need the road inclination to correlate an engine speed to a power load, on a ship the demand for power is subject to the sea state and wind loads and it is subject to a great deal of uncertainty. Furthermore, due to the limited capabilities of the vessels to provide regenerative paths (as described previously), charge depleting (instead of charge sustaining) implementations seem to be more attractive for maritime applications, given that there is a possibility to get connected to the grid in a frequency that allows for suitable battery unit recharging to match the operational profile of the vessel (similar to Plug-in Hybrid Electric Vehicles - PHEVs). Such implementations have yielded fuel savings of 6%-17%, in tug-boat applications, compared to the previous controllers (rule-based) that did not utilise the on-shore grid energy [1, 34, 35].

# Chapter 2

# Literature Review

Energy Management Strategies (EMSs) [33, 36], sometimes also being referred to as Supervisory Control Strategies in literature [3,37], are control algorithms implemented in the controllers on board hybrid vehicles or vessels, that most often target to minimise fuel consumption. In some implementations EMSs include additional objectives, such as pollutant emission or battery life degradation minimisation, in their cost function/objective. On operator's input (e.g. throttle, speed lever) and taking into account various constraints, EMSs decide on the optimal power or torque split between the multitude of energy sources on board the hybrid vehicle, which correspond to the degrees of freedom in the powertrain (i.e. determining the torque, speed, or power set-points to the power converters, e.g. ICE's torque, EM's power, battery power output). Further clarification of the role of EMSs can be realised by following the narrative in [3]: In conventional powertrain architectures, the operator is using the accelerator (for cars, or lever for ships) in order to directly control the desired power (or shaft speed for ships). However, in hybrid architectures, in the absence of an EMS, the operator would have to control the power demand of each one of the power converters (ICE, EM) with multiple inputs. That would, of course, yield sub-optimal results and input complexity. Thus, an EMS aims to provide an additional layer between the operator and the power converters in order to receive a single demand input from the operator and decide on an optimal power split according to predefined optimisation objectives.

Below follows an extensive literature study that examines the state-of-the-art in the automotive and microgrid powerplant industry. This approach is also taken in an another recent literature study [2]. The motivation behind the automotive section of the present study is the notion that hybridisation, and especially hybrid power supply, has been greatly affecting the automotive industry long before its recent applications on ships (of course with some exceptions e.g. submarines), and the corresponding literature and research is much more extensive. Looking into the literature on Microgrid control is also an advisable approach due to the number of existing similarities with

maritime power-trains. On most ships, power generation is achieved by a network of different energy converters serving the purpose of meeting the operating power demand of the vessel. Hybridisation of maritime vessels is highly correlated to topologically complex power-trains. Uncertainty is a primary characteristic of the propulsive load demand, due to the weather dependency and the non-fully-determined operating profile. Terrestrial Microgrids (MGs) demonstrate similarities with maritime power-trains both in terms of topological complexity and uncertainty. That said, the power scheduling of MGs is not only subject to high levels of uncertainty on the demand side, as with maritime applications, but also on the power supply side. This is due the de-centralised (or distributed, as opposed to centralised) power supply which typically includes renewable energy sources (e.g. photovoltaic, aeolic) that are subjected to weather-induced uncertainty. Given these similarities and the limited literature of energy management in maritime applications, a review of MG energy management (or tertiary control as classified in [38, 39]) research is presented in this section.

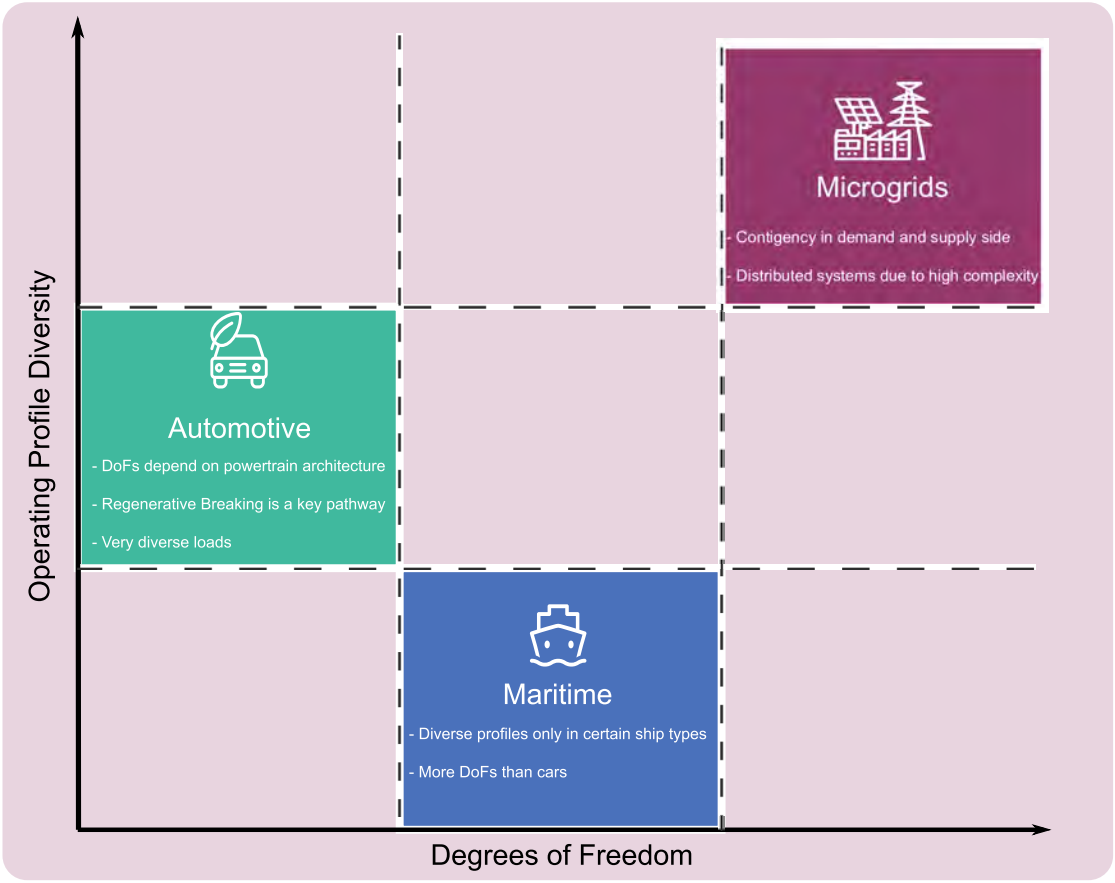


Figure 2.1: Hybrid Energy Generation in Different Industrial Sectors

Finally, the state-of-the-art in EMSs in the Maritime Industry is examined, the literature gaps are identified, and, extrapolating from the other sectors, a systematic approach to address the key

problem of realistic prediction utilisation is devised.

## 2.1 EMSs in the Automotive Industry

In this section an attempt to systematically present the extensive research into EMSs for Hybrid Electric and Plug-in Hybrid Electric Vehicles (HEV and PHEV) in the automotive industry has been made. The distinction between the two categories is made on the basis that HEVs attain fuel savings by keeping the State of Charge (SoC) of the energy storage device (i.e. batteries) relatively stable (charge-sustaining CS - all the energy is derived from the fuel [3]), while PHEVs deplete the energy in their energy storage (charge-depleting CD), and utilise electric power from the inland electric grid by being recharged between driving cycles (a more extensive analysis of the two types is given in Section 3.3).

Without going into much depth in terms of the formulation of the problem, an EMS minimises a cost function $J$ (corresponding to energy consumed, gas emissions, etc.), by choosing the optimal control law $u(t)$ for the power split over the driving cycle $[t_0, t_f]$. Regarding this control problem, in [40], a general formulation of the cost function is given as:

$$J = \int_{t_0}^{t_f} P_f(u(t), t) + \alpha P_b(u(t), E_b(t), t)dt \tag{2.1}$$

where $P_f \in [0, P_{f,max}]$ the instantaneous power from fuel consumption, $P_b \in [P_{b,min}, P_{b,max}]$ the instantaneous power from battery charge/discharge, $E_b \in [E_{b,min}, E_{b,max}]$ the energy state of the battery at t (which also corresponds to the SoC), and, for PHEVs, $a = \frac{e_b}{e_f}$ that correlates the well-to-wheel efficiency for the battery $b$ and the fuel $f$, correspondingly. For HEVs, $a = 0$, and also the following global constraint is considered for charge sustenance:

$$\int_{t_0}^{t_f} P_b(u(t), E_b(t), t)dt = 0 \tag{2.2}$$

Finally, the power demand $P_{dem}(t)$ must meet the power delivered at the wheels, which for an in-series architecture with no planetary gear box equals to the power of the electric motor $P_m$.

The available literature has been reviewed in a number of studies [3, 32, 33, 36, 37, 41]. The abundance of automotive research on EMS compared to that for ships, is due to a number of identified relative advantages such as (see also Section 1.1):

- suitable energy density of lithium-based battery units [28], ultracapacitors (UC) and fuel cell (FC) units (i.e. PEMFC units) [42] for the typical energy requirements of inland vehicles [43, 44]. Developments in Energy-Storage System (ESS) topologies for HEVs and PHEVs. [45]
- stricter regulatory framework regarding emissions (especially CO, HC, NOx and PM) of land-based vehicles ( [36], EURO 1-6 and I-VI emissions standard for EU/EEA members states:

there is series of directives, each amendments to the 1970 Directive 70/220/EEC [46], US emissions standard managed by EPA [47])

- highly diverse driving cycles (due to i.e. altitude variations, city traffic, different loads, etc.) and frequent starts and stops [32]
- the regenerative braking energy pathway capable of recovering part of the vehicles kinetic energy [3, 32]
- the increasing capability of connecting to the inland grid, in combination with fast-charging lithium battery technology [28]
- the relatively simpler and significantly less powerful powertrain architecture and topology (i.e. one small ICE and a battery pack with at most four motors, whereas ships often have multiple large ICEs and several generator sets with high-power consumers such as pumps)
- prediction of driving cycles by the recently developed and very capable Intelligent Transportation Systems (ITSs) and car movement pattern data [48], [49]
- the realisation of the opportunities presented above by regulating parties, consumers, and the highly competitive global automotive industry, leading HEVs, PHEVs and battery electric vehicles (BEVs) into mass production

As stated in [32] and shown in the expression for the cost function $J$ in Eq. 2.1, the main objective of the EMS is not to minimise the fuel flowing into the engine at each instant of time, but the total fuel consumed during a driving cycle. Perfect information of the driving cycle or even information on the length of the mission time, yields greatly different results than partial cycle knowledge when implementing the control strategy. In fact, the optimal trajectory can be found only if the driving cycle is known in advance [3]. Test-drive cycles by regulators conveniently provide a very well defined route (FUDS in the US and MVEG-95 in the EU [32]), on which the performance of the vehicle is assessed. In real implementations this is obviously not possible. Perfect knowledge can only be used as a benchmark of the EMSs real-time implementations, or to tune parameters of pseudo- and sub-optimal approaches. In combination with exhaustive solutions (i.e. Dynamic Programming), perfect knowledge can yield an optimal control sequence for the optimal trajectory, minimising the cost function [3]. To address that problem, automotive applications frequently utilise on-board Integrated Navigation Systems (INSs), like GPS, for future driving cycle prediction [49–53].

### 2.1.1 Hybrid Electric Vehicles

A number of comparative studies for different EMSs on HEVs can be found in the literature [3, 37]. Following is a review of the advanced EMSs applied in HEVs, with the stationary feedback

implementations not being extensively reviewed here, as they yield non-optimal and non-charge-sustaining control sequences. With that being said, heuristic rules or fuzzy logic laws in combination with stochastic dynamic programming can yield satisfactory results, while addressing most of the drawbacks present in other implementations of stationary feedback [54].

An extensively researched EMS implemented in HEVs, addressing charge-sustenance and easy implementation in real-time applications [3], is the Equivalent Consumption Minimisation Strategy (ECMS), initially proposed in [55]. This approach utilises the charge sustenance property of HEVs and treats the battery as an auxiliary reversible "fuel tank", by introducing a virtual equivalent consumption term for the use of the rechargeable ESS of the vehicle $\dot{m}_{virtual}$ [3]:

$$\dot{m}_{equivalent} = \dot{m}_f + \dot{m}_{virtual} = \dot{m}_f + \frac{s}{LHV} P_{electric} \tag{2.3}$$

where $\dot{m}_f$ the actual fuel consumption, $LHV$ the lower heating value of the fuel, $P_b$ the delivered electric power from or to the batteries, and $s$ the equivalency factor, that contains the information regarding the connection between using the battery "fuel" and using fuel from the actual fuel tank.

This means the electricity used when discharging the battery unit has to be replenished later by the engine using fuel [3]. The optimality of such an approach is highly dependent on the selection of an appropriate parameter $s$. This parameter was originally constant for charging and discharging (two different constant values for s, one for the charging and one for the discharging mode), however, these values depend on the driving cycle and are very critical to the strategy's success. They can be obtained with a numerical optimisation procedure, such as DP [3]. In fact, ECMS is derived from optimal control theory [32], in that there is an analytical derivation of ECMS that can be obtained from Pontryagin's Minimum Principle (PMP) [3]; ECMS is an implementation of PMP if the equivalence factor is time-varying, depending on the vehicle and driving cycle, while standard ECMS implementation can be assumed to be an approximation of PMP.

To that end, the standard ECMS has been augmented and improved, in particular regarding the means to calculate the optimal value of $s$, in order to be more applicable in realistic, real-time implementations [3]. This is because non-perfect information of the future driving profile cannot yield optimal or charge-sustaining control sequences, thus, the future profile has to be estimated. Such strategies are adaptive ECMSs (A-ECMSs) and telemetry ECMS (T-ECMS). In one A-ECMS implementation, data from a brief period of the current driving cycle (1-2 minutes) together with GPS data are utilised and auto-regressed in order for the $s$ value to be calculated periodically online [37, 56]. Another implementation of A-ECMS is realised by grouping together cycles with similar statistical properties and calculating a set of corresponding $s$ values offline; then, by means of pattern recognition, an appropriate $s$ value is selected online [57, 58]. On the other hand, T-ECMS [51] is utilising information from an on-board telemetry system, capable of identifying obstacles on the road, together with an altitude profile of the route that is assumed to be known from the GPS, in

order to estimate the optimal value of $s$.

In Model-Predictive Control (MPC) the future driving conditions estimation over a set horizon span ($T$) is made online using a simplified model, to mitigate the computational load. Then, with that information, a QP or DP solution is used to find the optimal control sequence [32,59,60]. MPC is computationally expensive and requires an accurate model of the system to yield satisfactory results, while, in order to be effective, prediction techniques must be used [3]. In [49], an MPC real-time EMS is proposed, utilising Intelligent Transportation Systems (ITS) for driving cycle prediction. A combination of route prediction from the telematics system together with MPC for the Power-Train-Control (PTC) has also been implemented in [52]. Online implementations of predictive control with information supplied by the GPS and the traffic-flow information systems can yield near-optimal results [53], with 0.3% more fuel consumed compared to an ideal controller, on a specific route for which enough data are available to be accurately modelled as a stochastic process.

In Table 2.1.1, an attempt to compare the EMSs for HEVs found in the literature is made. Advantages and drawbacks of each method, found in the literature reviews [3, 32], are given to provide some insight into possible applications. Relevant reference studies for these strategies are given, from which the presented results can be derived. Direct quantitative comparison is only indicative of the qualitative relation between the different strategies, as the results presented here are aggregated from greatly different sources, with implementations of different case studies, driving cycles and hybridisation architectures. There is no "common denominator" for all the results, and in some cases the amount of evidence for certain EMSs is very low. In this attempt for comparison, the performance of each strategy is compared to a global solution, or the closest comparative result to a global solution which is directly or indirectly available.

Table 2.1: Energy Management Strategies for Hybrid Electric Vehicles in the Automotive Industry

| Method | Advantages | Drawbacks | Consumption w.r.t. Global Solution* | Reference |
|---|---|---|---|---|
| **DP** | Closest approximation to optimal results | Requires perfect cycle information | - | [61] |
| | Can be used to tune parameters for rulebased methods or ECMS-based methods | Not directly implementable | | |
| | Can be used to benchmark other control strategies | | | |
| **SDP** | Close to DP results with enough data | Requires statistical information about a specified route | +3%with no position knowledge | [53] |
| | | Time invariant heuristic control | +0.2%GPS, traffic flow and statistical data | |
| **MPC** | Very good results with a known reference trajectory | Computationally expensive | +1.12% to +2.12%** | [49] |
| | More applications due to increasingly powerful processing units | Prediction of the disturbance vector must be made | +0.02%(horizon of 1/4 of the mission) | [59] |
| | | Requires an accurate model | +0.53%(horizon of 1/120 of the mission)*** | |
| **ECMS** | Implementable online only for very similar driving conditions | Sensitive to the equivalency factors s | +0.26% with single optimal s value [51] | [55], [56], [51] |
| | Unlike MPC only s must be determined to find the co-state | Optimality or charge sustenance not guaranteed for non-optimal s values (depend on the drive cycle) | +2.45% with realistic values for driving conditions [56] | |
| | Optimallity that is derived from Pontryagin's minimum principle | Relies on information for future driving conditions | | |
| | Can be extended to account for multiple objectives | Chattering between states | | |
| | | Factors s are fixed | | |
| **A-ECMS** | Online equivalent factor adaptation to the driving cycle | Computationally expensive, simplified for only one s | +0.66% | [56], [37] |
| | Meaningful real world application | | | |
| **T-ECMS** | Utilise telemetry to estimate future speed profile | | +1.48%**** | [51] |
| | Realistic implementation | | | |
| | Varying s(t) | | | |

*DP and QP are assumed here to all yield globally optimal solutions as stated in the corresponding literature

**indirect comparison of MPC in [49] with global solution, by using results from [56] and [51], respectively

***It must be noted that the driving cycle is varying periodically, unlike other case study in this comparison

****Found against ECMS with cycle-specific global optimal s and to which the +0.26% is added to compare against DP

*Note: The a) high variance in the results due to great non-uniformity between the different cycles and case studies available in the literature and the b) low amount of evidence for certain EMSs, only allow for a qualitative comparison of the EMSs performance to be inferred*

### 2.1.2 Plug-in Hybrid Electric Vehicles

Technological developments in ESSs [45] and recent technological breakthroughs in battery technology [43] are able to provide ESS solutions with high power and energy density on board vehicles, capable of increasing the portion of electrical drive and of allowing vehicles to be charged from the grid [62]. The total emissions of such vehicles rely on how green is the electricity production that powers the grid [43], so in order to evaluate the impact of such vehicles in a holistic manner, central electricity production emissions should be taken into account. While fuel consumption is the most common cost function for the optimal control problem in the case of HEVs, PHEVs' performance may be more appropriately evaluated with an energy consumption cost function [3, 63], but, this is rarely the case in literature.

In [63], implementations differ in terms of the hybrid architecture (combination of engine motor size, battery size, and ICE engine size) and control concept (charge depleting - charge sustaining or CD-CS and blended-mode or BM strategies, both being evaluated using DP). The CD-CS (also found as electric-vehicle-centric) control strategy uses the motors and batteries to meet all traction demand, whenever that is possible, while the ICE engine is only used if the power demand cannot be covered, or the SoC of the batteries is too low. CD-CS can be implemented with a rule based control strategy. The BM strategy optimally uses the engine power over a set distance so that the system is most efficient, however, deviations from this target distance ends up in higher fuel consumption compared to the electric-vehicle-centric mode, with the latter ultimately being the recommended strategy for any cycle where specific distance is not known [63]. This indicates the importance of information on the driving cycle.

As described in [44] (where DP is also being used to evaluate the control approaches and the trip length and driving profile are modelled as stochastic variables), in order to minimise fuel cost, the ESS has to be fully depleted between two charges. On the other hand, if the distance between the charges has exceeded the range of the PHEV, turning on the engine in a blended control fashion is, in most cases, more energy efficient, resulting in a 1-4% decrease in fuel costs, even if little is known for the trip length.

In [40], it is shown by means of DP that if the $\alpha$ in Eq.2.1 is above a critical value $\alpha_c$, the final $E_b$ of the PHEV (i.e. battery energy state) is higher than the minimum allowed (i.e. no depletion occurs), which means that the end constraint is not applied, and the optimisation cost function is dominating the control strategy; the value of $\alpha_c$ depends on the driving cycle and the battery size. Qualitatively that can be understood as follows: if the size is bigger and the mission's requirement for power lower, $\alpha_c$ will be lower and the end constraint is not as limiting for the strategy, but the global cost function is at play. This is very useful because from $\alpha_c$ and the corresponding driving cycle the minimum battery size can be found (see also Section 3.3).

A number of benchmark studies have been conducted for PHEV EMSs. In [41], MPC and A-

ECMS are implemented on a PHEV and compared against a rule-based controller, both yielding up to 10% reduced fuel consumption, with A-ECMS being 15% faster. In [33, 36, 64] and [65] it is stated that a fully electrical operation of charge depletion (CD) followed by a charge sustaining (CS) policy, known as CD-CS, is not optimal. On the other hand an optimal EMS shall yield a blended strategy. In [33], a benchmark PHEV control problem was presented, taking into account both the fuel efficiency performance compared to an exhaustive, perfect information, global PMP-based solution, and CPU with memory use. Nine solutions from different research teams were tested, with unknown driving profiles, yielding a BM, map-based ECMS as the winning strategy, that was able to yield near-optimal performance in two different driving routes. Online BM is implemented in ECMS with what is known in literature as co-state adaptation, that uses a decreasing value for $\xi_{ref}$, which, however, requires a prior estimation of the total distance to be covered.

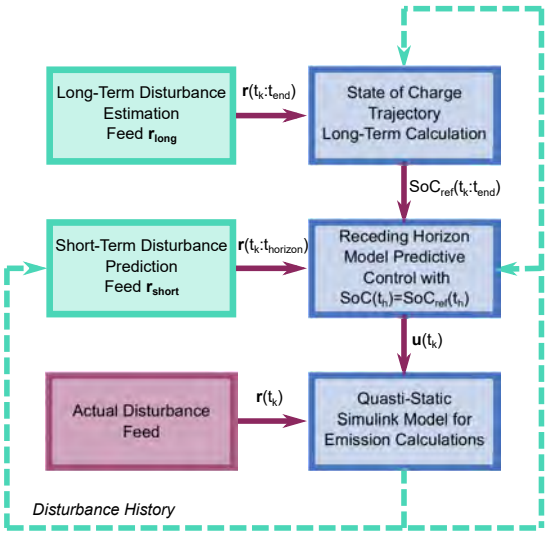


Figure 2.2: EMSs framework utilising MPC and supervisory SoC planning, adapted from [65]

A recent review study [36], indicates a general trend towards EMSs that implement BM and optimal control, while utilising ITSs. The same study also includes an extensive review of a plethora of new EMSs implementations utilising Derivative-Free methods (i.e. PSO, GA, DIRECT, Simulated Annealing), which are difficult to implement online, Convex Programming (CP), Neural Networks (NN), Sliding Mode Controller (SMC), and Game Theory (GP). It is indicated that BM strategies are performing better than CD-CS strategies, however, they require trip information, i.e. some form of mission prediction, with or without GPS, GIS or ITS utilisation. Following this paradigm, as it can be seen in Fig. 2.2, in [65], a conventional MPC was combined with a supervisory SoC planning scheme, utilising traffic information, and yielding results that are exceptionally close to DP solutions (when using dynamic traffic information, 94% fuel optimality is achieved on average, compared to the 100% optimal DP).

## 2.2 Microgrid EMSs

MGs are low voltage intelligent power distribution systems [66] which include Distributed Energy Resource (DER) units to supply power to various local loads. The form of power supply is typically electric or thermal. Terrestrial MG loads commonly consist of residential or industrial loads (e.g. HVAC of buildings [67], parks [68], etc.). DERs are divided into Distributed Generation (DG) and Distributed Storage (DS) units. Some key advantages of MGs include keeping the DER units locally for the consumers in the vicinity and the corresponding low losses, especially for thermal energy applications [69], flexibly selling and buying energy to the grid [67], and being compatible with the localised and distributed characteristic of Renewable Energy Sources (RESs). DER units can either be rotary units such as engines and turbines coupled with generators, or electric energy suppliers and storage systems (i.e. fuel cells and batteries, correspondingly) coupled to the grid with power electronic converters. DGs may include renewable (RDGs, non-controllable) units such as Wind Turbines (WT), or controllable units (CDGs) such as engines and Micro Turbines (MT) [70]. Thus, by combining fossil-fuel and renewable power sources with energy storage, they are a form of hybrid power supply [2].

Terrestrial MGs can be connected to the medium voltage grid [71] through the substation transformer (grid-connected mode) or they can be disconnected from the grid to autonomously supply enough power to sustain full or partial load, in what is called the islanded mode [66, 68].

Narrowing the scope to only electric energy supply, from standardisation efforts regarding MG control (ANSI/ISA-95) in [39] and [38] a hierarchical classification scheme has been proposed, consisting of four control levels (Level 0-4), which have been adopted to the considerations presented later in this section of this study, and are also shown in 2.3:

- zero (individual module) level inner control loops for voltage and current output
- primary (droop) control for system stability and dampening
- secondary control which corrects deviations in frequency and amplitude, while also has the ability to support the (dis)connection of the MG from the grid by the inclusion of a synchronisation control loop. Power flow is also regulated by this level of control
- tertiary control for the energy production of the MG; optimal operation control

It must be noted that, albeit the effort, the classification levels and distinctions in MG control are neither clear nor consistent in the literature. For example, tertiary control in [39] and [38] is considered to be active only during connection with the main grid; in fact, in [38] it is stated that when in islanded mode, secondary control becomes the highest hierarchical level and optimal strategies are implemented at the MGCC; however, it is not stated if there is energy management present when there is no connection with the grid. Other studies, such as [72] considers a distributed

EMS being implemented by communication between the local unit controllers (LSs) and the MGCC to be able to also function in islanded mode.

For the scope of the present study, a distinction between secondary and tertiary control is made in order to provide the much needed clarity and consistency within MG literature, but also in automotive and maritime research studies. This physical distinction regards as secondary control any relevant control for power flow management, and tertiary control any control strategy that provides control output with energy-based decisions. Such an approach was also selected in [2]. To avoid the additional confusion due to the ability of energy management problems to be formulated as Optimal Power Flow (OPF) problems (as in [72]), the distinction here essentially aims to decouple highly transient control from quasi-steady state control (also see Section 2.3). In more detail, tertiary control is thought as energy management where the objective minimisation is realised by implementing an EMS. The control inputs are the imported and exported energy (grid - connected mode), the commitment and dispatch of the DERs, the market operations (between the grid and the MGCC) and the controllable loads [72]. It should be noted that with this definition, even in the case of the islanded mode, the tertiary control still serves to optimally distribute the available energy and cover the load demand within the MG. Finally, such a classification provides a direct correspondence between terrestrial MG literature and maritime applications, where islanded mode is the most common for a ship-bounded MG operation [2].

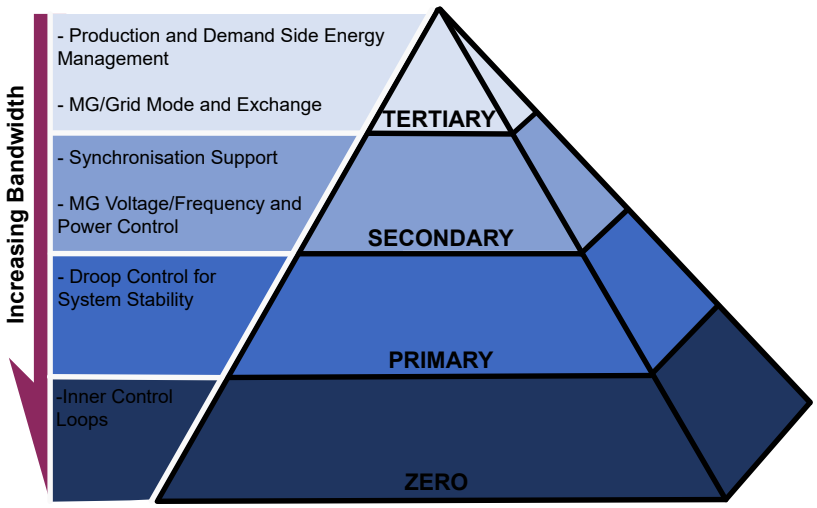


Figure 2.3: Microgrid Hierarchical Control Levels, adapted from Guerrero et. al (2010) [39]

Controlling the relatively big number of topological degrees of freedom compared to the automotive and maritime applications introduces considerable challenges regarding the control of the corresponding energy flow management. Due to the "on-off" characteristic of the network of DER units, such optimisation problems focus on the energy supply side and are characterised as Unit Commitment (UC) problems in the literature [73, 74], as opposed to Economic Dispatch (ED) in

which the control decisions for the power output setpoints of the DER units are being made and where there are continuous variables rather than binary. IC and ED are interdependent [67].

A considerable number of studies regarding the optimised MG operation are available. MG optimal operation and energy management is comprised of the optimisation in the [67]

- supply side, involving UC, ED, grid market decisions etc., while also taking into account uncertainty (primarily for RES [69])
- energy storage's role, which is crucial especially when coupled with RESs, where power production is inherently intermittent and weather reliant, in order to achieve a consistent output
- demand side (load management or DSM), which can only be optimised if there is the possibility of some of the non-critical loads to be rescheduled or curtailed, and also consider the possibility of providing (selling) power back to the grid (grid-connected mode only).

These different elements can be optimised separately (achieving, of course, sub-optimal results), or as a whole (system optimisation) in order to achieve true optimality, at the cost of significantly increasing the complexity of the problem [67]; in any case, forecasting (i.e. load or wind forecasting) is crucial for the optimality of the energy management. It should be noted that the implications of MG Demand Side Management (DSM), when considered for maritime applications, are quite interesting. In most cases the EMSs on board ships consider all loads as being critical and rescheduling or curtailing some loads has not been the subject of any prior research. Particularly interesting can be to classify loads based on their importance in different scenarios, especially in critical situations, for example when a frigate loses certain operating capabilities due to damage or when the propulsion of a cruise ship fails.

A brief presentation of the literature follows, according to the paradigm in [38], by classifying the MG operation studies based on their EMS approach; the EMS can be either implemented centrally, at the Microgrid Central Controller (MGCC), or using a distributed approach, where MGCC handles part of the control responsibilities.

### 2.2.1 Centralised EMS

Centralised implementations of MG EMSs at the MGCC formulate a nonlinear optimisation problem with no exact solution [66], with the number of binary decisions being significantly higher than those found in corresponding automotive approaches, due to the "on/off" characteristic of terrestrial loads and complex DER networks; that said, such implementations are correlated with a number of disadvantages, as identified in [72]:

- high computational demand for the MGCC
- low efficiency and scalability

- no plug and play capability of future DER units [71, 75]
- information gathering requirements that may violate privacy in several terrestrial scenarios

For maritime applications, only the first three disadvantages are relevant in most cases. However, privacy issues might arise in certain scenarios, for example if a naval vessel is connected to the shore grid (although the MG boundaries would have to include part of the shore grid in order for privacy concerns to arise). Plug and play capability is very important, but mostly in the form of redundancy, meaning that the ship-bounded Microgrid might need to be able to adapt in the event of loss of DERs (which for a ship can be the main engine, the batteries, the fuel cells etc.).

In early research for UC [73], Dynamic Programming (DP) is utilised, incorporating a heuristic scheme to deal with the exponential complexity of DP. The strategy employs a variable search window (as opposed to the fixed search window of earlier implementations) in order to get the priority list truncated and reduce the search space. Experimental (model) results on a system consisting of 26 thermal power generation units, tested for various load profiles, support reduced execution time of the approach, while it still delivers results of the same quality. As with any DP solution, online implementation of such a strategy is not possible. Another approach for dealing with UC problems is found in [74], where an Enhanced Adaptive Langragian Relaxation (ELR) algorithm is proposed. This algorithm is of linear computational complexity, while compared to other heuristic solutions not only it performs faster, but also better, especially for a larger number of DG units (in the order of several decads).

In [70], Mixed Integer Programming (MIP) optimisation model is used as the MG EMS for a grid-connected mode, capturing only the uncertainty in energy demand, but not the the uncertainty in energy production from RDG units. The objective function of the EMS is cost minimisation. MIP is particularly useful to deal with the large number of binary "on-off" constraints for the CDGs that are active at any moment. The study conducts sensitivity analyses on the demand response (which is the change of energy demand by the users based on market prices or additional incentives), the RDG power generation to simulate uncertainty (as it is not part of the problem formulation), and the storage capacity. However, the performance of the strategy is not compared against any other result.

A number of approaches have been implemented in EMSs for MGs. Sequential Quadratic Programming (SQP) has been used in [76] in order to optimise the production capabilities and the costs of a 23 bus 11kV MG, while using the same verification scheme, a Fully Connected Neuron (FCN) network has also been implemented in [77] in order to lower real-time computational load. A study which uses Particle Swarm Optimisation (PSO) for real-time application of a multi-objective EMS [78] yields promising results on a relatively small MT, WT and battery standalone hybrid plant, when compared to SQP optimisation.

### 2.2.2 Distributed EMS

In [71] it is described that the MGCC is connected to the medium voltage grid and its Distribution Network Operator (DNO) and Market Operator (MO) (one level above), while it is also interfaced with the lower level Local Control (LC) units (Micro Source Controllers or Load Controller) which are responsible for local decision making at the DER unit level. While the DNO controller manages the technical interfacing of the low-voltage MGCC with the medium-voltage grid, the MO is responsible for the market functionality, energy pricing etc. A distributed approach would decentralise the control decisions from the MGCC to the LC units, in an attempt to mitigate the problems presented in Section 2.2.1.

In the same study [71] the organisation of such a control network scheme is realised by using a MultiAgent System (MAS), which, in brief, gives every agent (or DER controller in this case) the autonomy to take decisions given a certain a) tendency and b) behaviour (refer to the citation for further information), and communicate with other closely related agents (e.g. photovoltaic DER unit and battery), but without information of the full system or MG. This way data flows in a complex network are minimised and the communication overhead is reduced [69]. The paper [71] implements an auction algorithm to solve the symmetric assignment problem which succeeds in achieving deals with the MO, while every DER agent decides what is best for them locally.

A number of distributed algorithms for distributed control coordination, similar to linear-iterative algorithms, are presented in [79]. Another EMS implementing a dual decomposition based algorithm preserves privacy of the customer behaviour, while it allows for energy flow scheduling within the MG [80].

A distributed strategy which prioritises robustness in order to deal with the uncertainty correlated to RES is presented in [69]. More specifically, a grid-connected mode optimal EMS, also based on dual decomposition, is considered for cost minimisation, taking into account both the supply and demand side of the MG, plus the transaction prices. Numerical tests on a MG that involves a significant numbers of RES have been conducted, however no comparison with other solutions has been made.

In [75], a distributed Additive-Increase-Multiplicative-Decrease (AIMD) algorithm is introduced, for optimal power generation in a MG, with the goal of minimising communication overhead and minimising utility (i.e. a financial cost function). The results were simulated in MATLAB®.

A more sophisticated approach is presented in [72] for the distributed EMS of both the supply and the demand side. The study takes into consideration the exact distribution network of the Microgrid and realistic constraints, by not assuming the connection of all DERs and loads to a single bus.

## 2.3 EMSs in the Maritime Industry

Although EMSs are an extensively researched topic in other industries (e.g. an abundance of studies concerning hybrid cars and energy-hubs/micro-grids is available), in the maritime sector there are recent developments yet to be applied, in order to further optimise the required objectives, taking into account the specific characteristics of marine systems.

Before delving into the analysis of the existing literature, a clarification needs to be made, at least for the needs of the present study. Following the paradigm of land-based vehicles and micro-grid hierarchical structures, EMSs that optimise fuel consumption typically do not need to take into account transient phenomena, and quasi-stationary models are used instead, which can be easily implemented online due to their reduced computational load [1, 32, 35]. Thus, if the timescale of the studies are in the order of several seconds, the strategies are classified as power management strategies or secondary control [38] and commonly also take into account transient phenomena of the components (i.e. rate of power delivery increase by the ICE, discharge rates etc.). For completion, a couple of examples are given. Studies such as [81], in which the power demand fluctuations in various sea states due to the propeller load (which are in the order of few seconds) are mitigated by means of power management on an electrical cargo ship propulsion power-train, or [82], where nonlinear ship response of an Offshore Support Vessel, due to environmental disturbances is taken into account to control ship speed in the surge direction, in dynamic time frames, also at a scale of few seconds, are examples of power management strategies. Similar implementations are found in [83–85]. On the other hand, studies done for the operating profile of whole missions, that do not take into account transient dynamics, such as [34], are typical examples of EMS or tertiary control.

In a recent literature study [2], research on EMSs, or tertiary energy management, for ships with hybrid electric supply has been discussed, presenting the following main strategies found in maritime applications:

- Heuristic Control Strategies, where the operating mode of the onboard hybrid power plant is determined by either logical rules [86] or multidimensional maps. As described in the previous section, heuristic control can be fast (computationally) so it is suitable for online implementation and also can perform well if correctly tuned, however, it yields sub-optimal results, while optimal control strategies such as ECMS are generally superior; back to automotive applications, in [33], a benchmark of plug-in HEV EMSs has been done, and (by taking into account only the dominant solutions of a Pareto front with fuel savings and computational effort for its axis) the dominant ECMS strategy saves 16.2% more fuel than its rule-based counterpart. On the other hand, the ECMS strategy performs 14.2% slower than the RB approach, although it uses 89% more memory. Another point worth noting is that in [1] and [34], baseline RB approaches were charge-sustaining, and not of plug-in nature, thus yielding big differences when

compared to PHEV strategies.

- ECMS, which performance has also been described in the previous section regarding automotive applications. Maritime applications include the hybrid ferry MV Hallaig, which is effectively a PHEV as it utilises batteries that are recharged from the grid overnight, yielding up to 38% in fuel savings compared to a conventional similar-sized vessel (24% in fuel savings due to grid utilisation, plus 11% fuel savings due to implementing optimal ECMS control, according to [2]). Another implementation of ECMS and A-ECMS is shown in [1].
- The EMS presented in [34], called *Power* Management through Operating Load Estimation over Subsequent Horizons, which does not take into account transient dynamics of engines or batteries, or provide a quantitative analysis of their effect, thus, it is classified under EMS here to prevent confusion. The formulated optimisation problem is solved by the constrained nonlinear minimisation Interior Point Algorithm (IPM) in MATLAB ®. Unless the Hessian matrix is provided, such a nonlinear solver may be fairly computationally expensive. Online implementation capabilities are not discussed in the paper, thus it is not known if the time step $\Delta t$ of 2 minutes in the paper is sufficient for the optimisation problem to be solved. Since the batteries are depleted, the tugboat is operating as a PHEV. The proposed EMS yields around 2% fuel savings compared to a rule-based (and much cheaper computationally) controller [2]. Compared to a charge sustaining, HEV operation, in the case when the mission's load demand is known, this strategy, compared to a charge-sustaining rule-based controller, yields 9.31% in fuel savings and 8.90% when the demand is predicted by a simple novel predicting scheme that utilises previous operating load data [34].

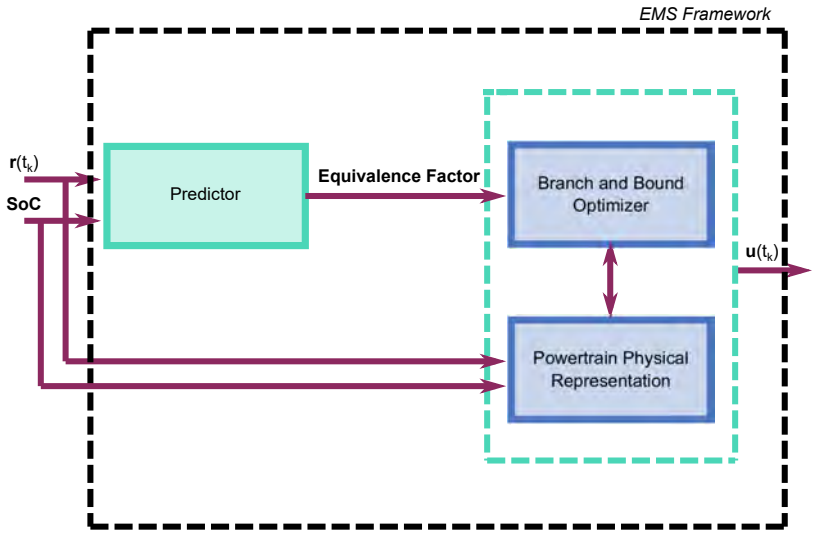


Figure 2.4: A-ECMS Supervisory Controller Scheme used in [1], adapted illustration

Recent research in the field [1], in which the EMS is described as secondary but due to the

reduced quasi-state model used and the timescale of the implementations it is classified as tertiary according to the previous discussion, has indicated that the application of a novel ECMS-based strategy, utilising the Branch & Bound method with Convex optimisation, in PHEV operation yields a 4-6% reduction in fuel savings, compared to the previously used RB, HEV strategies, while exhaustive solutions (DP) with perfect information indicate another 2-3% headroom for further reduction. The novel EMS solves the corresponding non-linear optimisation problem formulated, while it is quick enough to be implemented online. In more detail, a comparison between DP, rule based control, ECMS-based and A-ECMS-based has been made over 7 different operating profiles of tugboats to evaluate the controller. For the A-ECMS, the equivalence factor has been adapted based on estimations for the operating profile, using the methodology in [34].

Similarly in [35], concerning implementation on all-electric tugboats, an ECMS strategy has been implemented and compared to a conventional HEV rule-based strategy, yielding 17.6% in fuel savings.

Contrary to automotive applications, the time steps for the maritime applications can be in the order of a few minutes (instead of a few seconds), due to the slower dynamics of the power demand profile. This alleviates some of the computational burden maritime application have due to the additional degrees of freedom in their powertrain (i.e. additional DEs and EMs etc.). In [34], the time step interval for solving the EMS control problem for a tug boat is 2 minutes, thus providing a guide towards the appropriate length of the EMS times steps in maritime applications. Furthermore, since tugboats generally have a more dynamic propulsion power demand profile than most other ship types (e.g. power demand changes drastically during tug operation, as opposed to a cruise ship), even larger time step intervals may be implementable for certain applications.

## 2.4 Operating Profile Forecasting and Integrated Bridge Systems

It has become evident in the previous discussion that a key component of EMS performance is the accurate estimation of the future loading profile and mission length. To tackle this challenge, a number of approaches are discussed, which are applied or are potentially applicable in the maritime industry, while the Integrated Bridge Systems (IBSs) on ships are also being presented as means to potentially gather useful information before and during a mission.

It is also possible for a multitude of prediction schemes with different horizons to be part of the same EMS approach, as shown in [65], where a long-term and a short-term scheme coexist. The first is providing a globally optimal disturbance estimation (in that case state of charge of the batteries) and the latter is providing an estimation to be utilised in a traditional MPC-scheme.

### Prediction Schemes

The operating profile load demand was predicted in [87] and [34], with a *2n-period generation* scheme, utilising the typical time spent in different load levels (low, medium, high) during the mission, found in historical operating profiles of tugboats. The load prediction is performed for a short horizon into the future, that shifts forwards with each time step. For the duration between the present time $t$ until the set horizon $t + T_{horizon}$ the sub-optimisation problem is being solved. In [1] the same prediction scheme was utilised in order to adapt the equivalence factor in an A-ECMS approach.

However, this prediction scheme only utilises past information and, thus, its predictive capabilities are limited for a PHEV approach. On the other hand, in [36] (see previous Section 2.1.2) it is made clear that in order for BM strategies to perform better than CD-CS strategies, trip information is required. To that end, there is a trend for the prediction schemes applied in automotive vehicle EMSs to utilise GPS, GIS or ITS for their driving cycle predictions.

ITS in automotive vehicles, such as Google Maps, include traffic monitoring systems and a series of road traffic sensoring solutions, which in combination with GPS and the available 3-D maps are able to provide in real time accurate information about the environment and the future operating profile of a vehicle, given its destination [65].

Although there is not a perfect parallelism between ITSs and IBSs, a strong correspondence is present, and the potential of IBSs to provide insight into the future operating cycle should not be neglected. Following is a brief description of IBSs on-board maritime vehicles.

### Integrated Bridge Systems

Integrated Bridge Systems (IBSs) are regulated by perfomance standards (Resolution MSC.64(67) and SOLAS chapter V), by IMO [88], which defines them as a combination of interconnected systems that allow for central access to information (i.e. from sensors, from authorities) and for command from workstations, in order for the ship to be managed in a safe and efficient way by qualified personnel.

Modern IBSs integrate a number of maritime aids, such as the Electronic Chart Display and Information Systems (ECDISs), navigation aids (GPS, radar and automatic radar plotting aid - ARPA), the Auto-Pilot system, the NavTex message system, sensor information (e.g. echosounder, anemometer), etc. [89], [90]. ECDISs obtain weather forecasts and display various electronic charts, that are designed according to the requirements of IMO, IHO (International Hydrographic Organisation) and IEC (International Electrotechnical Comisssion), in order to produce comprehensive environment information for ship navigation, route planning and route monitoring [91]. The NavTex message system transmits safety information of a certain urgency (i.e. warnings, forecasts, etc.) [90].

In [92], it is described that the IBSs are designed to allow for usually a single person to perform ship management operations with safety and reduced stress. IBSs also integrate functions such as Dynamic Positioning, Automatic Route Keeping, Radio Communications, Safety System etc.

In a more methodical approach [91], IBSs are described to be comprised by a navigation and an automation system. The navigation system consists of the ECDIS, Conning, Auto-pilot and corresponding sensors, Radar etc., while the automation system is comprised by a number of control systems for various operations in the engine room (e.g. engine and propulsion control, bilge and ballast control, HVAC, alarm and monitoring systems etc.).

The Automatic Identification System (AIS) and Long-range Identification and Tracking (LRIT) system are also part of the ECDISs and can also be used for Vessel Traffic Monitoring and Information Systems (VTMISs) or to detect potential collisions [91].

In [90], the Estimated Time of Departure (ETD) and Estimated Time of Arrival (ETA) are discussed. The Auto-pilot system of ECDISs can provide the navigator with route planning. Weather routing that takes into account adverse weather conditions and the corresponding increased fuel consumption and added risk is also discussed. Route planning can also be done manually by the navigator by finding several "way-points" to the destination, taking into account the information provided by the on-board systems. In the same study it is also pointed out that there can be different route types, each corresponding to different objective, such as the shortest path route, the least time route, the least cost route the best comfort route, and combinations of the above [90].

## 2.5 Literature Gap

After clarifying key differences in the theory, with the most important clarifications being between PHEVs and HEVs, CD-CS and BM discharge, and power management and energy management, research potential is easier to be discerned. A number of gaps have been identified in the literature and in this review:

1. Lack of generalised objective functions of EMSs on ships which also account for objectives such as sound emissions and wear
2. Limited amount of implementations of advanced EMSs (as opposed to rule-based), especially energy (not power) management utilising MPC
3. The potential of demand planning following the Demand Side Management paradigm of Microgrids has not been researched, to the knowledge of the author
4. A holistic approach to account for the energy consumption optimisation including the energy from land charging, especially to examine PHEV functionality, has not been researched
5. Enabling the EMSs to be fed with realistic online information is not researched adequately, as BM is highly reliant on the information accuracy.

Focusing on the last point and following the extensive review of the state-of-the-art regarding supervisory controllers on hybrid ships, it is apparent that the available information assumptions of the current implementations of advanced EMSs are idealistic. This is showcased in the following instances:

- Tuning of the equivalence factor for the ECMS according to certain missions, while not showing robust behavior in changes of the profile length or substantial load deviations [1].
- Comparisons are done between PHEV and HEV operating modes [1, 34], while, in the case of [34], the marginally less efficient control without mission information (8.90% instead of 9.31%) is not clear whether it results from the depletion of the SoC or not

Any information that can be retrieved regarding the operating profile and its duration has the potential to greatly affect the online EMS controller, especially when the end SoC of the ESS can get significantly lower (PHEV approach), and if the strategy is designed to adapt to the real-time information stream (i.e. T-ECMS, A-ECMS, MPC). Several automotive applications and research of such EMS implementations, that utilise ITS, have been discussed previously (see Sections 2.1.1 and 2.1.2), with [53] for HEVs and [65] for PHEVs being perfect examples.

In this regard, the motivation behind the present study is to enable the EMS scheme on board to utilise online information regarding the mission of the vessel. This is important, as the state-of-the-art in maritime supervisory controllers can only be tuned before the mission. To that end,

a direction that presents research possibilities is to treat the IBSs on board ships, together with the navigators experience, as the maritime equivalent of ITS in automotive vehicles, and to examine ways in which available information from these systems can be utilised for pragmatic operating cycle prediction.

Furthermore, although there are plenty of MPC implementations in ships for secondary control, or power management control, with timescales of several seconds (see Section 2.3), there are not any implementations of such a strategy for EMS control, with timescales that correspond to a substantial part or even whole missions. Such research has been conducted in automotive vehicle energy management [65], yielding an implementable MPC strategy that is able to produce near-optimal performance, by utilising information from the ITS for load prediction. This research is considered to be key in implementing a realistic prediction-enabled EMS framework on a ship.

The research directions presented above constitute a substantial and interesting opportunity which may yield advanced energy management control methodologies with great potential for maritime applications, addressing in that way the challenges arising from hybridisation of maritime vehicles and providing solutions for greener alternatives.

## 2.6 Research Questions

After presenting the gap identified in the available literature and setting up two distinct research directions, research questions can be framed explicitly. The reason of posing these question is to further clarify the scope of this work, provide a preliminary framework for the assumptions that are going to be made and identify the contribution opportunities.

The present study addresses the following questions:

1. How can Model Predictive Control (MPC) be implemented for a plug-in based, energy management strategy on ships for fuel consumption minimisation?
    - How can a real-time information feed be combined with MPC to yield an effective Energy Management Strategy (EMS)?
    - What are the benefits of realistically utilising the Integrated Bridge Systems (IBSs) in combination with the navigator's decisions in order to provide a real-time information feed regarding the future velocity profile or power demand of the present mission, in the context of the EMS framework of a ship's hybrid propulsion power train?
2. How can such an EMS be implemented in a case study for naval vessels?
    - How can the vessel system together with the EMS control system be modelled in order to provide insight into the behaviour of this EMS.
    - What level of modelling detail does the simulation model need in order for the EMS control approach to be fast enough to be able to be implemented online, while still being effective and accurate enough?
    - What is the performance of such an approach and how does it compare against a) the current EMS implementations and b) the exhaustive solutions (i.e. DP solutions with perfect operating profile information)?

Considerations to be taken into account for the scope of this study are the following:

- MPC and T-ECMS are found to be the only EMSs capable of utilising an online future information feed regarding the mission, while also providing a flexibility in matching the horizon span with the available degree of this information.
- Although the battery capacity on-board a ship is small compared to the total energy demand of a naval mission, implementation of such a plug-in EMS approach for naval applications during parts of the mission where optimal battery depletion can be crucial provides important opportunities (range maximisation and power output reserve preservation)

- A combination of the IBSs and the operator's human input will be treated as an input to the system, however, attention will be given into keeping any assumption for the available level of information realistic.

# Chapter 3

# Concepts Regarding Vessel Hybridisation

## 3.1 Powertrain Architecture: Series and Parallel Configurations

Hybrid-electric powertrain architectures can be classified into series, parallel and hybrid (series-parallel), and they correspond to different degrees of freedom (DoFs) in the energy flow [32]:

- Mechanical powertrains have 0 DoFs [1]
- Parallel powertrains have 1 DoFs, corresponding to the node of the gearbox combining the mechanical energy flow from the induction machine and the IC engine towards the propeller
- Series powertrains have 1.5 DoFs; 1 DoF for the node where the flow from the battery and the generator meet and half of a DoF corresponding to setting either the speed or the torque of the IC engine
- Hybrid powertrains have 1.5 or 2 DoFs depending on whether or not the engine-generator node and the engine-motor node are mechanically connected (latter has 1.5 DoF).

[1] transmission ratios are not taken into account

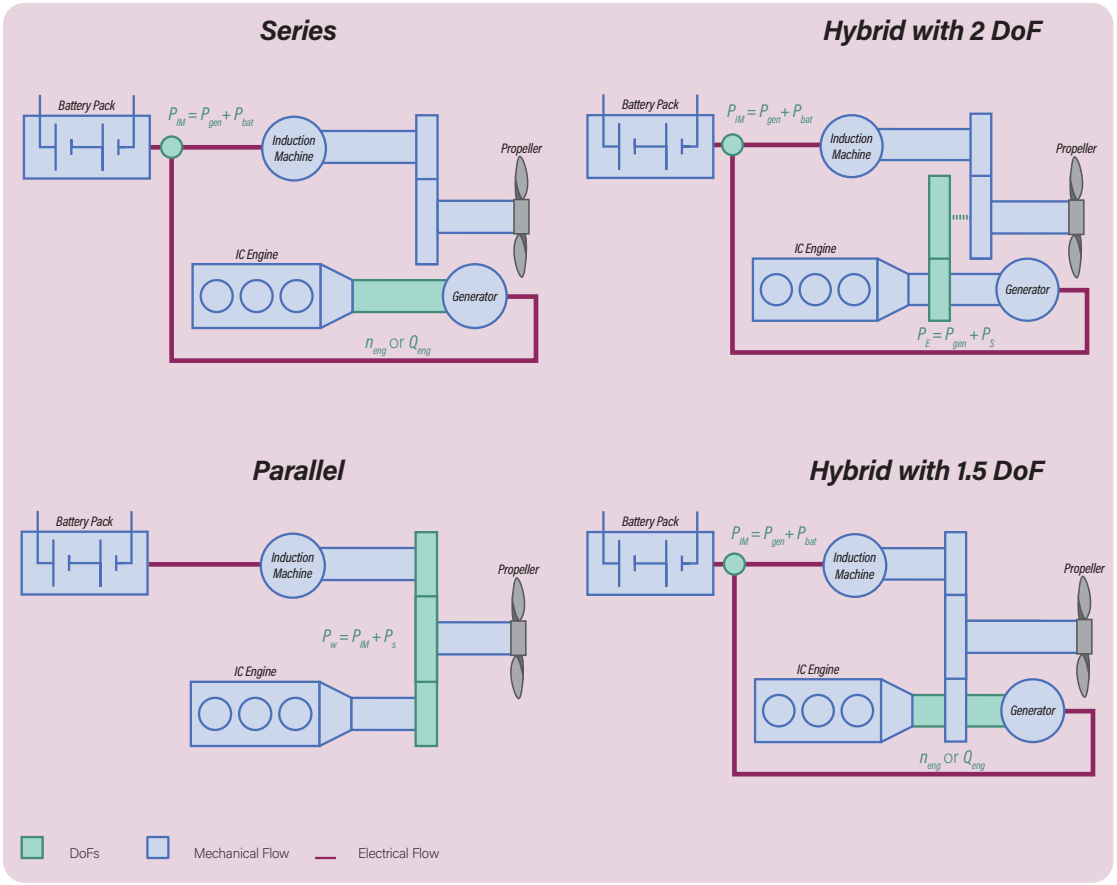


Figure 3.1: Different powertrain architectures, adapted from [32] and [93]

The different architectures are shown in Fig. 3.1, where the DoFs in the powertrains are indicated with green: series and hybrid architectures have an electrical node where 3 electric power flows meet (battery, generator, IM), while mechanical nodes where 3 mechanical flows meet are found in the hybrid configuration with 2 DoFs (propeller, IC, generator) and the parallel (IM, propeller, IC). Half DoFs, where either the shaft speed or torque can be chosen arbitrarily, are indicated with the green shafts, found in the series and the hybrid with 1.5 DoFs configurations.

A scenario showcasing the difference in the two hybrid configurations is when the IM is not rotating and the power for the wheel is provided entirely by the IC engine (2 DoFs). If the IM, the generator, and the IC engine are coupled mechanically and are unable to clutch-out (1.5 DoF scenario), that would not be possible.

In [2] it is observed that the above classification has no application for naval powertrains due to their additional complexity, with multiple power generation (i.e. IC engines, gas turbines, fuel cells), power conversion (i.e. motor/generators), and energy storage (i.e. batteries, ultracapacitors) units commonly found onboard. Although the suggested classification based on the propulsion and

the power supply is very useful and explained in detail in Section 3.2 of this chapter, the previously analysed classification [2] offers a helpful approach for identifying the DoFs in powertrains, however complex they might be, and subsequently assisting in formulating the mathematical representation of the system. The DoFs in a powertrain yield the number of control variables needed in the system, and, thus, play a key role in the supervisory controller design procedure.

DoF also correspond to nodes of the power flow in the powertrain [32]. One DoF in the powertrain can be expressed as:

$$P_K(t) = P_A(t) + P_B(t) \tag{3.1}$$

which simply expresses that either the power flow A $P_A$ or power flow B $P_B$ can be chosen arbitrarily, as long as they add up to the power flow K $P_K$ for every time instance $t$. These quantities are algebraic and can also take negative values, switching the direction of the power flow.

In the case of half a DoF, the torque $Q$ or shaft speed $n$ can be chosen arbitrarily to yield the required power flow $P_K$ [32], carried by a shaft:

$$P_K(t) = n(t) \times Q(t) \tag{3.2}$$

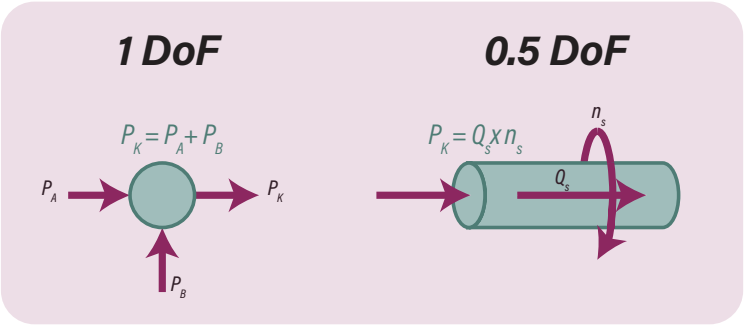


Figure 3.2: Half and whole nodes in powertrain architectures [32]

## 3.2 Hybridisation on Vessels: Hybrid Propulsion and Hybrid Power Supply

In a recent literature study [2], ship powertrains have been classified according to their power supply and propulsion and comparisons between the different groups have been made in terms of relative performance and applications. Such an approach allows for clustering together the complex ship architectures, something that cannot be done with the automotive classification analysed in the

[2] This classification is predominantly used in the automotive industry [32]

previous section (series, parallel, series-parallel). Following this paradigm, as it has been explained before in Section 1.2, a hybrid vessel can either refer to hybrid propulsion, hybrid power supply, or both, and this section presents the layout, key advantages and disadvantages, and the application of such different powertrain architecture configurations. From this chapter any propulsion train can be classified and consequently its advantages and challenges can be identified systematically. This chapter is based on the literature study [2] and the reader is referred to that study for further information.

### 3.2.1 Propulsion

Propulsive powertrains are in turn classified into electric, mechanical, and hybrid. Each architecture yields best results for different operating profiles, both in terms of propulsive and hotel power demand.

#### Mechanical

In conventional mechanical propulsion, the propeller shaft is mechanically coupled with a prime mover, either directly or with the use of a gearbox. The few power conversions in a strictly mechanical powertrain correspond to a high efficiency, especially if the operating profile is uniform and close to the optimal operating point of the prime mover. The hotel load must be covered by a number of auxiliary generator sets, exhaust gas heat recovery systems, etc.

A series of disadvantages regarding mechanical propulsion have been aggregated in [2]. A load of less than 50% of the MCR of an IC prime mover dramatically decreases its efficiency, and subsequently the efficiency of the whole propulsion plant. Furthermore, the dynamic behaviour of IC engines at low load or high transient loads is poor due to its limited steady-state envelope, but also due to dynamic effects such as those induced by the turbocharger, providing bad manoeuvrability and making it unsuitable for implementations on ships with very diverse operating profiles (e.g. tugboats).

#### Electric

In electric propulsion powertrains, the motor is connected to the electric bus and is coupled with the propeller shaft to provide the thrust. This introduces high conversion losses especially if the electricity is provided by a generator set and not by e.g. batteries or fuel cells, which involves converting from mechanical to electrical power and back. Other problems are the inability to change the generator speed and stability issues in AC distribution systems with no variable frequency [2]. However, such electric propulsion architectures provide key advantages [3]:

[3] first two of which where identified in [2]

- If the hotel loads are a significant portion of the power demand and the overall operating profile is diverse, due to their versatility in covering both propulsive and hotel loads, electric powertrains are more efficient via appropriate use of a power management strategy which makes best use of the engines. For example, this way, instead of two engines running at a low-efficiency part-load point, one can be switched off and one can run at optimal load to attain overall efficiency gains.

- The $NOx$ emissions, which are low at high-speed engines due to the lower residence time [94], may be reduced due to the high-speed engines in generator sets, compared to $NOx$ emissions in medium-speed four-stroke or two-stroke engines used in mechanical propulsion. An indicative comparison that accounts for the specific fuel consumption difference [4] has been done in [2], yielding a 33% and 8% emission reduction in high speed engines compared to their two-stroke and medium-speed four-stroke counterpart. On the same study it is noted that the higher speed is not just the only reason for lower $NOx$ emissions, but also the better allocation of power generation to the engines allows for their operation to be close to the design speed.

- the readiness of such architecture to utilise other types of power supply, such as electrochemical (e.g. fuel cells), or supply from electric storage systems (i.e. batteries and ultra-capacitors), although a rectifier is needed.

Other advantages are the easier and modular maintenance that does not require halting operation, the absence of a gearbox and the corresponding noise emissions [5] [2] and space requirements.

Taking the above into consideration, electrical propulsion is found on cruise ships, a number of different naval vessel types including capital ships and submarines, icebreakers or vessels with Azipod systems [27] and others.

## Hybrid

To achieve the best of both worlds, hybrid propulsion combines electrical and mechanical propulsion by using a mechanical coupling between the shaft of the motor and the shaft of the prime mover. This combines the high efficiency of the mechanical powertrain at design speed with the high efficiency and manoeuvrability of the motor at low loads. An extra functionality arises with the possibility of using the motor as a shaft generator through a PTO gearbox [2, 95], contributing in that way to the electric power production of the auxiliary gensets to ultimately cover hotel loads. In the case of gas turbines, where the efficiency of part load is particularly low, shown in [29], and where

[4] which means that the $NOx$ generated are compared on a g/kWh basis

[5] although the FPP commonly used with electric propulsion produce more noise via cavitation and in general noise emission studies are scarce

most applications concern naval vessels (e.g. destroyers) with a significant operating time in part load, hybrid propulsion is especially efficient, while in the same study, the PTO functionality yields 85% more fuel savings than a purely motoring functionality. Utilising the electric machine can also bring considerable reductions in $NOx$ emissions of the prime mover, with the $\lambda$-maintaining strategy introduced in [11], being capable of achieving a 16% $NOx$ reduction during manoeuvring. An extensive review of the hybrid applications can be found in [2]. Briefly summarising the advantages of hybrid propulsion:

- It reduces fuel consumption if low-load operation ($< 15\%$ of MCR) is a big part (in terms of time spent in such operation) of the operating profile [2], while a close to design point operation is also important to justify a non-fully-electric propulsion solution.
- Since in the case of mechanical propulsion, auxiliary engines are already installed as they are also needed to cover the hotel loads, regarding the hardware, the additional costs of hybridising the propulsion are limited to a motor/generator unit and the mechanical coupling unit (i.e. gearbox). [6]
- $NOx$ savings, covering loads by functioning as a PTO, and improved availability are additional advantages of hybrid propulsion.

Similar to its automotive counterpart, hybrid propulsion introduces an additional DoF at the mechanical node where the electric machine and prime mover shafts meet. Depending on the implementation, if the mechanical coupling allows for clutching off and changing of ratios through a gearbox, it corresponds to a whole DoF, while a fixed mechanical coupling corresponds to half a DoF. After presenting the different propulsion architectures, similarities between the electric and series, and hybrid and series-parallel topologies can be noted, which were presented in the previous section.

### 3.2.2 Power supply

The notion of power supply, although it might appear specific at first, is not a clear one. A unit that converts energy from one form to another is typically considered to supply power to cover the propulsive and hotel loads of the powertrain. However this conversion should be from an energy resource. Gas heat recovery heat exchangers and electric motors are not considered to be power supply units, in the sense that they do not change the form of the energy or, if they do (electric motors), they are not converting any resource. On the contrary, a steam turbine of a gas heat recovery system can be thought of as a power supply, however not a primary one.

[6] However, a complex automation system is also needed, which might correspond to higher costs.

### Classification and Clarifications

To approach such a notion more systematically, HFO fuel in a fuel tank, hydrogen stored in a metal hydride cylinder, and wind power can all be described as primary resources, in the sense that they are inputs to the ship as a system. In this example, the first two resources can be depleted and the ship has to refill her bunkers, while in the case of wind power, a ship as a system cannot provide any wind, only tap into its energy by means of conventional or rotor sails. Furthermore, if energy is being rejected by the ship, recovery of such energy should be also a resource, but secondary, because it can only be equal to a portion of the primary resources, from where it originates. That is, the secondary resources produce energy from within the ship system.

Following the paradigm of the microgrid analysis in Section 2.2, these resources can be further divided into controllable (fuel and hydrogen) or non-controllable (wind). Secondary resources can also be controllable (Exhaust Gas Heat Recovery Systems - EGHRSs) or non-controllable (Energy Saving Devices ESDs).

A unit that converts resources into other forms of energy is a power supply. Examples are IC engines, converting chemical energy into mechanical energy, and fuel cells, converting chemical energy into electric energy. Moreover and continuing to follow the microgrid theory, apart from generator power supply units, there are also storage power supply units, such as batteries, flywheels and ultra-capacitors. They are, essentially, reversible resources. To examine the robustness of these definitions, batteries are in fact classified under power storage only due to their recharging functionality. If it was not for this function, a battery would have been a power generation unit. In fact, strictly speaking, in a plug-in functionality where the end charge of a battery is lower than the beginning (charge depletion) the battery has to function as a power generating unit for the total amount energy that is being depleted, as this energy is provided by shore charging and not within the boundaries of the ship as a system.

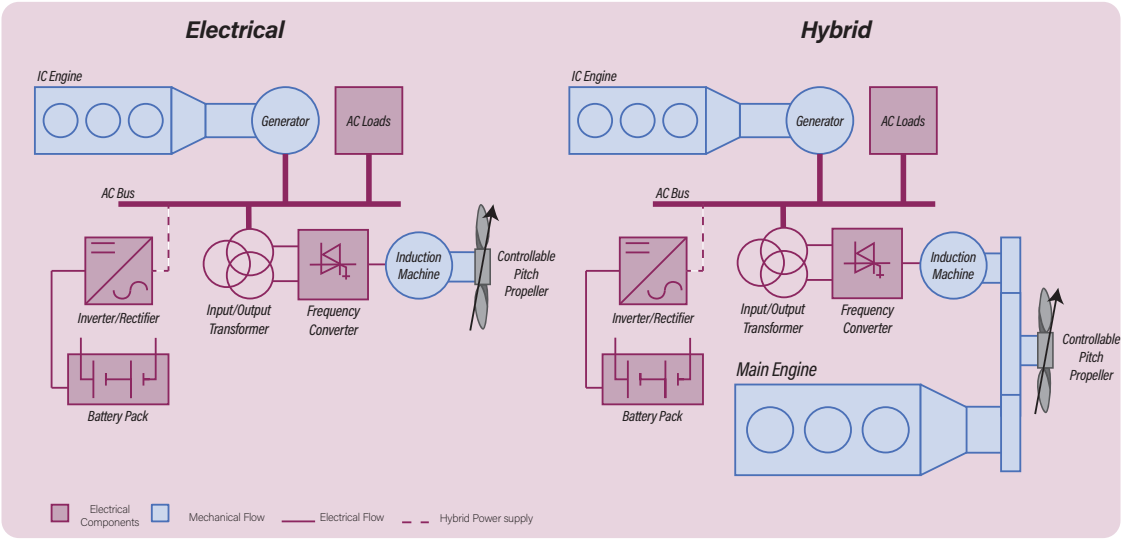


Figure 3.3: Electric and Hybrid Propulsion. With the dotted line the power train turns into a Hybrid Power Supply configuration. Adapted from [2]

## Advantages of Hybrid Power Supply

After the above classification, the most common power supply configurations found on ships are discussed: conventional, electrochemical supply, and hybrid with energy storage. Conventional power supply is delivered by IC engines or gas turbines converting fuel energy into mechanical energy. In the case of prime movers, that mechanical energy is transferred through a shaft and an optional gearbox to the propeller shaft, while in the case of auxiliary engines, it is converted via a generator to electrical energy and fed to the distribution network.

Electrochemical power supply is attained by using fuel cells, however such a discussion is not in the scope of this study and for more information the reader is referred to [2, 96]. Moreover, when the charge of the batteries is depleting during the mission it should be regarded as electrochemical power supply [7], Batteries in a charge sustaining configuration, and by considering the entire mission, do not provide power supply but act as energy storage. Thus, regarding batteries with a charge-sustaining functionality as power supply would be equally incorrect as regarding a flywheel or any other energy storage system as power supply. With that being said, in many cases and in literature, that nuance might be overlooked and battery power supply may be regarded as power supply, even in a charge-sustaining configuration.

Although full battery operation has only been implemented on the 1MWh battery ferry Ampere [97], which operates on a 5.7km route in Norway and gets recharged over 10 minutes from ashore, other such implementations are not found [2]. Battery packs, consisting of multiple cells are used

[7] (see also Section 3.3)

in combination with other power energy supply units, such as IC engines, in electric and hybrid propulsion powertrains. Other less common and more niche energy storage units are the ultra-capacitors, which allow for high power output in a short discharge, a functionality needed on board military vessels for weapons.

The most important advantages of using batteries in a hybrid power supply configuration, either in electric or hybrid propulsion architectures are once again identified in [2, 7, 12]:

- Energy storage can feed the powertrain or can be charged up to allow for the gensets to run at optimal load, thus reducing, amongst others, their fuel consumption, emissions, and wear. This allows for optimal energy management in covering both propulsive and auxiliary loads.
- Load levelling of the engines [7], [12] [6] can be a solution to power demand fluctuation during certain operating conditions, resulting in fuel consumption reduction and lower maintenance costs. This can be attained with a charge-sustaining configuration, by utilising the batteries to keep the propulsion plant efficiency higher.
- Utilisation of shore energy is possible on a charge-depleting powertrain, where the end charge of battery (when the mission is over) is lower than the charge at the start.
- The power reserve is bigger due to the power output of the batteries

## 3.3 Hybrid Electric Vessels with Energy Storage: Charge Sustaining and Charge Depleting Vessels

Similar to the Hybrid Electric and Plug-in Hybrid Electric Vehicles (HEVs and PHEVs) in the automotive industry, ships may also be divided into Charge Sustaining and Charge Depleting Vessels, based on whether or not the State of Charge (SoC) of the battery at the end of the mission is the same as in the beginning, or it is being depleted and recharged between missions from ashore. In [1], a comparison between a rule-based controller (RB) that keeps the SoC constant, and an optimal Dynamic Programming (DP) controller, which enforces minimum SoC at the end of the mission, yields an average reduction of 8.6% in fuel consumption, from a plethora of tugboat missions. Furthermore, the same study concludes that this reduction is primarily due to the utilisation of the battery packs, while the RB controller and DP controller have only 1% difference if the SoC of the optimal controller is set to constant. This may be attributed to the restriction of a constant SoC at 100%. If both the RB and DP were deployed in a tugboat operating in e.g. 70% SoC, which is common for HEV automotive applications [49], allowing for both charging and discharging of the batteries, the optimal controller might have performed better. Furthermore, in the same study it is stated that the regenerative pathways on ships are limited, and since similar studies [34] have also

shown fuel consumption reduction when comparing depleting SoC to sustaining SoC, it is evident that charge depletion is an important mechanism for fuel savings on hybrid ships.

Before explaining the two approaches in more depth (Charge Sustaining and Charge Depleting), a preliminary formulation of the optimal control problem is needed.

The powertrain can be formulated as a system where, if its state vector is $\mathbf{x}$, its control input vector $\mathbf{u}$, the output vector $\mathbf{y}$, and its disturbance is $\mathbf{r}$, can be expressed as [65]:

$$\dot{\mathbf{x}} = f(\mathbf{x}, \mathbf{u}, \mathbf{r}) \tag{3.3a}$$

$$\mathbf{y} = h(\mathbf{y}, \mathbf{u}, \mathbf{r}) \tag{3.3b}$$

Formulating the cost functional $J$ of the fuel consumption minimisation control problem yields [3, 98]:

$$J(\mathbf{u}(t)) = \phi(\mathbf{x}(t_f)) + \int_{t_0}^{t_f} \sum_i \dot{m}_{f,i}(\mathbf{u}(t), \mathbf{x}(t), t) + G(\mathbf{u}(t), \mathbf{x}(t), t) \quad dt \tag{3.4}$$

where $\dot{m}_{f,i}$ the fuel consumption of the $i$-th engine, as a function of the control input vector $\mathbf{u}$, state variable vector $\mathbf{x}$, and time $t$, $G$ an additional function typically implemented to prevent *chattering* issues [3, 65], meaning turning the engines on/off very frequently. Moreover $t_0$ and $t_f$ are the initial and final time instants, correspondingly, and $\phi$ is a function weighing in the final constraint to the state vector $\mathbf{x}$.

The optimal control problem can now be expressed as [98]:

$$arg\min_{\mathbf{u}(t)}(J(\mathbf{u}(t)) \tag{3.5a}$$

subject to

$$\dot{\mathbf{x}}(t) = f(\mathbf{x}(t), \mathbf{u}(t), \mathbf{r}(t), t) \tag{3.5b}$$

$$\mathbf{x}(t_0) = \mathbf{x}_0 \tag{3.5c}$$

$$\mathbf{x} \in \mathcal{X}(t) \subset \mathbb{R}^m \tag{3.5d}$$

$$\mathbf{u} \in \mathcal{U}(t) \subset \mathbb{R}^n \tag{3.5e}$$

$$\mathbf{x}(t_f) \in [\mathbf{x}_{min,f}, \mathbf{x}_{max,f}] \tag{3.5f}$$

where $\mathcal{X}$ and $\mathcal{U}$ are the subsets of allowable values for the states $\mathbf{x}$ and control input variables $\mathbf{u}$, of dimension $m$ and $n$, correspondingly. In Eq. 3.5f an explicit constraint on the final state is being imposed.

### 3.3.1 Charge Sustaining Control

Following the above formulations, a CD controller imposes either as a *soft* or a *strong* constraint the final state of charge, $SoC(t_f)$, to be equal to the initial state of charge, $SoC(t_0)$. This $SoC$ is one element of the state variable vector of the problem, $SoC = x_1$, with other state variables typically being the number of running engines $NoE$ [65], needed in the formulations in order to penalise the switching on/off of the engines, and to prevent chattering, as explained previously. So a typical state vector would be:

$$\mathbf{x} = \begin{bmatrix} x_1 \\ x_2 \end{bmatrix} = \begin{bmatrix} SoC \\ NoE \end{bmatrix} \tag{3.6}$$

A soft constraint is imposed by the first term in Eq.3.4, taxing the state when it gets out of bounds by introducing additional cost to the cost function. On the other hand, a hard constraint is imposed by using the explicit constraint in Eq. 3.5f.

During CD control, the vessel is never charged and the $SoC$ is kept within a window via the constraint in Eq. 3.5d, which limits its allowed values to ensure the high efficiency and life expectancy of the batteries [3]. Together with the final soft and/or hard constraints the $SoC$ is maintained. Subsequently, in CD control, the vessel is using only its fuel as its primary energy resource, and any charge in its batteries is from that fuel energy.

### 3.3.2 Charge Depleting control

In the case of CD (or PHEV in automotive), the end state constraint (soft or hard) is imposed to be equal to the bettery's depletion state, that is $SoC_{min,f} = SoC_{depl}$. It must be noted that, in the case of CD control, a modification to Eq. 3.4 must be made in order to account for the production of the electric energy used to charge the batteries. This was not necessary before (in CS) because all of the energy was coming from the fuel tank anyway, and there was no charging from outside of the system taking place (i.e. from ashore), an energy that now has to be compared in terms of production costs with burning fuel on board. The implementation in [40] accounts for this factor by including an extra term:

$$J(\mathbf{u}(t)) = \phi'(\mathbf{x}(t_f)) + \int_{t_0}^{t_f} \sum_i P_{DE,i}(\mathbf{u}(t), \mathbf{x}(t), t) + G'(\mathbf{u}(t), \mathbf{x}(t), t) + \alpha P_b \quad dt \tag{3.7}$$

where $\dot{m}_{f,i}$ has been replaced by $P_{DE,i}$ (a simple conversion that just requires multiplying with the engines' SFOC), $P_b$ is the power of the battery and $\alpha$ is a factor taking into account the cost of using the energy from recharging compared to the energy from the fuel. This value can be chosen according to environmental or financial criteria, e.g. by correlating the CO2 emissions, emitted by the supplier of the power required, for a given amount of charge of the battery with the corresponding

C02 emissions to produce the same energy from the IC engine. The correlation must be done taking into account all the conversion efficiencies until the point in the powertrain when that energy is available.

As already discussed in Section 2.1.2, in [40] the recharging-to-fuel correlating factor $\alpha$ is shown to have a critical value $\alpha_c$ above which, for a given mission and battery capacity, the optimal control no longer chooses to deplete the battery, even if the mission's length allows for depletion, as shown in Fig. 3.4. More formally, the choice of the controller to not fully deplete the batteries means that the end state explicit constraint (Eq. 3.5f) is no longer affecting the solution and is not active. On the other hand, values of $\alpha$ below this critical value, all result in the controller choosing to deplete the batteries, thus acting the same, independently of the $\alpha$ value.

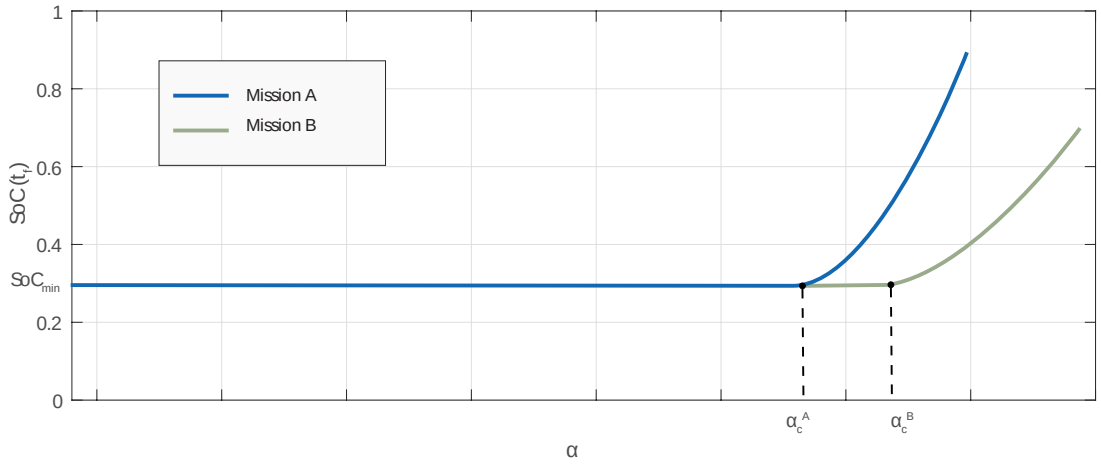


Figure 3.4: End state of charge $SoC(t_f)$ plotted against correlating factor $\alpha$. Critical value $\alpha_c$ above which the battery is not depleted ($SoC(t_f) > SoC_{min}$) is shown, for different missions A and B (in mission B battery usage is more efficient compared to A due to e.g. harsher off-design load on the engine). Adapted from [40]

## Battery Sizing

In the same study, another important point regarding CD control and battery sizing has been shown at a given mission and by varying $\alpha$ and battery size (Fig. 3.5). Starting from the infinite battery capacity case, by varying $\alpha$ and plotting it against the total energy used in the given mission, the optimal controller yields a characteristic line, which for low correlating factor values, $\alpha < \alpha_{saturation}$, corresponds to complete electric power supply (Battery Electric Vehicle - BEV mode, saturation zone), and for values above $\alpha_c$ the optimal control starts to opt for less battery power (which for the infinite capacity case is abundant). Then by lowering the battery capacity new characteristics can be obtained as a function of $\alpha$. The diminishing battery efficiency at lower states of charge of the battery influences $\alpha_C$ and, subsequently, the amount of total battery energy used

by the controller.

For example, if the capacity of the battery pack is $Q_a$, the part where its characteristic line coincides with the characteristic line of the infinite battery , which is also the point of $\alpha_c$, would determine the region where the battery will get depleted and the end constraint will be activated (below the line), and the region where the end constraint is not activated and a global optimum is achieved (above). This is important because a global optimum will yield the best solution, so the battery size correlated to that is found via this procedure. Any capacity $Q < Q_a$ will get depleted and any capacity $Q > Q_a$ will not. However, bigger capacities do affect the efficiency and, subsequently $\alpha_c$. Furthermore, the capacity at which there is almost no difference with the infinite capacity can be found, by looking at what capacity there is no separation in the characteristics. It is also noted that for finite battery capacities, the part before their characteristic meets the infinite characteristic would have been flat, if it has not been for the battery efficiency deterioration at lower charge states.

Such graphs can be useful during the design phase in order do decide on the best battery capacity for a given application [40].

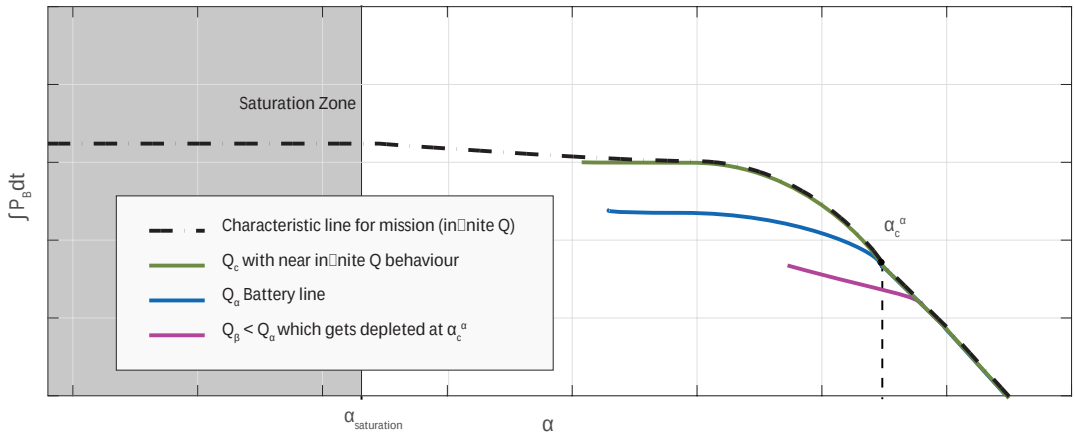


Figure 3.5: Correlating factor $\alpha$ plotted against total battery power used $\int P_B dt$ at a given mission. Different battery capacities yield different characteristic lines. Adapted from [40]

## Charge Depleting - Charge Sustaining and Blended Mode

A classification of CD control is based on the way the batteries are discharged when the total mission of the vessel is bigger than the battery, when it cannot be covered entirely by the battery energy installed on board.

Following the discussion in Section 2.1.2, there are two approaches to controlling the discharge of the battery, the *charge depleting - charge sustaining* (CD-CS) or *electric-vehicle-centric* mode

and the **blended** mode (BM). In [63], it is explained that the CD-CS approach uses just battery energy, while it uses the engines, only if the power demand exceeds the battery power supply capabilities. When the battery gets depleted the vehicle uses only the IC engines and the battery charge is sustained at the lowest level. On the other hand, in blended mode the battery discharge is distributed in a wider time interval in an attempt to use the battery when it is the most efficient. DP solutions with perfect information are capable of providing optimal blended discharge trajectories. On the other hand, CD-CS trajectories are sub-optimal when the mission is longer than the radius of the battery mode.

In [44], regarding automotive parallel PHEVs, it is found that the savings of BM over a CD-CS mode are $1-4\%$, even if the information on the trip (length and profile) is limited, with the best results given in the case of no or moderate underestimations of the trip length, and for trips 75% longer (in terms of distance) than the range of the battery mode. However, even slight overestimation of the trip length can lead to the CD-CS strategy performing better than the BM, while the driving profile specifics seem to also affect considerably the BM performance (e.g. in the overestimation case, the CD-CS performs $4-8\%$ better). The study in [63] also notes that an optimal BM discharge at a given trip length is not optimal for other lengths. DP is used in both studies to yield the optimal blended discharge.

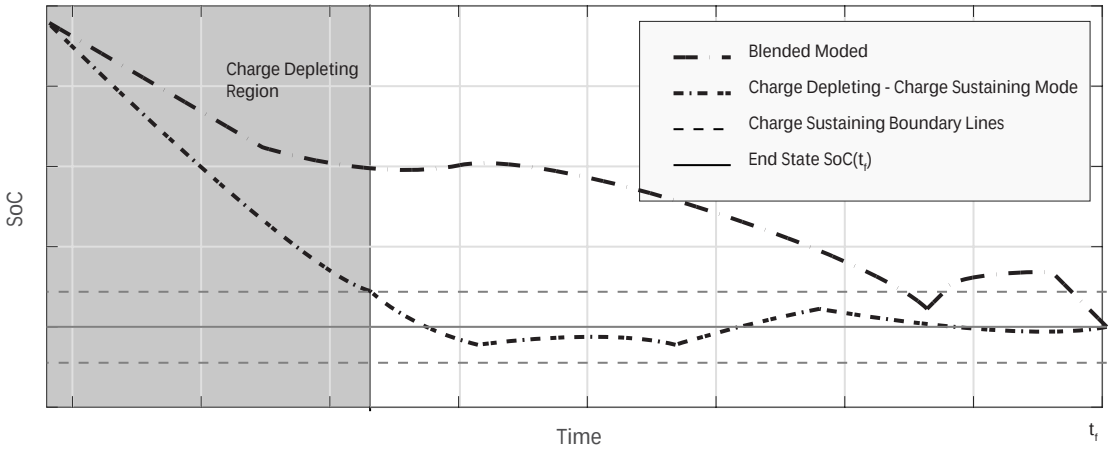


Figure 3.6: Charge depletion: Blended Mode and CD-CS. Adapted from [44]

# Chapter 4

# Energy Management Control on Ships: Model Formulation and Optimal Control Problem

In Sec. 2.3 it is stated that, at least for the scope of the present study, Energy Management Control Strategies (EMSs) are differentiated from the Power Management Control Strategies (PMSs), primarily on the basis of the time scale these two control levels are acting on, with the latter deciding over power demand and transient behavior control setpoints. Furthermore, in the case of batteries, this distinction is also consistent with the electric ESS recommended practice booklet from DNV GL [99], where the high-level control, or Energy Management System [1], which determines when and how fast the battery module is charged or discharged, depending on the functionality of the system, is differentiated from the low-level Battery Management, which is responsible for keeping the batteries within the operating limits (in terms of e.g. temperature, current) and which directly affects the power flow.

In further detail, and now regarding the propulsive plant as a whole, in [2] PMS is explained as the control module performing secondary control, in the sense of:

- keeping the voltage and frequency stable in transient conditions
- providing automatic switching off/on of the gensets to protect them from overloading
- protective control to prevent black-outs

[1] not to be confused with Energy Management Strategy - EMS; an EM system typically has an Energy Management Strategy together with some other functions (e.g. manoeuvring and emergency modes). This is also found as tertiary control in [2], however, the terminology should be used with caution as it is not consistent in literature, especially across different sectors (maritime, microgrid, automotive)

It can be easily inferred that PMSs are implemented regardless of the existence of hybrid power supply on the vessel. In fact, a number of decisions regarding the number of online gensets and their loads have to be made.

When a hybrid power supply is present, however, the need for an additional level of control arises, aiming to strategise on how to utilise the available energy sources over a long-term time scale. The EMSs or supervisory controllers decide on the setpoints of the components in the powertrain, optimising for the main objective of energy consumption minimisation, subject to various constraints, while still meeting the power demand of the operator [100]. Unlike automotive applications where the power output is managed by the control strategies and a correlation between the accelerator pedal and a torque demand is made, on ships most commonly the captain requests a certain shaft speed [1], which for a given seastate and pitch of the propeller (simplified case, other parameters also play a role) corresponds to a power demand. The powertrain on a ship with hybrid power-supply typically includes:

- a battery pack and a number of generator sets which provide the electric power demand for the electric motor and the hotel demand
- a prime mover (main engine) for each powertrain

Another point is that the number of online generator sets can vary in order to optimally allocate the load amongst them and have them operate at optimal, in terms of fuel consumption, setpoints. This supervisory control level may exist regardless of the existence of hybrid power supply.

## 4.1 Model Formulation

In this section a general quasi-static formulation of a ship's hybrid-power-supply hybrid-propulsion powertrain is given. Quasi-static models are sufficient to be used for fuel consumption minimisation supervisory control, as dynamic models add unnecessary computational load, while contribute very little in the minimisation of a cumulative quantity [1]. Simpler topologies can be derived from this formulation by eliminating terms. The formulations below follow the powertrain from the propeller to the power resource and are based on [8]. Simplifications have been made in the formulations, while also caring to not oversimplify and keep the required level of accuracy of the representation of conversion losses and component efficiencies, necessary for the generation of accurate optimal control output for fuel consumption minimisation [3]. This study does not focus on the performance of the model, as most of the formulations have been verified and validated in [1, 101]. However few improvements have been made, namely in the genset power allocation, by providing a way of penalising the frequent on/off switching with minimal computational load, and the battery SoC estimation, by using the electrochemical efficiency instead of the Ragone efficiency [1]. Finally, effort has been

made to keep the formulations below generic enough to be readily applied in a variety of propulsive powertrains.

### 4.1.1 Propeller

In the general case, the propulsive demand is divided between $k_p$ Controllable Pitch Propellers. The case of e.g. one fixed propeller is a sub-case of that general case for $k_p = 1$ and a set pitch $P/D = \varepsilon$ (common for all propellers). Assuming that the propeller law stands, if $v_s$ is the ship speed, $n_p$ the shaft speed, and $C_3$ a function of the pitch, then:

$$n_p = C_3(P/D) \cdot v_s \tag{4.1}$$

and ship resistance is given by

$$R = C_1(v_s) \cdot v_s^2 \tag{4.2}$$

where the effect of the ship speed on the coefficient $C_1$, in the sense that at higher speeds the resistance grows faster with the speed due to Froude effects, is explained in [8].

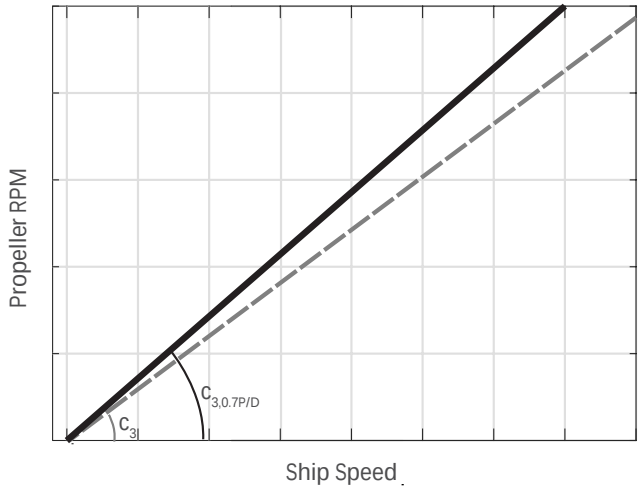


Figure 4.1: Qualitative effect of a pitch reduction (e.g. from 100% to 70%) on the propeller law relationship, shown with the change in the slope, $C_3$. Adapted from [8]

The ship curve is constant for a constant number of propellers online and given by:

$$K_T = C_7 \cdot J^2 \tag{4.3}$$

where $K_T$ the thrust coefficient, $C_7$ constant and $J$ the advance ratio. Now, on the Open Water Diagram (OWD), where the ship curve meets the propeller's thrust coefficient curve, the operational point is defined. Then from the torque coefficient curve, $K_Q$ and, subsequently, the propeller power

demand $P_{P,load}$ can be found, as a function of shaft speed:

$$P_{P,load} = \frac{2\pi\rho D^5}{\eta_R} K_Q \cdot n_p^3 = C_4 \cdot n_p^3 \tag{4.4}$$

More specifically, in Fig. 4.2 it is shown that the effect of the non-cubic Froude effects and the corresponding increase of $C_1$, changes $C_7$ through the equation:

$$C_7 = \frac{1}{\rho D^2} \cdot \frac{C_1}{k_p \cdot (1-t) \cdot (1-w)^2} \tag{4.5}$$

where, $D$ the propeller diameter, $\rho$ the water density, $t$ the thrust deduction factor, and $w$ the wake factor. This moves the ship curve upwards (bottom figure, black curve), in a similar fashion that added resistance would. The effect of a change in propeller pitch is also shown (top figure).

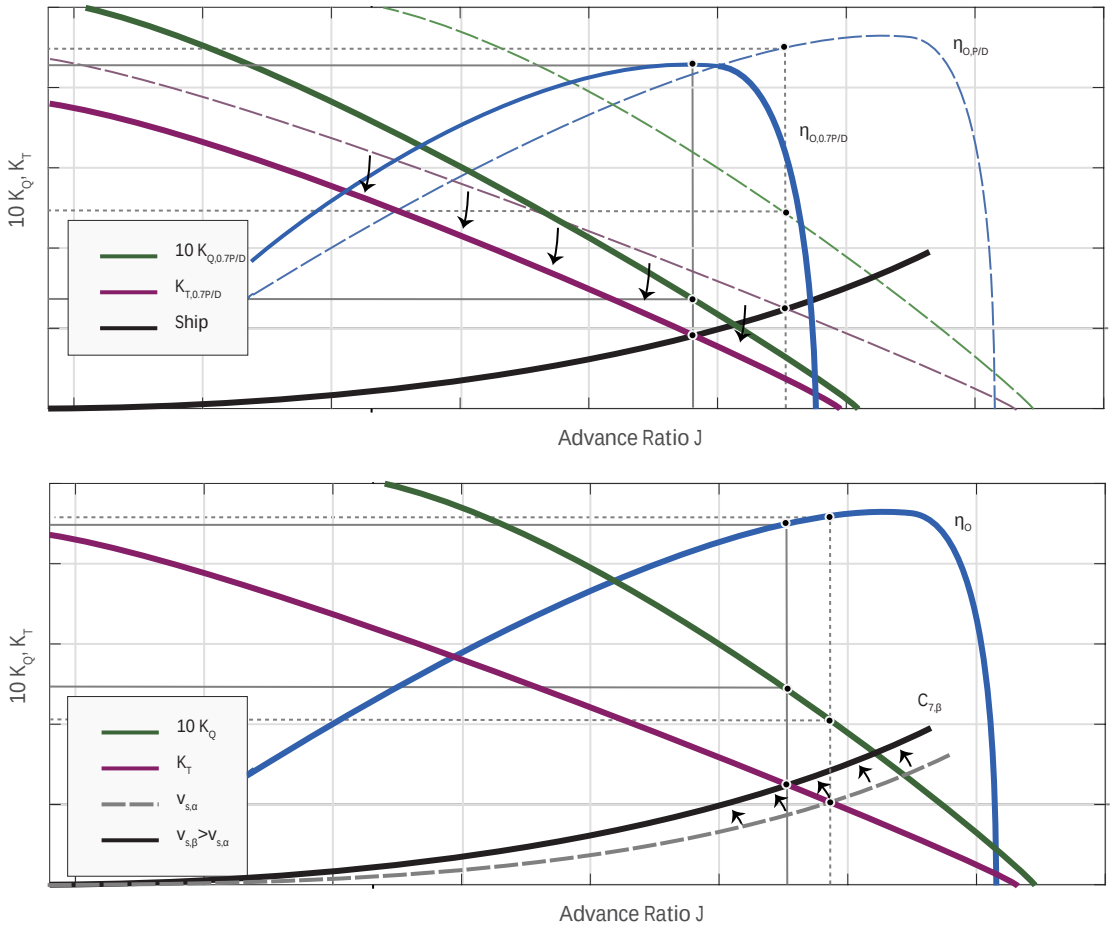


Figure 4.2: Off-design conditions: Effect of a decrease in propeller pitch (top) and an increase in ship speed (bottom), plotted on the Open Water Diagram. Adapted from [8]

If there is a possibility for switching off $m$ number of propellers (trailing propellers), the number of the propellers would change $k_p' = k_p - m$ and the resistance would increase due to the rudder and

the trailing propeller effect $C_1' = \alpha C_1, \alpha > 1$. The new ship curve would have the new coefficient $C_7$, given by:

$$C_7' = \frac{k_p}{k_p - m} \cdot \alpha \cdot C_7 \tag{4.6}$$

From which a new $K_Q'$ can be found at the OWD, leading to a corresponding propeller demand relationship, just by substituting $K_Q'$ in Eq.(4.4) and subsequently a new $C_4'$. Other sailing *off-design* conditions might include

- If the $P/D$ changes, the propeller law coefficient changes to $C_3'$ but the ship curve on the OWD is the same, allowing to find a new $K_Q'$ and, thus, a new $C_4'$
- If the resistance changes (due to sea state, hull fouling, displacement change, shallow waters, etc.), the case described for the trailing shaft can be used (Eq. (4.6), without the $\frac{k_p}{k_p - 1}$ factor)
- If additional thrust has to be exerted as an external load that is constant and not a function of the ship speed (as part of e.g. tugging a static load) it can be added with an extra term $T_{ext}$ in $R = C1 \cdot v_s^2 + T_{ext}$, resulting in the following expression for the ship curve:

  $$K_T = C_7' J^2 + \frac{T_{ext}}{\rho n^2 D^4 k_p (1-t)(1-w)^2} \tag{4.7}$$

  From then on, the procedure to find the $C_4'$ is the same as the other cases.
- a change in speed will also change the resistance, and if the speed change is substantial, $C_1$ in Eq. (4.2) will also change and alter the ship curve, falling under the resistance change case

From the above, a vector of different coefficients $\boldsymbol{C}_4 = [C_4\ C_4'\ C_4''\ ...\ C_4^{[N]}]^T$ can be devised, for $N$ different sailing conditions, in order to provide a piecewise propeller demand equation for any sailing condition, (as a single case or a combination of cases from the above options):

$$\boldsymbol{P}_{P,load} = \boldsymbol{C}_4 \cdot n_p^3 \tag{4.8}$$

or by use of Eq.(4.1) and taking into account an appropriate vector $\boldsymbol{C}_3 = [C_3\ C_3'\ C_3''\ ...\ C_3^{[N]}]^T$ for the different sailing conditions:

$$\boldsymbol{P}_{P,load} = \boldsymbol{C*}_4 \cdot v_s^3 \tag{4.9}$$

where $\boldsymbol{C*}_4 = [C*_4\ \ C*_4'\ \ C*_4''\ \ ...\ C*_4^{[N]}]^T = \boldsymbol{C}_3 \odot \boldsymbol{C}_4$ (element-wise or Hadamard product). The corresponding $i-$th element of vector $\boldsymbol{P}_{P,load}$ can be chosen for the sailing condition $i$.

Alternatively, the propulsive demand can be given together with the shaft speed, as disturbances to the ship model.

### 4.1.2 Transmission

Transmission losses involve the losses at the shaft, the losses at the gearbox, and the electric machine (power take-off - PTO, or take-in - PTI).

Commonly, shaft losses are given by empirical models, as a function of torque $M_s$ and revolution speed $n_s$:

$$M_{loss,shaft} = f(M_s, n_s) \tag{4.10}$$

Assuming that no speed loss is present from the propeller to the shaft, $n_s = n_p$, while $M_s = M_p - M_{loss,s}, M_{loss,s} < 0$ and $M_p = \frac{P_p}{2\pi n_p}$, the following expression can be acquired:

$$M_{loss,s} = f\left(\frac{P_p}{2\pi n_p} - M_{loss,s}, n_p\right) \tag{4.11}$$

or, if the loss formula allows solving for $M_{loss,s}$:

$$M_{loss,s} = g_s(P_p, n_p) \tag{4.12}$$

In terms of efficiency:

$$\begin{aligned} \eta_s &= \frac{P_p}{P_s} \\ &= \frac{P_p}{P_p - M_{loss,s} 2\pi n_p} \end{aligned} \tag{4.13}$$

or by using Eq. (4.12)

$$\eta_s = \frac{P_p}{P_p - g_s(P_p, n_p) 2\pi n_p} = h_s(P_p, n_p) \tag{4.14}$$

Gearbox losses can be calculated similarly with the empirical model found in [1,102], which uses a quadratic fit, as a function of the normalised shaft speed and total input torque, $\eta_{GB} = f(M_L, n_L)$. It is assumed that the gearbox is coupled with the propeller shaft, while the electric machine (EM) is coupled with the engine shaft as a PTO/PTI either directly ($i_{PTO/i} = 1$) or via a gearbox (which is the more general topology). The effect of the electric machine on the power equilibrium is measured as a load $P_{PTO/I}$. Before the load, the power is equal to $P_L$, so $P_B \cdot k_e = P_L + P_{PTO/I}$, and the following equation holds [8]:

$$P_B = \frac{1}{k_e} \cdot \left(\frac{P_s}{\eta_{GB}} + P_{PTO/I}\right) \tag{4.15}$$

where $k_e$ is the number of connected engines per powertrain. Now focusing on the gearbox losses with the expression found in [102], and using the generator law values for the coefficients, the following can be derived:

$$M_{loss,GB} = M_{loss,GB,nom} \cdot \left(a_{GB} \cdot \frac{M_L}{M_{L,nom}} + b_{GB} \cdot \frac{n_L}{n_{L,nom}} + c_{GB}\right) \tag{4.16}$$

or

$$M_{loss,GB} = f_{GB}(M_L, n_L) \tag{4.17}$$

and similarly with the derivations for the shaft losses:

$$M_{loss,GB} = g_{GB}(P_p, n_p) \tag{4.18}$$

and

$$\eta_{GB} = h_{GB}(P_p, n_p) \tag{4.19}$$

Now the total transmission losses can be expressed as

$$M_{loss,TRM} = g_{TRM}(P_p, n_p) \tag{4.20}$$

and

$$\eta_{TRM} = h_{TRM}(P_p, n_p) \tag{4.21}$$

The above assumptions and formulations provide the possibility to express the propulsive load at the shaft after the gearbox (or point $L$) as a function of the propeller power demand $P_p$, and shaft speed $n_p$.

$$\eta_{TRM}(P_p, n_p) = \frac{P_p}{P_L} \tag{4.22}$$

Furthermore, if Eqs. (4.8,4.9) are used, the propulsive demand can be expressed by only one quantity, propulsive power $P_p$, shaft speed $n_p$, or ship speed $v_s$, so e.g. expressing the efficiency in terms of propeller shaft speed yields:

$$\eta_{TRM} = \mathcal{H}_{TRM}(n_p) \tag{4.23}$$

Then, taking into account the mechanical couplings, the following equations hold:

$$P_B = \frac{1}{k_e} \cdot (\frac{P_p}{\eta_{TRM}(n_p)} + P_{PTO/I}) \tag{4.24}$$

or

$$P_B \cdot k_e = \mathcal{F}(n_p) + P_{PTO/I} \tag{4.25}$$

and due to the reduction ratios of the gearbox at the end of the propeller shaft, and the gearbox of the PTO/PTI, the shaft speed relations are:

$$\begin{aligned} n_L &= i_{GB} \cdot n_p \\ n_{Drive} &= i_{PTO/I} \cdot n_L \end{aligned} \tag{4.26}$$

It is noted here that if the EM requires a constant rotational speed $n_{Drive}$ due to lack of power electronics to convert a varying frequency voltage and subsequent inability to feed an AC distribution network [8], then the propeller must be a CPP. In that case, the propeller torque or power can be used as disturbances to the ship's powertrain system.

The amount of power getting out of the shaft at the PTO gearbox is $M_L - M_B = M_{PTO/I}$.

$$\begin{aligned} P_L - P_B &= P_{PTO/I} \\ n_L(M_L - M_B) &= n_L \cdot M_{PTO/I} \\ M_L - M_B &= M_{PTO/I} \end{aligned} \tag{4.27}$$

And at the PTO/I gearbox during PTI functionality:

$$\begin{aligned} P_{Drive} + P_{loss,PTI} &= P_{PTI} \\ n_{Drive} \cdot (M_{Drive} + M_{loss,PTI}) &= n_L \cdot M_{PTI} \\ M_{Drive} + M_{loss,PTI} &= \frac{1}{i_{PTO/I}} M_{PTI} \end{aligned} \tag{4.28}$$

and during PTO functionality:

$$\begin{aligned} P_{Drive} &= P_{PTO} + P_{loss,PTO} \\ n_{Drive} \cdot M_{Drive} &= n_L \cdot (M_{PTO} + M_{loss,PTO}) \\ M_{Drive} &= \frac{1}{i_{PTO/I}} (M_{PTO} + M_{loss,PTO}) \end{aligned} \tag{4.29}$$

The torque losses during PTO are positive $M_{loss,PTO} > 0$, when the torque is going in the electric machine, $M_{Drive} < 0$, and can be expressed as:

$$M_{loss,PTO} = M_{loss,nom} \cdot \left( a_{PTO} \cdot \frac{|M_{PTO}|}{M_{nom}} + b_{PTO} \cdot \frac{n_L}{n_{nom}} + c_{PTO} \right) \tag{4.30}$$

and the torque losses during PTI are negative $M_{loss,PTI} < 0$, when the torque is going out of the electric machine and $M_{Drive} \geq 0$ can be expressed as:

$$M_{loss,PTI} = -M_{loss,nom} \cdot \left( a_{PTI} \cdot \frac{|M_{Drive}|}{M_{nom}} + b_{PTI} \cdot \frac{n_{Drive}}{n_{nom}} + c_{PTI} \right) \tag{4.31}$$

however, $M_{Drive} = \frac{M_{PTI}}{i_{PTO/I}} - M_{loss,PTI} = \frac{|M_{PTI}|}{i_{PTO/I}} + |M_{loss,PTI}|$, which yields:

$$M_{loss,PTI} = \frac{M_{loss,nom} \cdot M_{nom}}{M_{loss,nom} \cdot a_{PTI} - M_{nom}} \cdot \left( \frac{a_{PTI}}{i_{PTO/I}} \cdot \frac{|M_{PTI}|}{M_{nom}} + b_{PTI} \cdot i_{PTO/I} \cdot \frac{n_L}{n_{nom}} + c_{PTI} \right) \tag{4.32}$$

The coefficients used for the PTO functionality are the generator law coefficients given in [102], while the coefficients for the PTI functionality are the propeller law coefficients. Eqs. (4.32,4.30) can be combined, together with $n_L = n_B$ to yield the following piecewise expression:

$$M_{loss,PTO/I} = \alpha_{1,j} \cdot |M_{PTO/I}| + \alpha_{2,j} \cdot n_p + \alpha_{3,j} \tag{4.33}$$

where $j = 1$ corresponds to the PTO and $j = 2$ corresponds to the PTI functionality. Multiplying with the rotational speed gives an expression of the following form:

$$P_{loss,PTO/I} = \mathcal{K}(M_{PTO/I}, n_p, i_{PTO/I}, i_{GB}) \tag{4.34}$$

and finally:

$$P_{Drive} = P_{PTO/I} + P_{loss,PTO/I} \tag{4.35}$$

where $P_{PTO} < 0$ and $P_{loss,PTO} \geq 0$, $P_{PTI} \geq 0$ and $P_{loss,PTI} < 0$. The power of the PTO/I can easily be expressed as a function of the variables in Eq.(4.34):

$$P_{PTO/I} = M_{PTO/I} \cdot n_{Drive} = i_{GB} \cdot i_{PTO/I} \cdot M_{PTO/I} \cdot n_p \tag{4.36}$$

### 4.1.3 Electric Machine

The PTO/I consists of a gearbox, which is on the shaft connecting the engine with the propeller gearbox, and an electric machine with a variable speed drive (VSD). The losses of the frequency VSD can be integrated into the electric machine losses, $P_{loss,EM}$, or a constant value can be used. The electric machine power losses are again a function of torque and shaft speed, expressed with another piecewise fitted equation in [1], and by converting the rotational speed to the disturbance $n_p$ an expression of the following form is obtained:

$$P_{loss,EM} = \mathcal{L}(M_{PTO/I}, n_p, i_{GB}, i_{PTO/I}) \quad , \quad M_{PTO/I} \in [0, M_{EM,max}] \wedge n_{PTO/I} \in [0, n_{EM,max}] \tag{4.37}$$

where the operating limits are given by the manufacturer.

Thus, the PTO/I power is:

$$P_{PTO/I} = P_{EM} + P_{loss,EM} \tag{4.38}$$

where $P_{PTO} < 0$ when the electric machine works as a generator and $P_{PTI} \geq 0$ when it works as a motor. From the previous equation and Eqs. (4.34-4.36), an expression for the electric machine demand/supply $P_{EM}$ from/to the distribution bus $P_{EM}$ can be obtained, solely as a function of the PTO/I torque $M_{PTO/I}$, the reduction ratios $i_{GB}$,$i_{PTO/I}$ and the propeller shaft speed $n_p$:

$$P_{EM} = P_{PTO/I} + P_{loss,PTO/I} - P_{loss,EM} = \mathcal{M}(M_{PTO/I}, n_p, i_{GB}, i_{PTO/I}) \tag{4.39}$$

### 4.1.4 Main Switchboard Electric Balance

The power from and to the electric machines $P_{EM,j}$ , $j = 1, 2, ..., k_p$ of the propulsion trains $k_p$, together with the power from the $k_g$ generator sets $P_{gen,j}$ , $j = 1, 2, ..., k_g$ are met on a high voltage AC or DC distribution bus. In the case of an AC architecture, DC power sources/storage systems

are connected to the system via inverters/rectifiers. Such power sources are fuel cell units, and such storage systems are battery units and supercapacitors. However, only batteries are within the scope of this study. Finally, the aggregated electric power demand of the consumers is expressed with the quantity $P_{hotel}$, which corresponds to the total hotel load demand [2]. The total electric power balance on the main switchboard can be expressed as follows:

$$\sum_{j=1}^{k_g} P_{gen,j} + \sum_{j=1}^{k_p} P_{EM,j} + P_{bat,AC} + P_{hotel} = 0 \tag{4.40}$$

### 4.1.5 Battery Unit

The battery unit is comprised of a number of parallel $n_{par}$ and series $n_{ser}$ battery cells to be able to provide both the necessary total capacity $Q_{0,pack} = Q_{0,cell} \cdot n_{par}$ and power output $P_b$.

Battery capacity is typically expressed in Ah because it depends on the (dis)charge current [100], or more commonly the non-dimensional C-rate, which indicates the amount of time in hours that it takes for a given current to fully (dis)charge the battery.

The State of Charge or $SoC$ of a single battery cell is defined as:

$$SoC(t) = \frac{Q(t)}{Q_0} \tag{4.41}$$

while the derivative of this equation yields the following expression:

$$\dot{SoC}(t) = \frac{1}{Q_0}\dot{Q}(t) = \frac{-\eta_c I_b(t)}{Q_0} \tag{4.42}$$

where $\eta_c$[3] indicates the *Coulombic* efficiency during battery charging which represents the irreversible effects of the charging process [100], while from this equation and by keeping track of the battery current $I_b$, the determination of the $SoC$ of the battery is possible. However, such approach can be inaccurate due to accumulated errors, resulting to what is described in the literature as $SoC$ drift [1].

[2] Commonly hotel electric demand and the AC input/output of the converted DC power supply/storage are on a low AC bus or a secondary bus, which is connected to the primary high voltage bus by means of a transformer [8]

[3] $\eta_c = 1$ for discharging

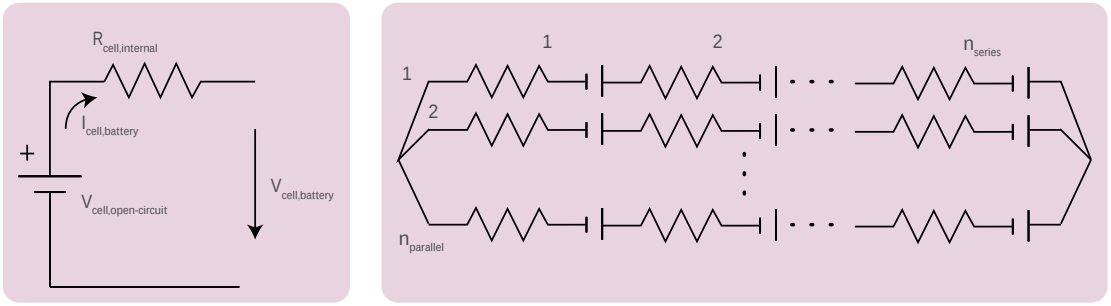


Figure 4.3: The equivalent circuit for the steady state description (left), and the battery pack (right). Adapted from [100]

Since the modelling approach is not dynamic, a simple steady-state description of the battery cell is chosen [100]:

$$V_{cell,bat} = V_{cell,open} - R_{cell,int} \cdot I_{cell,bat} \tag{4.43}$$

where both the open voltage $V_{cell,open}$ and internal resistance $R_{int}$ of the cell are first-order functions of the $SoC$:

$$\begin{aligned} V_{cell,open} &= \beta_1 + \beta_2 \cdot SoC \\ R_{cell,int} &= \beta_3 + \beta_4 \cdot SoC \end{aligned} \tag{4.44}$$

The connection between the battery cell and the battery pack is given by $V_{pack,open} = n_{ser} \cdot V_{cell,open}$, $R_{pack,int} = R_{cell,int} \cdot \frac{n_{ser}}{n_{par}}$ The performance of this model has been demonstrated to provide sufficiently accurate steady-state results when compared with a more accurate double R-C branch model [1]. From Eq. (4.43) and $I_{cell,bat} = \frac{P_{cell,bat}}{V_{cell,bat}}$:

$$V_{cell,bat}^2 - V_{cell,open} \cdot V_{cell,bat} + R_{cell,int} \cdot P_{cell,bat} = 0 \tag{4.45}$$

while solving for $V_{cell,bat}$ and keeping the suitable solution gives:

$$V_{cell,bat} = \frac{V_{cell,open}}{2} + \frac{\sqrt{V_{cell,open}^2 - 4R_{cell,int}P_{cell,bat}}}{2} \tag{4.46}$$

and by dividing with $R_{cell,int}$, an expression for $I_{cell,bat}$ is gained:

$$I_{cell,bat} = \frac{V_{cell,open}}{2R_{cell,int}} + \sqrt{\left(\frac{V_{cell,open}}{2R_{cell,int}}\right)^2 - \frac{P_{cell,bat}}{R_{cell,int}}} = \mathcal{M}(SoC, P_{cell,bat}) \tag{4.47}$$

The operating limits for the power output of the battery cell $P_{cell,bat}$ and current output $I_{cell,bat}$ are:

$$P_{cell,bat} \in \left[\frac{I_{cell,bat,min}}{R_{cell,int}}, \frac{I_{cell,bat,max}}{R_{cell,int}}\right] \quad and \quad I_{cell,bat} \in \left[I_{cell,bat,min}, I_{cell,bat,max}\right] \tag{4.48}$$

From Eq. (4.42) the State of Charge of a cell is:

$$\dot{SoC} = -\frac{I_{cell,bat}}{Q_{cell,0}} \tag{4.49}$$

and by discretising this equation with a timestep of $\Delta t$:

$$SoC(t + \Delta t) = SoC(t) - \frac{I_{cell,bat} \cdot \Delta t}{Q_{cell,0}} \quad , \quad SoC \in [SoC_{min}, SoC_{max}] \tag{4.50}$$

where $P_{cell,bat} = \frac{P_{bat}}{n_{par} \cdot n_{ser}}$ and $I_{cell,bat}$ can be calculated from Eq.(4.47).

Finally, if the battery is connected to an AC bus via a rectifier/inverter (for charging $P_b < 0$ / discharging $P_b \geq 0$, correspondingly), its efficiency is also taken into account, correlating the power at the battery pack side $P_{bat}$ with the power of the AC bus side $P_{bat,AC}$ with:

$$\eta_{inv/rec}^{sgn(P_{bat})} = \frac{P_{bat,AC}}{P_{bat}} \tag{4.51}$$

The above allow for expressing the new $SoC$ of a battery cell as a function of the previous $SoC$ and the battery pack power $P_{bat,AC}$:

$$SoC(t + \Delta t) = \mathcal{N}(SoC(t), P_{bat,AC}(t)) \tag{4.52}$$

## Electrochemical Efficiency

An alternative way of calculating the $SoC$ at the next time step is by using the electrochemical efficiency of the battery, if it is available, as it allows for more complex expressions for describing the open circuit voltage. The *electrochemical power*:

$$P_{ech} = V_{open} \cdot I_{bat} \tag{4.53}$$

is defined as the power of the battery without taking into account the internal losses [100], and it is connected to the battery power with the *electrochemical local efficiency* $\eta_b$, available as a function of battery power output $P_{bat}$ and $SoC$[4]:

$$\eta_b^{sgn(P_{bat})} = \frac{P_{bat}}{P_{ech}} = \frac{V_{bat}}{V_{open}} = f(P_{bat}, SoC) \tag{4.54}$$

Assuming a more complex expression of the open circuit voltage [1]:

$$V_{open,cell} = \alpha_1 \cdot e^{\alpha_2 \cdot SoC} + \alpha_3 + \alpha_4 \cdot SoC + \alpha_5 \cdot SoC^2 + \alpha_6 \cdot SoC^3 \tag{4.55}$$

and combining Eqs. (4.53,4.54) while also converting from the pack to the cell:

$$I_{cell,bat} = \frac{P_{pack,bat} \cdot \eta_b^{-sgn(P_{bat})}}{n_{par} \cdot n_{ser} \cdot V_{open,cell}} \tag{4.56}$$

By substituting $I_{cell,bat}$ into Eq.(4.50), and by taking into account the inverter/rectifier losses, another expression for $SoC(t + \Delta t)$ is obtained, that is again solely a function of $SoC$ and $P_{bat,AC}$:

$$SoC(t + \Delta t) = \mathcal{N}^*(SoC(t), P_{bat,AC}) \tag{4.57}$$

[4] Where $P \geq 0$ corresponds to the battery discharging

### 4.1.6 Diesel Engines

For EMS purposes aiming for fuel consumption minimisation, quasi-static models are typically modelled by fuel consumption maps, or fitted functions, as dynamic behaviour is of secondary importance [3].

#### Generator Sets

As generators coupled with diesel engines run at a constant speed, the fuel oil consumption $\dot{m}_f$ of the generator can be approximated with a quadratic function of the power output $P_{gen}$ [1]:

$$\dot{m}_{f,gen} = \sum_{i=0}^{2} \alpha_i \cdot P_{gen}^i \quad , \quad P_{gen} \in [P_{gen,min}, P_{gen,max}] \tag{4.58}$$

where the minimum and maximum power output is key to defining the operating limits, which are important for the EMS, especially if the number of active generator sets is a state variable. The generator and transformer losses are integrated within the above polyonomial fit.

#### Main Engine

The static fuel consumption of the main diesel engine can be approximated by a polynomial function of the power output $P_b$ and the shaft speed $n_b$ [1]:

$$\dot{m}_{f,DE} = \sum_{i=0}^{2} \sum_{j=0}^{2} a_{i,j} \cdot n_B^i \cdot P_B^j \quad , \quad \begin{bmatrix} n_B \\ P_B \end{bmatrix} \in \mathcal{E} \subset \mathbb{R}^2 \tag{4.59}$$

where domain $\mathcal{E}$ the operating envelope of the diesel engine, bounded by the turbocharger limit $P_1 = g_1(n_B)$, the torque limit $P_2 = g_2(n_B)$, and the minimum and maximum shaft speed, expressed as a function of shaft speed $n_B$ according to specifications by the manufacturer:

$$\mathcal{E} = \{ \quad \begin{bmatrix} n_B \\ P_B \end{bmatrix} \in \mathbb{R}^2 \quad | \quad P_B \leq g_1(n_B) \ \wedge \ P_B \leq g_2(n_B) \ \wedge \ n_B \in [n_{B,min}, n_{B,max}] \quad \} \tag{4.60}$$

### 4.1.7 Model Description Formulations

The hybrid powertrain model of a ship can be aggregated into the following set of equations. Eq. (4.25) corresponds to the mechanical coupling in the gearboxes and power balance, and by using the PTO/I torque $M_{PTO/I}$ instead of the power Eq. (4.36):

$$f_1(n_p, M_{PTO/I}, k_e, P_B, i_{GB}, i_{PTO/I}) = 0 \tag{4.61}$$

while the electrical node in Eq. (4.40) can be expressed as:

$$f_2(P_{gen}, k_g, M_{PTO/I}, k_p, P_{bat,AC}, P_{hotel}) = 0 \tag{4.62}$$

The above two equations represent two power balances and correspond to the 2 whole DoFs in the powertrain, one for the mechanical node and one for the electrical node. This is in accordance with the DoF analysis in Section 3.1.

The new state of charge of the battery unit is expressed by Eqs. (4.52,4.57), as a function of the current state of charge $SoC(t)$ and the battery power $P_{bat,AC}$.

Finally, the fuel consumption of the main engines and the generator sets are expressed in Eqs. (4.59,4.58), as a function of the load $P_B$ and shaft speed $n_B$, and as a function of load $P_{gen}$, correspondingly.

The model is also subject to a number of constraints, physically expressing the operating limits of the components of the powertrain. In the mathematical sense, these constraints define the domains of the descriptive functions of the components.

## 4.2 Optimal Control Problem

Once the ship model is described by a set of equations, the optimal control problem (OCB), discussed in Section 3.3, can be formally defined. Again, the system is described by Eq.(5.1), which is repeated here:

$$\dot{\mathbf{x}} = f(\mathbf{x}, \mathbf{u}, \mathbf{r})$$
$$\mathbf{y} = h(\mathbf{y}, \mathbf{u}, \mathbf{r})$$

First the state vector $\mathbf{x}$ has to be decided. Following the mathematical background in [65] to solve the problem, the state of charge $SoC$ and, optionally, the number of running generator sets $NoE$ are the states of the control problem:

$$\mathbf{x} = \begin{bmatrix} SoC \\ NoE \end{bmatrix} \quad , \quad SoC \in [SoC_{min}, SoC_{max}], k_g \in [0, 1, ..., k_g] \tag{4.63}$$

The disturbances of the control problem $\mathbf{r}$ are the loads to the powertrain, which could be fully described by the hotel power $P_{hotel}$, the propeller speed $n_p$ and the coefficient $C_4^*$.

$$\mathbf{r} = \begin{bmatrix} P_{hotel} \\ n_p \\ C_4^* \end{bmatrix} \tag{4.64}$$

The control input vector $\mathbf{u}$ has the same dimensions as the DoF of the system, which is 2. The battery output $P_{bat,AC}$, and the PTO/I torque $M_{PTO/I}$ are typically selected as the control inputs.

$$\mathbf{u} = \begin{bmatrix} P_{bat,AC} \\ M_{PTO/I} \end{bmatrix} P_{bat,AC} \in [P_{bat,AC,min}, P_{bat,AC,max}], M_{PTO/I} \in [M_{PTO/I,min}, M_{PTO/I,max}] \tag{4.65}$$

Although the reduction ratios of the gearboxes ($i_{GB}, i_{PTO/I}$) may be able to vary (two-speed gearboxes), in this study they are assumed to be fixed. Another assumption has been made regarding the active powertrains, as for these study all main engines are considered to be always online. Discussion regarding the ability of the energy management controller to utilise turning main engines on and off has been discussed in [1], where additional saving in the order of $2-3\%$ have been found, however, the same study also expresses concern of such functionality potentially compromising reliability.

The output vector $\mathbf{y}$, which allows for the fuel consumption of the IC engines to be calculated, is defined as follows:

$$\mathbf{y} = \begin{bmatrix} P_{gen} \\ P_B \end{bmatrix} \tag{4.66}$$

The objective of the optimal control problem is to find the control input sequence $\mathbf{u}$ that minimises the cost function $J$, (i.e. $arg\min_{\mathbf{u}(t)} J$), as it has been discussed in Sec. 3.3, and has been expressed by Eqs. (3.4,3.5a-3.5f).

$$J(\mathbf{u}(t)) = \phi(\mathbf{x}(t_f)) + \int_{t_0}^{t_f} \sum_i \dot{m}_{f,i}(\mathbf{u}(t), \mathbf{x}(t), t) + G(\mathbf{u}(t), \mathbf{x}(t), t) \quad dt$$

The fuel consumption term inside the integral can now be specified:

$$\sum_i \dot{m}_{f,i}(\mathbf{u}(t), \mathbf{x}(t), t) = \sum_{i=1}^{NoE(t)} \dot{m}_{f,gen,i}(t, P_{gen,i}(t)) + \sum_{i=1}^{k_e} \dot{m}_{f,DE,i}(t, n_B(t), P_B(t)) \tag{4.67}$$

where it is assumed that the load on the main engines for each of the powertrains is equally divided.

The $G$ term, which is used to reduce the frequency at which the generator set engines are switched on/off can be expressed as [65]:

$$\mu \cdot \delta NoE = \mu \cdot |NoE(t + \Delta t) - NoE(t)| \tag{4.68}$$

where $\mu$ is a parameter to tune the effect of the term on the total cost.

The constraints in Eqs. (3.5a-3.5f) can also be specified. The differential equation constraint is defined for the $SoC$ using Eqs. (4.52,4.57). The domain set for the state vector $\mathcal{X}$ is given in Eq. (4.63), and the domain for the input control vector $\mathcal{U}$ is given in Eq. (4.65). It is noted that both domain sets are not a function of time. The initial conditions for the state vector $\mathbf{x}_0$ can be chosen according to the initial $SoC$ of the battery, while the online diesel engines could use a typical initial value. Finally, the terminal condition of the state $\mathbf{x}(t_f)$, concerns only the SoC, while its value depends on whether the powertrain functions as a charge sustaining or a charge depleting vessel (See Sec. 3.3).

# Chapter 5

# The Long-term Feedback Enabled Framework: Theory and Implementation

## 5.1 Dynamic Programming

### 5.1.1 An Overview

The Dynamic Programming (DP) algorithm was introduced by Bellman in a technical report, back in 1956 [103], while he was working for the RAND corporation in Santa Monica, California, on a project for the U.S Air Force. The term *Dynamic Programming* was coined, in an attempt to make the mathematical theory of *multi-stage decision processes* sound less *"formidable"*. This is probably why little insight can be gained into the algorithm, just by the name *Dynamic Programming*.

Regarding DP applications and optimal control, Bertsekas' book [104] is a milestone for optimal control in literature. DP is capable of yielding an optimal controller if perfect knowledge of the future disturbances and reference outputs of the system are explicitly known a priori [98]. That is, DP is capable of finding the mathematically optimal solution for the optimal-control problem (OCP), while the requirement for perfect knowledge classifies it in the regime of a-causal controllers. However, for the DP algorithm to be implemented, descritisation of the OCP is required. For that reason DP practically yields close to optimal results, as the optimal solution is selected out of a discrete set of candidate solutions [3]. Of course it can be easily inferred that the optimality of the results depends on the density of the OCP problem's discretisation grid.

Classic DP algorithms are also characterised as deterministic, distinguishing them from the stochastic DP (SDP) algorithms. The computational complexity of a DP algorithm is exponential

with respect to the number of states and control inputs so attention must be given in order to minimise computational cost [98]. Most commonly, DP algorithms are used to benchmark (an extensive list of such applications is given in [3]) or tune other controllers (e.g. heuristic rule extraction [105]), due to, firstly, their close to optimal performance, and, secondly, their a-causal nature and computational burden, which renders their online implementation difficult. Nevertheless, as it is further discussed in Sec. 5.2 and 5.3, implementation of DP in online Model Predictive Controllers (MPC) (or receding horizon DP) is not an uncommon practice at all [65], [106], [59], [107]; in fact, this very study utilises exactly this approach to solve the OCP problem that emerges from the Energy Management Strategy (EMS) on-board ships.

### 5.1.2 Optimality Principle and Formulations

The DP algorithm fundamentals are described in the rest of this section, as found in [3, 98, 108]. DP is a numerical solution based on the **optimality principle**, which states that, *an optimal policy has the property that whatever the initial state and initial decision are, the remaining decisions must constitute an optimal policy with regard to the state resulting from the first decision* [103].

This means that, if the optimal solution path of a problem $P$ with initial state $O$, $(\mathbf{x}_0, t_0)$, passes through $M$, $(\mathbf{x}_m, t_m)$, then, a new optimal problem $P$', which is identical to $P$, but it is now starting from $M$, will have as a solution the remaining portion (after point $M$ and until the end) of the initial solution for $P$ [108].

This allows for the approach to start from the end state and work its way backwards, assessing at each time step the optimal path arc. Also, due to this, DP is **not causal**, since it does not start from the start of a time-marching problem. Shortest path problems are a typical example of the dynamic programming algorithm [108] and can provide insight into its behaviour.

For control problems, when considering a continuous system in time that has continuous variables as states and control inputs, a discretisation into a grid has to first take place. The resulting system description, as found in [3], is of the form:

$$\mathbf{x}_{k+1} = f(\mathbf{x}_k, \mathbf{u}_k) \quad , \quad k = [1, 2, ..., N],\ \mathbf{u}_k \in \mathcal{U}_k,\ \mathbf{x}_k \in \mathcal{X}_k \tag{5.1}$$

where $N$ are the total time steps of the problem, $\mathcal{U}_k$ and $\mathcal{X}_k$ the allowable control input and state vectors at a given time instant $k$, correspondingly. This description is crucial as it commonly describes the dynamics of a system, as a result of the Euler integration approximation for a differential equation ($dx/dt = (x_{k+1} - x_k)/\Delta t = F(x, t)$, and then isolating $x_{k+1}$).

Every control input vector $u_k \in \mathcal{U}_k$ applied on a system state vector $x_k \in \mathcal{X}_k$ is associated to a cost for the $N$ time steps of the problem. That association is described by a cost function $h_k(u_k, x_k)$. This way, the control input, or control effort, and its associated cost, for every state transition, can be mapped.

The final cost, due to the state transition to the end state, is given by a different function $\phi_{N+1}(x_N)$, because it is solely a function of the end state [98]. This can be easily understood by substituting $N$ in the system description Eq. (5.1), and noticing that the final $u_N$ and $x_N$ already define $x_{N+1}$ via the system's dynamics, while the cost for $u_N$ has already been accounted for in $h_N$. Having a cost attributed to the final state is useful for control purposes, in the sense that finishing with the system in one state might be more favourable than in a different one. Furthermore, as it is discussed further on, constraints on the end state can also be enforced in a similar way.

Now, starting from all possible end states $\mathbf{x}_{N+1}$ and working backwards by one step to $N$, the costs of every possible transition can be mapped:

$$\mathbf{J}_{N,N+1} = \Delta\mathbf{J}_{N,N+1} + \mathbf{J}_{N+1} = \mathbf{h}_N(\mathbf{x}_N, \mathbf{u}_N) + \boldsymbol{\phi}_{N+1}(\mathbf{x}_{N+1}) \tag{5.2}$$

the dimension of $\mathbf{h}_N(\mathbf{x}_N, \mathbf{u}_N)$ is the same as all of the arcs connecting all of the allowable states in timestep $N$ to the states in timestep $N+1$, so it is $\mathcal{U}_N$ by $\mathcal{X}_N$.

For example, if the state of the system can be fully described by only one number $x_N$ belonging in a finite set of cardinality 3, e.g. $\mathcal{X}_N = \{0,\ 0.5,\ 1\}$ and the control effort to change to $x_{N+1}$ is fully described by a control input vector of size 2, $\mathbf{u}_N = [u_1\ u_2]$ in a finite set of cardinality 2 by 2, e.g. $\mathcal{U}_N = \mathcal{U}_{N,1} \times \mathcal{U}_{N,1} = \{0,\ 1\} \times \{0,\ 1\}$, then the resulting arcs than need to be evaluated are $N = N_x \times N_{u1} \times N_{u2} = 3 \times 2 \times 2 = 12$, which means that the size of $\mathbf{h}$ grows exponentially with the states and control input dimensions. Generalising, the exponential complexity of the problem becomes also apparent, as for each quantized state $\mathbf{x}_i$ of $N_{x,i}$ points, and each quantized control input $\mathbf{u}_j$ of $N_{u,j}$ points, the points that have to be evaluated become at each time step are:

$$N = \prod_i N_{x,i} \cdot \prod_j N_{u,j} \tag{5.3}$$

By working backwards and using the principle of optimality, the computational load can be significantly reduced. Such an approach can be thought of as a shortest path problem, where instead of path arcs, there are control input costs for all given allowable state transitions.

However, since for a specific state transition, the discrete control input vector $\mathbf{u}_M$ required does not necessarily result into one of the given discrete states $\mathbf{x}_i$, the closest state has to be chosen, or an interpolation can also yield a value between the discrete adjacent states.

Among these control efforts, for the $N^{th}$ state $\mathbf{x}_N$ there must be at least one control input vector $\mathbf{u}_N$ that minimises $J_N$:

$$J^*(\mathbf{x}_{N,N+1}) = \min_{\mathbf{u}_n \in \mathcal{U}_N} (J_N(\mathbf{u}_N)) \tag{5.4}$$

This is the optimal cost associated with state $\mathbf{x}_N$, and it corresponds to the best **cost-to-go** to the end state $N+1$. This cost corresponds to the optimal arc, connecting $\mathbf{x}_N$ to the optimal end state (cheapest), and it "hides" all other sub-optimal end states.

Now any intermediate state $\mathbf{x}_k$ can be considered to have an optimal sequence of least control effort $\pi_{\mathbf{x}_k} = \mathbf{u}_k,\ \mathbf{u}_{k+1},\ ...,\ \mathbf{u}_N$:

$$J^*(\mathbf{x}_{k,k+1}) = \min_{\pi_{\mathbf{x}_k} \in \mathcal{U}_k} \{J_k(\mathbf{u}_k) + J^*(\mathbf{x}_{k+1,N+1})\} = \min_{\mathbf{u}_k \in \mathcal{U}_k} \{\Delta J_{k,k+1}(\mathbf{u}_k)\} + J^*(\mathbf{x}_{k+1,N+1}) \tag{5.5}$$

This means that instead of evaluating every possible path, just the the optimal arc from $\mathbf{x}_k$ to the state $\mathbf{x}_{k+1}$ in $k+1$ should be evaluated, and then the cost-to-go from $\mathbf{x}_{k+1}$ to the end state $\mathbf{x}_N + 1$ is added (See Fig. 5.1). The optimality of the new path with the added new path arc added, is also optimal, due to the Bellman's principle of optimality. All suboptimal states leading up to state $k+1$ (starting from the end) are hidden and not re-evaluated.

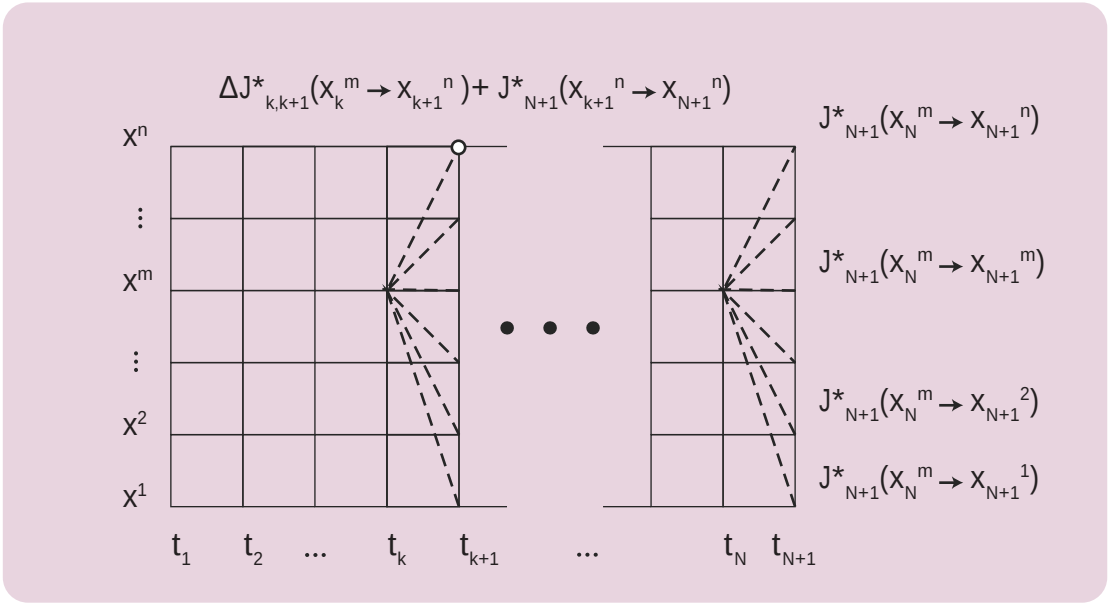


Figure 5.1: Evaluation of one optimal path for $x^m$ at stage k is equal to evaluating the state transition $x^m$ to e.g. $x^n$ from stage k to k+1 and then adding the optimal path that starts at $x^n$ at stage k+1, up until the final stage N+1 and then continuing evaluating all other states for stage k+1 to find the minimum [108]

Then, the control sequence or **policy** $\pi^*_{\mathbf{x}_1} = \{\mathbf{u}_1, \mathbf{u}_2, ..., \mathbf{u}_N\}$, leading up to the initial state and condition $\mathbf{x}_1$ is **optimal**, and it will be

$$J^*_\pi(\mathbf{x}_1) = \min_{\pi_{\mathbf{x}_1} \in \Pi} \{J^*(\mathbf{x}_{1,N+1})\} \tag{5.6}$$

The above cost functional can be extended to include a penalty term, $\theta$, for the state constraints [98], while the control constraints are dealt with through time-varying boundaries on the control input sets $\mathcal{U}_k$. The sets $\mathcal{U}_k$ for every $k \in [1, 2, ..., N]$ is a new set $\Pi$. Finally, the discretised description of the DP algorithm for optimal control essentially means finding the optimal control policy:

$$\pi^*_{\mathbf{x}_1} = arg \min_{\pi_{\mathbf{x}_1} \in \Pi} \{J_\pi(\mathbf{x}_1)\} = arg \min_{\pi_{\mathbf{x}_1} \in \Pi} \{\phi_{N+1}(\mathbf{x}_{N+1}) + \theta_{N+1}(\mathbf{x}_{N+1}) + \sum_{k=1}^{N} h_k(\mathbf{x}_k, \mathbf{u}_k) + \theta_k(\mathbf{x}_k)\} \tag{5.7}$$

The Eq.(3.4) can be written in that form in order to apply the DP algorithm to the optimal control of a hybrid vessel. The description of the dynamics need to be supplied, and can be found by an Euler discretisation to the differential equations for the states, $SoC$ and $NoE$, of the hybrid powertrain, such that:

$$\mathbf{x}_{k+1} = f(\mathbf{x}_k, \mathbf{u}, \mathbf{r}, \Delta t) \tag{5.8}$$

where $\Delta t$ the time step.

Then, term $h$ of the cost functional includes the terms inside the integral:

$$h_k(\mathbf{x}_k, \mathbf{u}_k) = \sum_{i=1}^{NoE(k)} \dot{m}_{f,gen,i}(k, P_{gen,i}(k)) + \sum_{i=1}^{k_e} \dot{m}_{f,DE,i}(k, n_B(k), P_B(k)) + \mu \cdot |NoE(k+1) - NoE(k)| \tag{5.9}$$

while the various operating constraints can also be given without need for new formulations.

A DP MATLAB® function, that is freely available by ETH Zürich, has been developed and validated for hybrid electric vehicles in a series of publications by Sunstrom and Guzella [98,109,110], allowing for utilisation in a wide range of OCPs, common of which are supervisory control problems for hybrid vehicles, with applications found in [3,111]. This software has been also used and verified in [1, 65], where the EMS implementations are similar to the approach of the present study, while the software also offers much needed end-state constraint capabilities.

## 5.2 Model Predictive Control

### 5.2.1 Latest Applications in Energy Management of Powertrains

The above formulations of a time-marching control problem allow for a transition into a discussion regarding a powerful, yet computationally expensive control strategy, Model Predictive Control (MPC). In MPC, a model description of the system is utilised in order to generate the optimal control input vector sequence, $\pi^*_{\mathbf{x}_1}$. In [112], it is shown that microgrids, the similarities of which with the marine propulsion systems were discussed in Sec.2.2, are suitable for MPC applications, which was traditionally applied in the process industry (e.g. for the control of temperature for certain reaction processes in chemical plants, etc). The slower dynamics in the process industry-related OCPs were appropriate for the computationally demanding utilisation of a model for control purposes, however, the faster processors of micro-controllers of today allow for the use of MPC in systems described by faster dynamics, also explained in [3], where two important implementation issues of MPC are noted:

- MPC is an accurate control strategy **if** the reference trajectory (for setpoint tracking) of the output is given and the disturbances are measurable, which is not the case for maritime vessels,

and, thus, a disturbance forecasting scheme should be utilised. [1]

- The model describing the system must be accurate enough to calculate the state, in order to correctly estimate the results of different control inputs, and provide correct control setpoints.

The advantages of MPC control are identified in [112], and those relevant to vessel applications are:

- MPC is able to cope with multiple variables and a bigger number of degrees of freedom for objective minimisation (bigger than most widely used EMSs e.g. ECMS)
- MPC is able to handle binary variables and non-linearities well, which is a key point in complex hybrid systems (e.g. for (dis)connecting generators, (dis)charging non-linearities, operating limits of the powertrain's components etc.)

### 5.2.2 Algorithm Description

The computational load of MPC can be understood with a more detailed description. In MPC, a series of control problems $P_k$ are being solved, one at each time step $t_k$. Each of these problems is solved for a set horizon length $T_h = N_h \cdot \Delta t$, starting at $t_k$, and up until $t_k + N_h \cdot \Delta t$ into the future. The solution of each of these problems is essentially an optimal control vector sequence $\pi^*_{J,k,k+(N_h-1)\Delta t}$, of which **only** the first control vector $\mathbf{u}_k$ is used as a control input to be applied on the known current state of the real system $\mathbf{x}_k$. In order for the solver to be able to find the solution, the disturbance vector $\mathbf{r}_{k,k+N_h\Delta t}$ must be either fully known, or estimated and supplied, and then the model description is utilised to evaluate the state transitions $\Delta J$ and pick an optimal route to minimise a cost functional $J_{k,k+N_h\Delta t}$, starting from the present sampled state $\mathbf{x}_k$. The rest of the control inputs $\mathbf{u}_{k+1}$, $\mathbf{u}_{k+2}$, ..., $\mathbf{u}_{k+N_h\cdot\Delta t}$ are discarded, the next state $\mathbf{x}_{k+1}$ is sampled from the real system, and the whole process is shifted to **k+1** and iterated. This is why MPC is described in the literature as a **receding horizon** control strategy [113].

Perplexing matters a bit further, the control horizon and the prediction horizon can be different ($N_c$ and $N_p$, correspondingly, with $N_c \leq N_p - 1$), with the control output staying constant after $N_c$, in order to reduce the decision steps and, consequently, computational effort. The question, however, arises as to why that extra prediction horizon $N_p - (N_c + 1)$ might be useful. This is because MPC has been usually used in literature for setpoint tracking, meaning that the output of the system is needed to follow a given reference trajectory, by commonly utilising an euclidian distance (or second norm) in the cost functional [112]:

$$\sum_{i=k}^{N_p} ||y(k + i \cdot \Delta t) - y_{ref}(k + i \cdot \Delta t)||^2_R \tag{5.10}$$

[1] However, the use of stochastic variables is another approach [112], that might be of particular interest to maritime applications, where the wave resistance is often modelled with stochastic variables

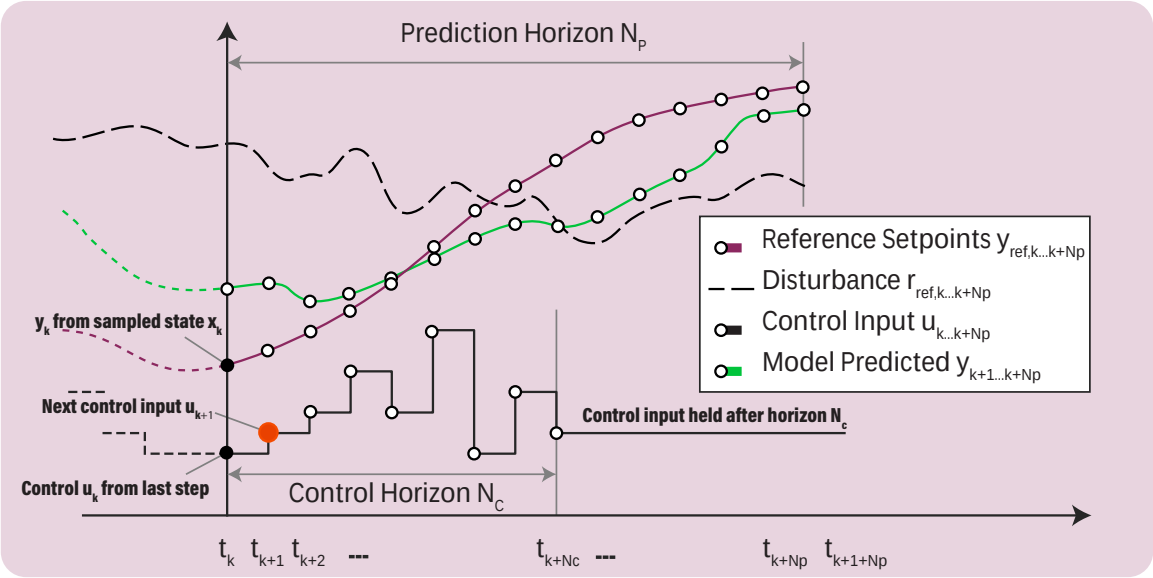


Figure 5.2: Model Predictive Control at time step k, adapted from [112, 113]

where R a weighing matrix (positive definite).

This term can be thought of as a penalty to further punish control sequences that do not end up with the output close to the reference value $y_{ref}(k + \lambda \cdot \Delta t)$ for some $\lambda < N_p$, and it can be very effective in identifying trajectories that converge to the reference, where the term above converges to zero.

Although the setpoint tracking nature of MPC might not have obvious applications for energy consumption minimisation purposes, reference trajectory tracking can be very effective for long term information utilisation of known disturbances [112] (e.g. common operating profile or scheduled mission drills), which is, after all, the approach of this study, explained in the next section.

Regarding the cost functional for the control horizon, EMS applications in [112] use familiar minimisation formulations, as found in other EMSs and written without losing generality in a fuel consumption-oriented form:

$$\sum_{i=k}^{i=N_c} \mathbf{w} \cdot \dot{\mathbf{m}}_f(k + i \cdot \Delta t) \tag{5.11}$$

where $\mathbf{w}$ is a weighing array and $\dot{\mathbf{m}}_f(k + i \cdot \Delta t)$ a column of the consumption of all engines in a propulsive powertrain. Such formulations can be very similar with the summation term $h$ in Eq. (5.9).

The above can be sequenced in the following algorithm:

1. The state $\mathbf{x}_k$ is sampled from the actual system, at time step $t_k$, while the state history and the past inputs and outputs, up until $\mathbf{u}_{k-1}$ and $\mathbf{y}_{k-1}$, correspondingly, are known. For setpoint tracking, an output reference trajectory should also be given $y_{ref}(k, k + N_p \cdot \Delta t)$

2. The disturbance to the system, $\mathbf{r}_{k,k+N_p\Delta t}$, is either known or estimated, and supplied to the system, for the full prediction horizon $[t_k, t_k + N_p \cdot \Delta t]$

3. The above are fed into a model description of the system, as the one formulated in Section 4.1, and together with a cost functional $J$, state transition control efforts are evaluated by a solver, and an optimal control policy is found $\pi^*_{J,k,k+(N_c)\Delta t}$, while also the prediction of the output trajectory of the system is generated for the prediction horizon, $y_{ref}(k, k + N_p \cdot \Delta t)$, commonly included in the cost functional.

4. The controller finally yields only the first control input vector $\mathbf{u}_k$ of the optimal sequence $\pi^*_{J,k,k+N_c\Delta t}$, while the rest of the control steps $\mathbf{u}_{k+1}$, $\mathbf{u}_{k+2}$, ..., $\mathbf{u}_{k+N_c\cdot\Delta t}$ are discarded.

5. The new state of the system $\mathbf{x}_{k+1}$ is now available to be sampled, and acts as the sole feedback to the controller. This final step coincides with the first step of this algorithm and it is continuously iterated by shifting the whole OPC by one time step

A demonstration of the above algorithm, at time step $k$ is given by Fig. 5.2. A typical MPC control block diagram is shown in Fig. 5.4(top figure), adapted from [112]. The latter diagram shows classical setpoint tracking, while the control horizon term is not shown but regarded to be included in the optimal control solver block. The data flows and actions in blue are iterated for the whole horizon.

An overview of the solver applications by MPC for hybrid powertrains is given in [65]. An opensource MATLAB®-based software is available in [114], utilising a Quadratic Programming (QP) solver and including several features for high performance, however, no applications regarding powertrains have been made. A full MPC code implementation on a hybrid powertrain with a battery module is also available in [115].

## 5.3 The Suggested Strategy Framework

### 5.3.1 Background Study

In a study for automotive vehicles by Sun et al. [65], MPC approaches are presented as a compromise between DP and ECMS strategies for energy management. On one hand, DP requires the load profile and duration to be known in advance, yielding a control strategy that is very sensitive and performs poorly when the actual load profile has even slight deviations from the profile used for the DP solution. For this reason, DP is predominantly used as a benchmarking strategy, as explained previously (Sec. 5.1). On the other hand, ECMS performs well when information is given only on the present time instant, however tuning the equivalence factor $s$, which depends on the load profile,

is not a trivial task, while adaptive implementations (A-ECMS) are required in order for this factor to change accordingly during a profile cycle, in order to yield greater fuel economy.

The methodology employed in the above study [65], in order to enable the energy management framework to utilise along-the-way mission information, is the "backbone" of the controller implementation in the present study, applied in maritime hybrid powertrains, and taking into consideration the slower dynamics and the differences in the nature of the disturbances with automotive applications.

### 5.3.2 Maritime Powertrain Considerations: Dynamics and Disturbances

In fact, the time step of the MPC implementation of [65] is 1 $s$, whereas, as it is also discussed in Section 7.2, for maritime applications a time step in the order of 20 $s$ is sufficient. The thought process behind this time step decision regards the nature of the disturbances that should be taken into account in a maritime powertrain EMS. As it is discussed in [116], while waves do not impose an oscillatory disturbance on the powertrain due to the ship's inertia, the disturbance on the wake field due to waves does play an important role on powertrain loading. A description of the wake speed $v_w$ at the centre of the propeller is given in [117]:

$$v_w = \zeta_w \omega_w e^{k_w \cdot z} cos((k_w \cdot v_s + \omega_w)t)$$

where $\omega_w$, $\zeta_w$, $k_w$ is the angular frequency, significant amplitude, and wave number of the wake wave, correspondingly, while $v_s$ shows the dependence of the wake wave angular frequency on the ship speed. $z$ is the distance of the centre of the propeller to the water surface. Note that since the description above is a single wave, it is not capable of providing bounds for the $v_w$. Only a single wave with significant wave height can be described [101]. In reality, a superposition of wave functions with various wave heights, phases, and encounter angles, can generate irregular waves [90] and subsequent extreme values that cannot be bounded (by means of an infimum and a supremum wake speed) by a single wave function. Such sets of waves are usually provided in phase-space from statistical measurements in expected sea states. Furthermore, since the ship speed is in the equation for the wake speed, the response amplitude operator (RAO) under these sets of waves and operating vessel speeds, for the surge direction, needs to be used in order to provide any adequate prediction of extreme values.

However, EMS control should not act upon the system based on such oscillatory disturbances, because that would interfere with lower-level controllers (e.g. controller of the fuel valve of the diesel engine or the pitch control). For that reason, a sufficiently larger time step is needed in a bigger order of magnitude than typical values of the wakefield disturbance frequency $2\pi(k_w \cdot v_s + \omega_w)$, so any potential interference or chattering is minimised. At the same time, the time step should not be too large, so in the model description used by the MPC, the discretised differential equation

describing the dynamics of the system (Eq. 5.8) is still accurate.

Regarding the nature of maritime disturbances which **should** be an input to the EMS controller, two major groups are identified:

- weather-dependent alterations and subsequent wave and wind resistance disturbances mainly due to a different sea state
- human decision-making, by the governor of the vessel, regarding the remaining mission

Since the quantification of the disturbance is crucial in MPC for the controller to work, such potential of these two disturbance groups is analysed further.

Integrated Bridge Systems (or IBS) typically offer sophisticated sea-state estimations, sometimes together with an added weather-routing functionality, thus, in realistic scenarios, the weather-dependent disturbance can effectively be obtained as a function of the time and the off-load resistance curve $d = f(t, C*_4(t))$ (See Eq.(4.9)). Using the formulations in Section 4.1.1, the resistance can be described in terms of shaft speed and load mode, or shaft speed and propulsive demand. In the case of a controllable pitch propeller, by using a certain combinator curve, a single virtual shaft speed is enough to describe the resistance. Moreover, since new predictions are available during a mission in a fixed or non-fixed interval, the disturbance can be described by a series of profiles $\mathbf{r}_{t_1},\ \mathbf{r}_{t_2},\ ...,\ \mathbf{r}_{t_F}$, available at each update time step $t_1,\ t_2,\ ...,\ t_F$.

Such profiles extent in much larger horizons (in the order of hours) than a short-term MPC horizon would (in the order of several minutes), due to mainly the big computational burden. It is noted here that every EMS, for both forward and backward simulations [113], assume that the speed profile must be followed, and does not decide on the profile. Usually large horizons would not have an impact on the ship consumption for a given speed profile, as there are either no DoFs in the powertrain, or the number of generator engines running requires only a few minutes of prediction depth to be optimal. In fact, if no transient phenomena are considered, which is typically the case with EMS due to their typical cumulative fuel consumption objective functions, the number of running generators is an OPC that requires a prediction depth of only one time step.

However, long-term information is important in the case of hybrid propulsion trains that utilise a battery module. Energy can be transferred to the battery at time $t_k$ and, ultimately, it may be optimal to be used at a much later time $t_{k+N\Delta t}$, where $N >> N_p$, with $N_p$ the span of the prediction horizon of the MPC controller. Furthermore, for plug-in functionality, optimal blended discharge of the battery requires the full mission cycle as an input (also see Section 3.3). This means that important information are not able to be given to the MPC controller as disturbances.

Now regarding human input, for naval, tug-boats and other types of vessels, where hybrid powertrains with batteries are more likely to be present, planned disturbances that are more or less measurable either by direct calculation or from historical data can be easily correlated with certain

mission parts, drills, or operations. For example, if the captain of a tug-boat decides that in 6 minutes a tug operation of a certain ship will start, will take approximately 20 minutes, and will use approximately 60% of the pulling power in intermittent pulses, the disturbance profile can be described very accurately, and can be given as an input to the controller. However, such inputs may reach way farther into the future than the prediction horizon span $N_p$ of the MPC, so there is again the need to input important information into the controller in another way.

### 5.3.3 Implementation Formulation

In order for the OCP to not be completely "oblivious" of the important information discussed above regarding the sea-state-related and the mission-related load trajectories, a reference discharge trajectory for the SoC of the battery module can be used, either in the summation term of the objective function, or in the end state constraint [65]. A reference SoC trajectory method has also been used in [118]. Since battery utilisation is the main reason for the importance of long-term information in the OCP, and since MPC has the ability of following reference trajectories, utilising information for the future disturbances, via an online-generated SoC trajectory, by the MPC, sounds a promising approach for maritime applications. The effectiveness of such a controller framework is the object of the present study and, simultaneously, its scientific contribution.

Reference trajectory generation[2] in automotive literature [65, 118] and utilises information for the future operating profile based on position (i.e. elevation or traffic data). This information is available from a GPS or GIP (see also Sec. 2.4). In maritime applications equivalent information come from the Integrate Bridge Systems (IBSs) and/or the governor's input regarding future load decisions, such the ones discussed above.

The Model Predictive Control Framework block diagram, including the SoC trajectory generation, and the corresponding data flows, is depicted in Figure 5.3.

#### Reference Trajectory Generation

If a long-term prediction of the disturbances $\mathbf{r}_{long}$ until the end of the mission is available, the optimal discharging trajectory of the battery module SoC can be found, $SoC(t),\ t \in [t_k, t_{N+1}]$, where $t_k$ is the current time at time step k and $t_{N+1}$ the final time step at the end of the mission. This is possible by using a model description of the powertrain, and solving the OCP for the full mission time with an exhaustive solution (PMP, or DP). The solver that has been chosen to be used is a DP solver for MATLAB® [98]. For this reason the implementation formulations are given in Section 5.1. However, the final term in Eq.(5.9) is omitted, even if the number of generator sets $NoE$ is included in the states of the OCP of the MPC. This is due to the added computational load

[2] also the term predictive reference signal generator (pRSG) is used

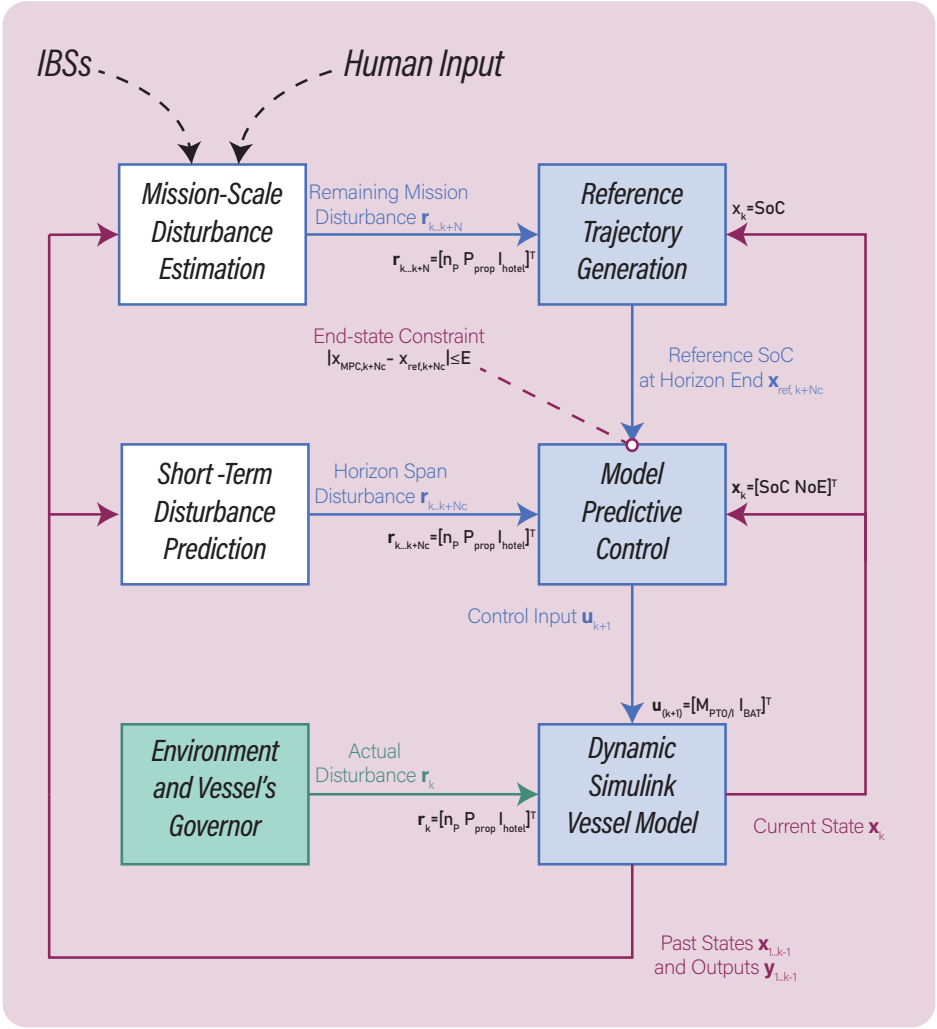


Figure 5.3: The Model Predictive -based, prediction enabled, Energy Management Control framework. In the figure the data routes are depicted for time step $k\Delta t$, adapted from [65]

and the smaller contribution of any future number of running $NoE$ to the present fuel consumption. Moreover, since the long-term DP solution does not directly provide the control inputs, including a term in the long-term OCP objective function, meant to prevent the frequent turning on and off of the generator sets, is redundant. The final cost functional, following the formulation in Eq.(5.7) and dropping the generator set on/off penalty term in Eq.(5.9), is of the form:

$$J_\pi(x_1) = \phi_{N+1}(\mathbf{x}_{N+1}) + \theta_{N+1}(\mathbf{x}_N) + \sum_{k=1}^{N+1} \dot{\mathbf{m}}_{f,k}(\mathbf{x}_k, \mathbf{u}_k) + \theta_k(\mathbf{x}_k) \tag{5.12}$$

where the constraints on the state vector are enforced with term $\theta_k$, while the end constraint function $g_(N+1)$ associates the end state with a cost (See also Sec. 5.1).

Regarding the generator sets, the total power to be covered is found with the power balance

Eq.(4.62), by solving for $P_{gen}$. In order to find how to divide that power between the number of available engines, the active number of engine generator sets can be found with an integer division $NoE = div(P_{gen}, P_{nom}) + 1$, and then, by dividing the power with this number, the consumption of each generator set is found to be:

$$P_{gen,i} = \frac{P_{gen}}{NoE} \ , \ i \in [1, 2, ..., NoE] \tag{5.13}$$

The above yields optimal results in the practically common case where a) the fuel consumption of the generator set is a convex function of its power demand, $\dot{m}_{f,i} = f(P_{gen,i})$ and b) the generators are identical. By considering two generator sets with power setpoints $P_{g,1}$ and $P_{g,2}$, what is essentially needed to be proven, in order for the above to be optimal, is that, if point $C$ is the common operation point of the two engines, there exist **no** points $A$ and $B$, that cover the power demand $P_{gen}$, such as:

$$\dot{m}_{f,a} + \dot{m}_{f,b} < 2 \cdot \dot{m}_{f,c} \iff f(P_{a,g,1}) + f(P_{b,g,2}) < 2 \cdot f(P_{c,g,12}) \ , \ P_{a,g,1} < P_{c,g,12} < P_{b,g,2} \tag{5.14}$$

This can be proven from the definition of convexity[3]:

$$f(tx + (1-t)y) \leq tf(x) + (1-t)f(y) \ , \ t \in [0, 1], x < y \tag{5.15}$$

Now, since point C is between A and B, it can be expressed in the form

$$P_{c,g,12} = t \cdot P_{a,g,1} + (1-t) \cdot P_{b,g,2} \tag{5.16}$$

Which yields:

$$t = \frac{P_{c,g,12} - P_{b,g,2}}{P_{a,g,1} - P_{b,g,2}} \tag{5.17}$$

and by substituting in the equation above the expression $2 \cdot P_{c,g,12} = P_{a,g,1} + P_{b,g,2} = P_{gen}$, which means that in both scenarios, the total power has to add up to the total power demand $P_{gen}$, yields that $t = 1/2$. From the definition inequality Eq.(5.15), and by substituting the $\dot{m}_f$ function, it is now:

$$\dot{m}_{f,c} \leq \frac{1}{2} \cdot \dot{m}_{f,a} + (1 - \frac{1}{2}) \cdot \dot{m}_{f,b}$$

or

$$2 \cdot \dot{m}_{f,c} \leq \dot{m}_{f,a} + \dot{m}_{f,b} \tag{5.18}$$

which can be generalised for more engines and which proves that the common power setpoint $P_{c,g,12} = P_{gen,i}$ from Eq. (5.13) is optimal. In the case of different engines, but their consumption functions are still convex, the formulation above can be extended, however, that case is not discussed here. Regarding the operating limits, the following inequalities should hold:

$$P_{gen,i} \in [P_{gen,min}, P_{gen,max}] \tag{5.19}$$

$$P_{gen} \leq k_g \cdot P_{gen,max} \tag{5.20}$$

[3] An important and helpful book on convex optimisation is written by S.P. Boyd [119], which is openly available

where $k_g$ the number of generator sets available on board the vessel.

The rest of the model description of a general maritime hybrid powertrain utilising batteries has been given in Section 4.1.

## Model Predictive Control with End State Constraint

MPC requires the utilisation of a solver and a model description. For a DP solver and hybrid maritime powertrains, most of the formulations have been covered in previous sections. However, the importance of the end-state constraint in the implementation of this study is discussed here.

The utilisation of the setpoint-tracking capabilities of MPC are key for enabling the controller to be updated with information about the future disturbances and these capabilities act as an information pathway, either by direct use of a corresponding term in the objective function, such as the term in Eq.(5.10), or by utilising the end-state constraint. This study takes the latter approach, which is the one followed in [65]. For that reason, there is not set-point tracking term and, subsequently, the MPC problem is only using the control horizon $N_c$.

Now, in Eq. (5.7) it is shown that term $\theta_{N+1}$ is penalising the objective of the control policy for the end-state. This is because the discretisation is based on the control inputs and not the states, meaning that a state resulting from a discretised control inputs might not fall exactly on one of the discritised end-states, thus an interpolation is done (See Sec. 5.1.2). The end-state constraint is formulated by a double inequality, providing a window of allowable values:

$$SoC_{min}(k + N_c \cdot \Delta t) \leq SoC(k + N_c \cdot \Delta t) \leq SoC_{max}(k + N_c \cdot \Delta t) \tag{5.21}$$

where $SoC(k+N_c \cdot \Delta t)$ the state at the end of the **control** horizon $N_c$, for the optimisation problem of time step $k$, with $SoC_{min}$ and $SoC_{max}$ being the minimum and maximum allowable values of $SoC(k + N_c \cdot \Delta t)$.

The generated trajectory $SoC_{ref}(t)$ has to be followed. However, not allowing for a number of end states around the reference value might lead to an infeasible problem, due to the disturbance alterations being big enough, due to a short control horizon, or due to grid discretisation considerations (e.g discrete state mismatch due to a coarser grid in the long-term DP problem). This may happen because, there might not be a possible path leading up to the current state $SoC_k$. For that reason a parameter $E$ is used, which is some function of the state and input control grid, $N_{\mathbf{u}}, N_{\mathbf{x}}$, the control horizon $N_u$, and the disturbance discrepancy $\mathbf{r} - \mathbf{r}_{ref}$, difficult to describe explicitly, so that:

$$|SoC(k + N_p \cdot \Delta t) - SoC_{ref}(k + N_p \cdot \Delta t)| \leq E \tag{5.22}$$

This parameter is practically chosen to be large enough for the DP solver to still be able to find a feasible solution.

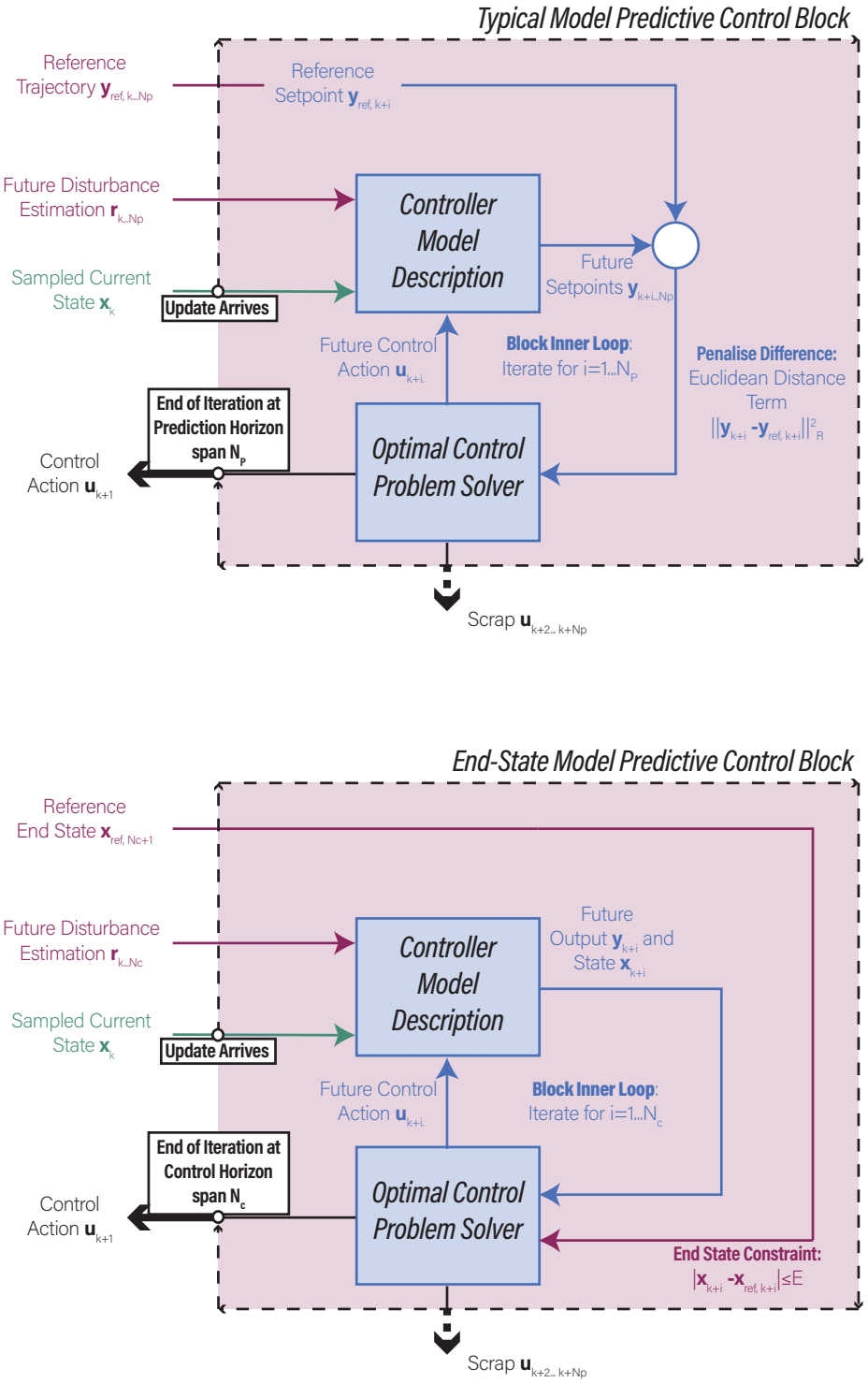


Figure 5.4: Different approaches for setpoint-tracking: Typical MPC approach with utilisation of the prediction horizon summation term, $||y - y_{ref}||^2_R$, (top), and the end-state constraint approach with a cost functional that includes only the minimisation term (bottom). The actions and data flows that are being iterated over the horizons (predictive and control, respectively) are shown in blue. Adapted from [112]

The difference in the two approaches are shown in Fig. 5.4. It is important to notice that, while in typical MPC a reference trajectory is given for every MPC control problem, in the end-state approach only a single value, the end-state reference is needed. Thus, regarding the whole mission, a typical MPC will utilise a series of reference trajectories, while the present approach will only utilise one **end-state reference trajectory**. This difference is showcased in Fig. 5.5. From all the above it is concluded that the end-state MPC approach is the most suitable for contingent state trajectories, which is the case for vessel missions.

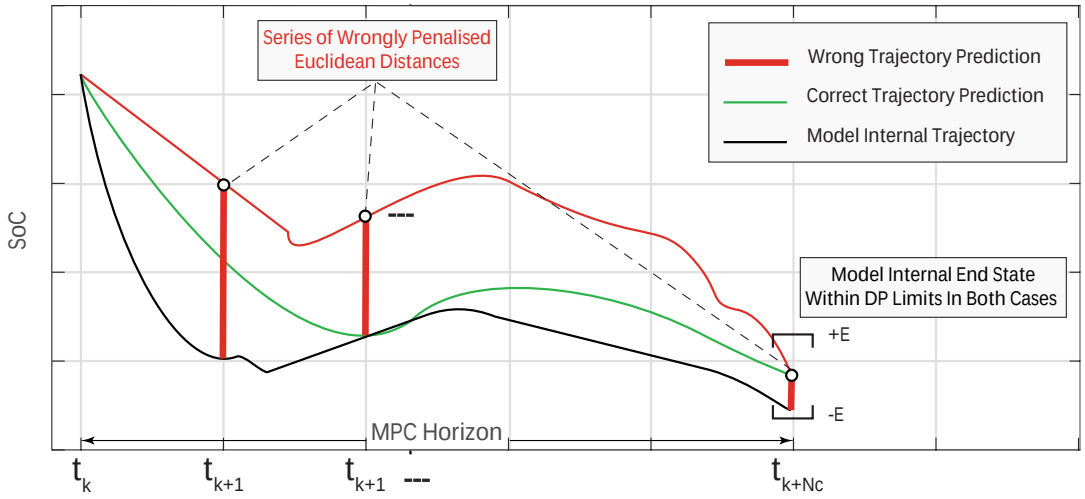


Figure 5.5: The effect of the different approaches for setpoint-tracking: in traditional setpoint tracking the wrong prediction is punishing correct candidate trajectories and restricts optimality, while in end-state MPC the optimal path is not eliminated as long as its final state falls within the end-state window

Apart from the data flow interface considerations correlated with the above fact, there is a deeper implication: By dropping the setpoint tracking term and imposing an end-state window, if the reference is re-estimated, the penalty imposed to the series of the time-marching optimal problems correlated with the initial false reference is conjectured to be much lower. Furthermore, by using a DP solver, which starts from the allowable end-states and does not take into account all of the trajectories, a form of state-tracking feedback to the MPC framework is still present.

## Short-Term Disturbance Estimation

In order for the Model Predictive Control to solve the Optimal Control Problem at each time instant $k$, the disturbance vector, $\mathbf{r}_k$, for the control horizon, $t \in [k, k + N_c \cdot \Delta t]$, has to be estimated and fed into the Dynamic Programming solver as an input. For the estimation of the disturbance, the past values can be utilised, from the start of the mission, $t = 0$, until the previous time instant, $t_{k-1} = (k-1) \cdot \Delta t$. Furthermore, historical data regarding typical operating profiles can also be

useful for an accurate disturbance estimation.

Since the horizon is smaller than the mission length, the estimation is expected to be more accurate than the full mission estimation, discussed before. Furthermore, the current information used for the full mission length estimation, such as information regarding weather and human input, may be utilised as well. A discussion regarding the naval capabilities of short term prediction has been made in Sec.2.4.

In more detail, several prediction schemes may be used:

- Historical data, *2n-period generation* scheme used in [34, 87]
- Neural Networks, such as the RBF-NN implementation in [65]
- Autoregressive Moving-Average (ARMA) models [120]
- Markov Chain Monte Carlo method which utilises historical operating profile data to generate a transition probability matrix [121].

### MPC Framework in the Scope of the Present Study

The long and short term disturbance predictions, for the SoC reference trajectory and the MPC future disturbance input, correspondingly, are a crucial part of the suggested framework. However, the inclusion of a specific prediction scheme would interfere with the performance results of the framework, while the present study focuses at enabling utilisation of future information. So, in order for the framework to be benchmarked regardless of the prediction scheme implementation, perfect predictors are used, and an information barrier is being introduced in order to showcase the importance of long-term information utilisation, and the corresponding impact of the presence of the long-term information feed pathway to the fuel consumption. Thus, the prediction implementations are not in the scope of the present work.

# Chapter 6

# Case Study: Formulation and Verification of the Components for the Reduced Model

## 6.1 Component Reduction for Reduced Model

The performance of the dynamic data -enabled energy management control framework has been tested on a Simulink® Mean Value First Principle (MVFP) model of a hybrid patrol vessel, provided by DAMEN® DSNS, and described, verified, and validated in the thesis of Dr. R.D. Geertsma [101] and a series of publications [1,116,117,122,123]. Details on the models can be found in the references. This section is concerned with the model reduction in order to provide the mathematical description of the powertrain of the vessel to be used by the controller framework.

The vessel consists of 2 powertrains, with each having a main engine, connected to the propeller shaft via a gearbox. Each propeller shaft has a PTO/I induction motor, which is attached with a 1:1 gear relation. The electric portion of the propulsive plant contains 4 diesel engine generator sets, providing power to a three-phase, high-voltage AC bus on which the hotel consumers, induction motors and batteries are connected. The battery pack is assumed to be attached on the high-voltage AC bus via a rectifier/inverter. The power plant of the vessel is shown in Fig. 6.1.

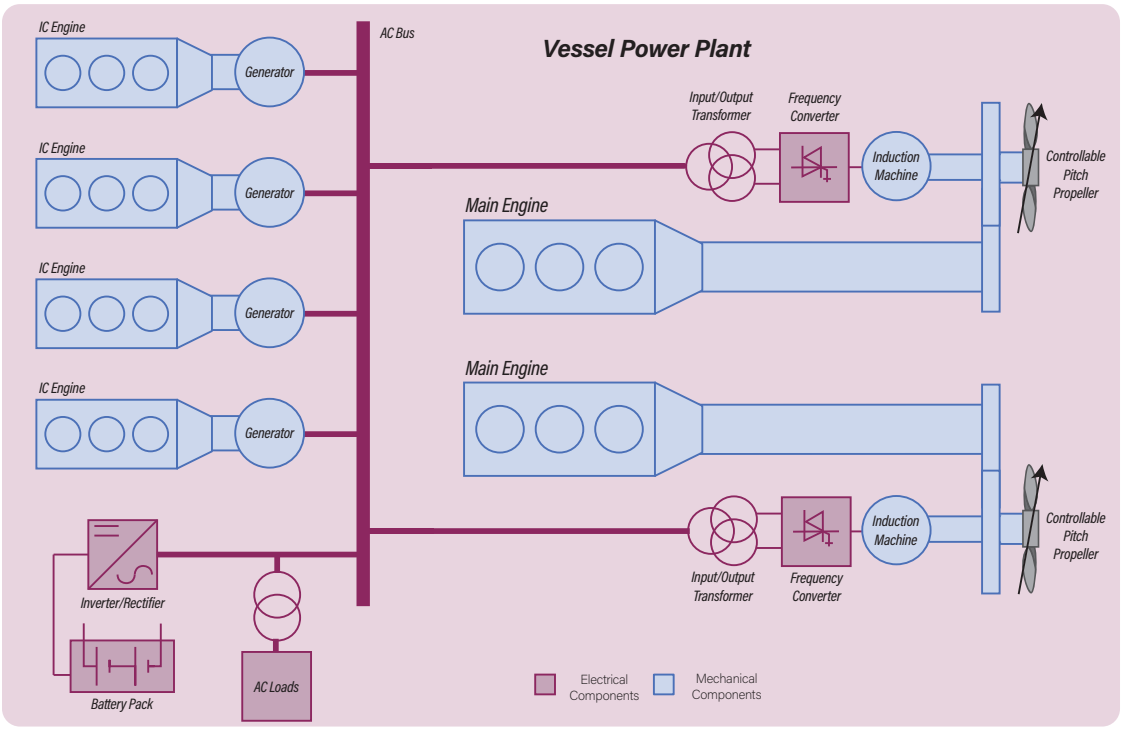


Figure 6.1: Vessel's power and propulsion plant. Adapted from [101]

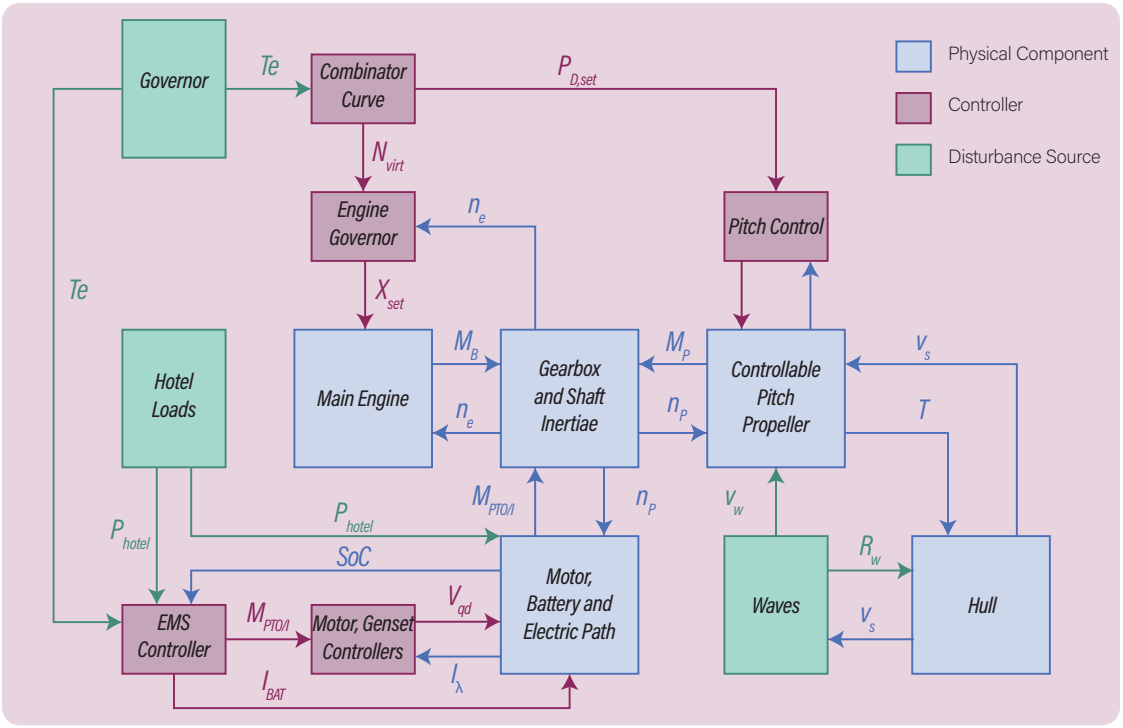


Figure 6.2: Vessel's dynamic model causality and block diagram, including the EMS controller. Adapted from [101]

It is noted that for this reduced model, the control inputs are the battery power current $I_{bat,AC}$ and the induction motor torque of each of the powertrains, $M_{PTO/I}$. The causation of the dynamic model block diagram can be seen in Fig. 6.2, together with the EMS controller. Details on the induction motor, the engine and the pitch controller can be found in Dr. R.D. Geertsma's work. Furthermore, the modelling of the waves and the periodic oscillation in the wake field that they induce, $v_w$, have been discussed in Sec. 5.3.2, however they have not been incorporated in the model due to the added complexity and certain implementation difficulties. Nevertheless, the level of detail such an inclusion provides should not be an obstacle to the demonstrative purpose of this case study.

### 6.1.1 Combinator Curve

Based on the documentation on the Simulink® dynamic model of the vessel, given in [117], the governor of the vessel is able to set the two inputs to the controllable pitch propeller -based propulsive plant, the virtual shaft speed, $N_{virt}$, and the desirable pitch ratio, $P_{D,set}$, via one sole input, the telegraph position, $Te$. The relationship between the telegraph position and the virtual shaft speed and pitch ratio, $[N_{virt}, P_{D,set}] = f(Te)$, is prescribed by combinator curves, and it can be programmed to alter with the operation mode, (e.g. transit or manoeuvring). Since the governors' actions are subject to non-deterministic circumstances and weather phenomena, the telegraph level and, subsequently, the virtual shaft speed and pitch ratio setpoint, are considered a disturbance to the vessel's powertrain.

The above disturbances to the dynamic model are the signal references for the controllers for the propeller pitch, induction motors, and engines. They yield the fuel consumption setpoint rate of the engine governor, and the propulsive demand from the propeller and hull system, while, by taking into account the induction motors and rotating inertia in the powertrains, ultimately, the actual shaft speed of the vessel is fed back to the controllers to be compared with the references again. This means that the dynamic vessel model is designed in a **forward** simulating fashion, with the information flow, or *causality*, starting from the governor (captain).

On the other hand, the **backward** simulation approach where the information flow starts from the load means that, quasi-static models have backward causality, with the power following a prescribed path[1]. This is in contrast to dynamic models which have forward (or realistic) causality, with the acceleration resulting from the propulsive power of the powertrain.

For the purposes of fuel minimisation and the reduced quasi-static model, a backwards information flow should be adopted, the inputs of which should be the propulsive $P_p$ and hotel loads $P_h$, while the output should yield the fuel consumed. For this reason, in the model reduction, the telegraph position, $Te$, has been directly correlated to the virtual shaft speed, $N_{virt} \in [N_{virt,min}, N_{virt,max}]$

[1] The reader is also referred to [113]

with the following simple scaling relationship:

$$N_{virt} = (N_{virt,max} - N_{virt,min}) \cdot Tg + N_{virt,min} \tag{6.1}$$

The operating boundaries where selected to be **limited**, so that they describe common main engine envelopes, without Sequential Turbocharging (STC), in order to demonstrate the MPC framework capabilities in **heavily bounded systems**. However, in Sec. 7.3.3, an implementation that takes into account the extended capabilities of the MVFP model, due to STC, has also been studied.

Now by varying the virtual shaft speed, $N_{virt}$, the actual engine speed, $n_e$, has been measured from the dynamic model. An interpolation method has been chosen to yield more accurate results than a polynomial or other analytic fit, as the fuel consumption of the engines is very sensitive to the shaft speed. Likewise, from the model's measurement data, the propulsive load $P_p$ is measured against the engine shaft speed, $n_e$ (Fig. 6.3). Such measurements are realistic also in case of a physical vessel.

This way, the complex dynamics that are involved in the ship's speed and resistance, the propeller pitch control, and the reaction of the engine and powertrain inertia to the load, have been simplified to a single propeller curve. More propeller curves can be generated for several sea states, or other off-design conditions, in a similar manner. Apart from the transient behaviour, which is of secondary importance when fuel consumption is concerned, this approach yields very accurate results (See Fig. 6.9.

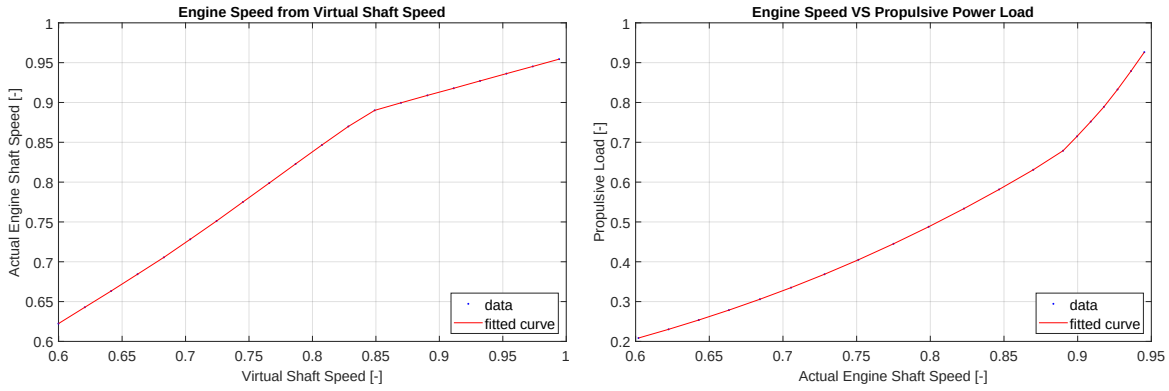


Figure 6.3: Normalised interpolated fits from model measurements for a given combinator curve. Actual engine speed, $n_e$, versus virtual shaft speed, $N_{virt}$, (left), and the propeller curve, propulsive power load, $P_p$, versus actual engine speed, $n_e$, (right)

### 6.1.2 Induction Motor

The induction motor has been modelled based on a piecewise polynomial fit, as in [1], where the normalised power losses, $P_{PTO/I,loss}/P_{PTI,loss,nom}$, including the variable speed drive losses, can be

expressed as a function of the normalised motor speed, $n_n$, and torque, $M_n$:

$$P_{PTO/I,loss,n} = \begin{cases} c_1 \cdot n_n + c_2 \cdot M_n + c_3 \cdot n_n^2 + c_4 \cdot M_n^2 + c_5 \cdot M_n \cdot n_n & , \ M_n > 0 \\ c_1 \cdot n_n + c_2 \cdot M_n + c_3 \cdot n_n^2 + c_6 \cdot M_n^2 - c_5 \cdot M_n \cdot n_n & , \ M_n < 0 \\ 0 \ , \ M_n = 0 \end{cases} \tag{6.2}$$

where $c_i, i \in [1, 2, ..., 6]$ fitted coefficients. In Fig. 6.4 it can be noticed that the generating mode has higher power losses, especially close to the maximum speed, justifying the use of a piecewise function for the two modes. In [1] it is stated that this fitted curve has higher errors when the torque is close to the zero point mark, however, a minimum absolute torque threshold equal to 30% of the nominal torque value has been used by the controller, $|M_n| \geq 0.3$, below which the motor is inactive and disconnected. This threshold has been introduced for the reduction of the occasionally observed chattering between low power setpoints, and should not affect optimality, as, even without it, the motor rarely operates in that region.

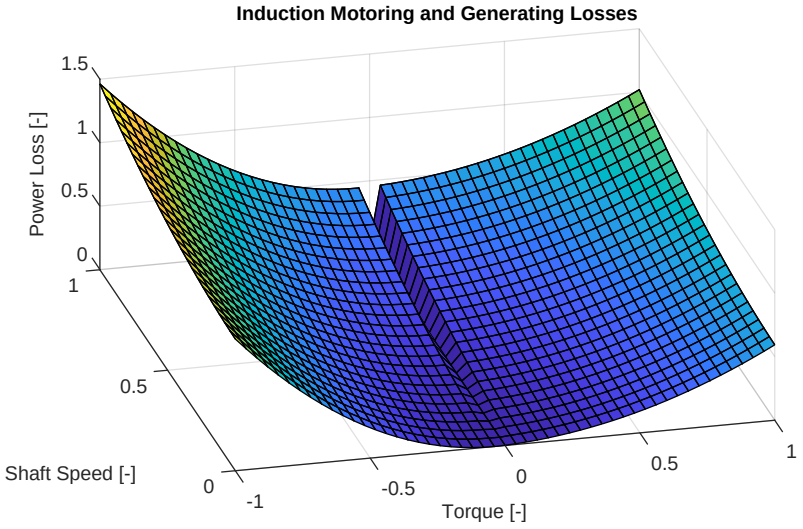


Figure 6.4: Power losses of the induction motor in motoring and generating mode (negative torque corresponds to PTO/generating). Adapted from [1]

### 6.1.3 Main Engine

The main engine fuel consumption has been measured from the dynamic model, by setting the power level, then varying the shaft speed to all allowable values, and then setting the next power level and iterating the procedure. The measurement does not include the power losses of the shaft and gearbox, due to the small impact they have on the fuel consumption. Then, a second order polynomial fit has been made on the fuel consumption per time unit (normalised from $[kg/sec]$), as a function of the normalised power and shaft speed:

$$\dot{m}_f = c_1 + c_2 \cdot n_{B,n} + c_3 \cdot P_{B,n} + c_4 \cdot n_{B,n}^2 + c_5 \cdot P_{B,n} \cdot n_{B,n} + c_6 \cdot P_{B,n}^2 \tag{6.3}$$

where $c_i, i \in [1, 2, ..., 6]$ fitted coefficients. The details of the fit are given in Fig.6.5. Note that the residuals are in the order of $10^{-3}$, yielding an accuracy that would be sufficient to register performance differences down to approximately 0.3%. A more accurate fit might be beneficial, although, it comes with an added computational burden.

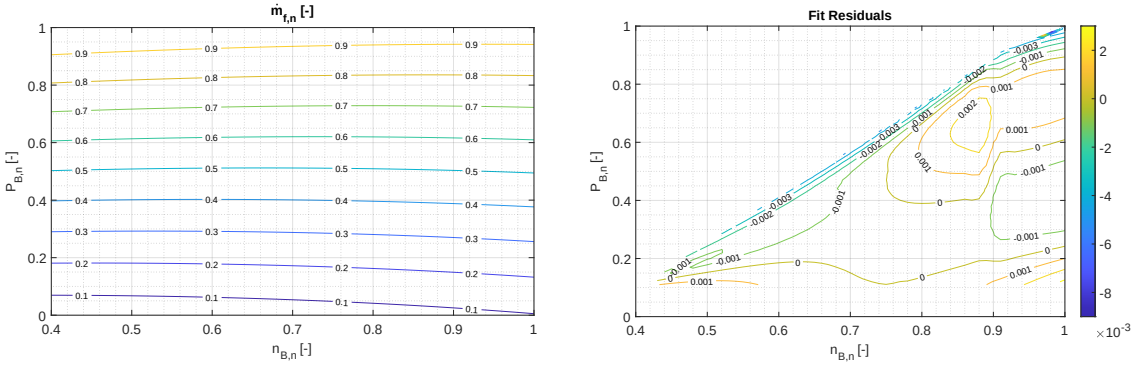


Figure 6.5: Polynomial fit for the normalised fuel consumption of the main engine, $\dot{m}_f[-]$ (normalised from $[kg/sec]$), as a function of the normalised engine power $P_{B,n}$ and shaft speed $n_{B,n}$. R-square: 1.

The operating envelope of the engine is divided into three different regions, the power limit, $n_{B,n} \in (N_2, N_{max}]$, the torque limit, $n_{B,n} \in (N_1, N_2]$, and the turbocharger limit, $n_{B,n} \in [N_{min}, N_1]$. The last limit is expressed in terms maximum power as a function of the shaft speed:

$$P_{B,max,TB} = \beta_1 n_B + \beta_2 n_B^4 \ , \ n_B \in [N_{min}, N_1] \tag{6.4}$$

where $\beta_1, \beta_2$ coefficients. A 0.95 safe factor has been used in the controller to ensure that the operating limits are not violated during operating point transitions, and the engine is stable.

### 6.1.4 Diesel Generator Set

The fuel consumption of the diesel generator set can be measured by varying the torque at a constant rotational speed. However, since the dynamic model has a simple cubic equation describing the engine's consumption, the reduction is trivial. The cubic relationship, normalised fuel consumption as a function of normalised genset power, is:

$$\dot{m}_{gen,n} = c_1 \cdot P_{gen}^2 + c_2 \cdot P_{gen} + c_3 \tag{6.5}$$

where $c_i \ i \in [1, 2, 3]$ are positive coefficients. The consumption of the generator set is also convex, as the second derivative is strictly positive, $\frac{d^2}{dt^2}\dot{m}_{gen,n} = 2 \cdot c_1 > 0$, which is needed for the optimisation of the number of generator sets running (See Sec. 5.3.3).

### 6.1.5 Battery Pack

The battery module current $I_{bat,AC}$, before the rectifier/inverter static converter, is correlated with the battery pack power output/input $P_{bat,AC}$ with the expression:

$$I_{bat,AC} = \frac{P_{bat,AC}}{V_{line} \cdot pf \cdot \sqrt{3}} \tag{6.6}$$

where $V_{line} = 440\ V$ the line voltage and $pf = 0.8$ the power factor of the AC bus.

Now, the per cell maximum continuous current of the battery is $I_{max} = 145\ A$, while the cell capacity is $Q_{0,cell} = 46.3\ Ah$. This gives a maximum C-rate of $C_{max} = I_{max}/Q_{0,cell} = 3.1317$ per cell, and for this value, the power output was measured to be $P_{cell,max} = 1847\ W$, resulting in a total power output of $P_{bat,max} = n_{ser} \cdot n_{par} \cdot P_{cell,max} = 6.387\ MW$. The rated voltage is $V_{cell,bat} = 13\ V$. The battery model uses a double RC branch circuit to emulate the batteries, described in [101].

Then, the static converter (rectifier/inverter) current losses, $I_{bat,cnv,los}$, are given by the following quadratic fitted relationship, assumed to stay the same for both converting modes:

$$I_{bat,cnv,los} = \frac{P_{cnv,los,nom}}{V_{line} \cdot pf \cdot \sqrt{3}} \cdot \left(c_1 \cdot I_n^2 + c_2 \cdot I_n + c_3\right) \tag{6.7}$$

where $P_{cnv,los,nom} = P_{nom} \cdot (1 - \eta_{cnv,nom})$ the nominal converter power losses, while $I_n$ is the normalised current $I_n = |I_{bat,AC}|/I_{bat,AC,nom}$, and $c_i,\ i \in [1, 2, 3]$ are fitting parameters. Moreover it is:

$$I_{bat,AC,nom} = \frac{P_{nom}}{n_{ser} \cdot V_{rat} \cdot pf \cdot \sqrt{3}} = 10287\ A \tag{6.8}$$

The $I_{bat,DC}$ can then be found as:

$$I_{bat,DC} = I_{bat,AC} + I_{bat,cnv,los} \tag{6.9}$$

Note that $I_{bat,cnv,los} \geq 0$ so that during charging , $I < 0$, the rectifier losses are subtracted from the current input towards the battery, while during discharging, $I > 0$, the inverter losses are added to the current demand from the battery. This inevitably leads to a **non-linear** mathematical model for the powertrain of the vessel.

This finally yields to the power at the battery module side:

$$P_{bat} = I_{bat,DC} \cdot pf \cdot V_{line} \cdot \sqrt{3} \tag{6.10}$$

and to find the power per cell the power has to be divided with the number of parallel $n_{par}$ and the number of series $n_{ser}$

$$P_{cell,bat} = \frac{P_{bat}}{n_{par} \cdot n_{ser}} \tag{6.11}$$

The electrochemical efficiency $\eta_{ech}$ which is a function of the power per cell, $P_{cell,bat}$, and the battery cell state of charge $SoC$, has been measured, and a piecewise polynomial fit has been used for its

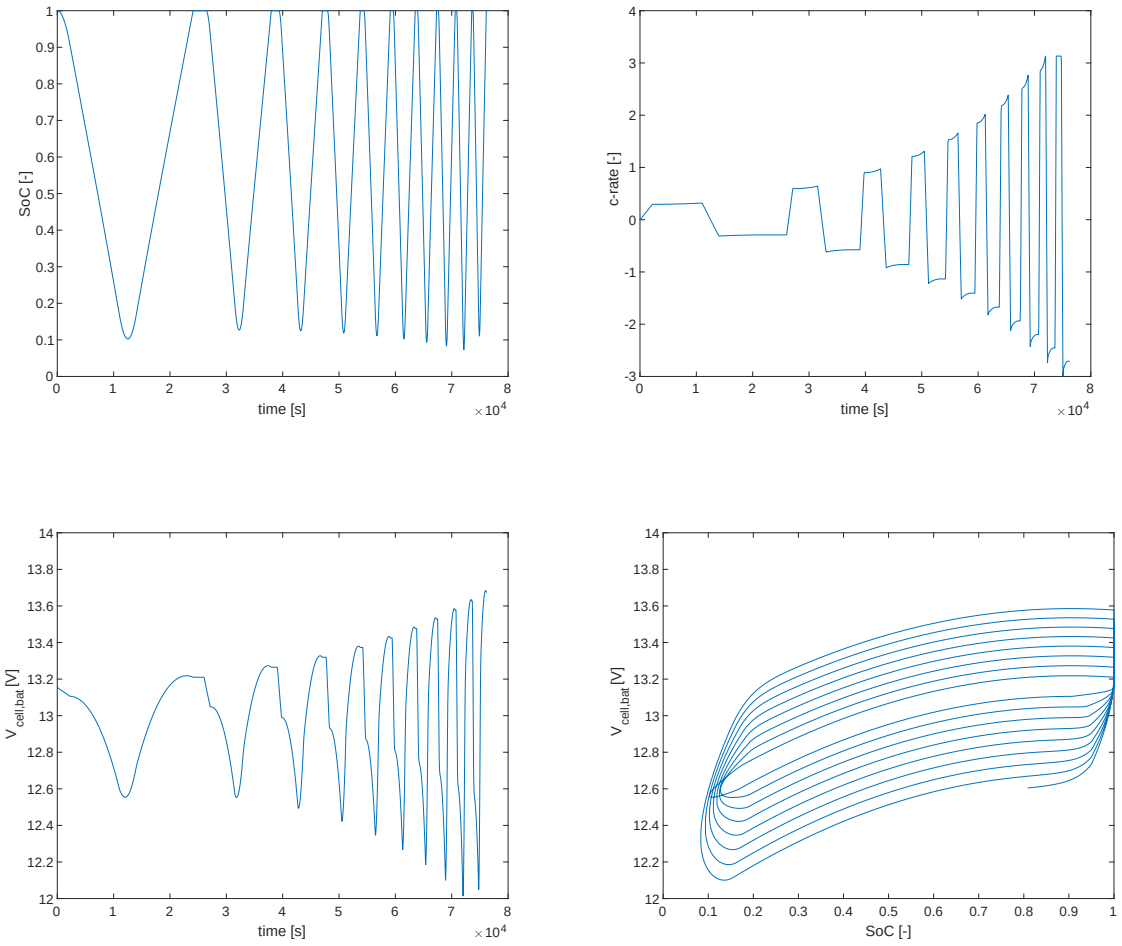


Figure 6.6: Battery cell cycles for different c-rates. Top-left to bottom-right: Evolution of the state of charge of the battery cell, $SoC$ as a function of time, evolution of the c-rate, evolution of the battery cell voltage, $V_{cell,bat}$, and plot of the $V_{cell,bat}$ against the $SoC$. The cycles where made in such a way so that different (dis)charging c-rates can fully deplete (SoC=0.2) and then fully charge the battery, while the electrochemical efficiency has been also calculated from this procedure, shown in Figs. (6.7,6.8)

approximation (See also Figs. 6.7,6.8). It is noted that the residuals do not affect the online implementation, as it can be seen in Fig 6.14:

$$\eta_{ech} = \begin{cases} c_1 + c_2 \cdot SoC + c_3 \cdot P_{norm} + c_4 \cdot SoC^2 + c_5 \cdot P_{norm} \cdot SoC + c_6 \cdot P_{norm}^2 & , \ P_{norm} \geq 0 \\ c_7 + c_8 \cdot SoC + c_9 \cdot P_{norm} + c_{10} \cdot SoC^2 + c_{11} \cdot P_{norm} \cdot SoC + c_{12} \cdot P_{norm}^2 & , \ P_{norm} < 0 \end{cases} \tag{6.12}$$

where $P_{norm} = P_{cell,bat}/P_{cell,max}$ and $c_i, \ i \in [1, 2, ..., 12]$ the fitting coefficients.

The open circuit voltage $V_{cell,open}$ is found with Eq. (4.55), as a function of the state of charge $SoC$, and with the electrochemical efficiency $\eta_{ech}$ and Eq. (4.54) the $V_{cell,bat}$ can be found:

$$V_{cell,bat} = V_{cell,open} \cdot \eta_{ech}^{sgn(P_{bat})} \tag{6.13}$$

Now everything in Eq.(4.56) is known, and the current of the battery cell, $I_{cell,bat}$, can be calculated:

$$I_{cell,bat} = \frac{P_{bat}}{n_{ser} \cdot n_{par} \cdot V_{cell,bat}} \tag{6.14}$$

Finally, the next state of charge of the battery cells $SoC(t + \Delta t)$ can be expressed explicitly as:

$$SoC(t + \Delta t) = SoC(t) - \frac{I_{cell,bat} \cdot \Delta t}{Q_{cell,0}} \tag{6.15}$$

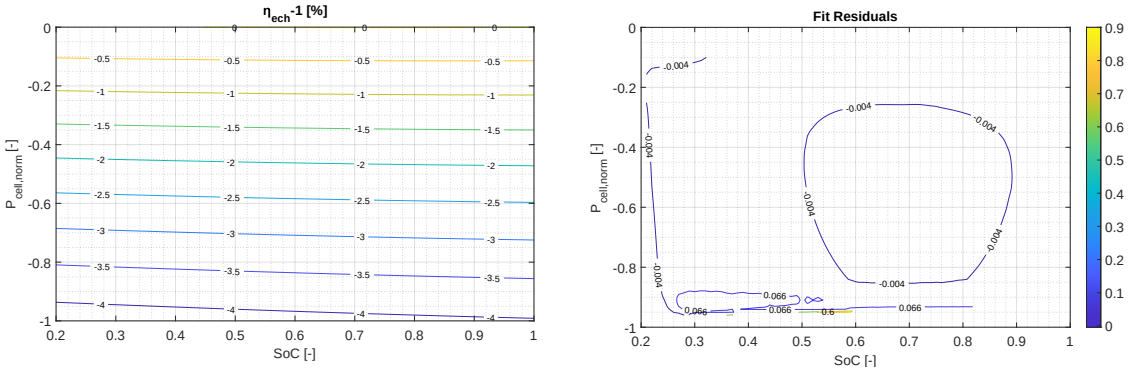


Figure 6.7: Polynomial fit for the electrochemical efficiency when charging minus one, $\eta_{ech} - 1[\%]$ as a function of the normalised cell power $P_{cell,norm}$ and state of charge $SoC$. R-square: 0.9996. Note that only a small region for maximum charging current at the region close to $SoC = 0.55$ presents significant residuals. (Positive values: overestimation)

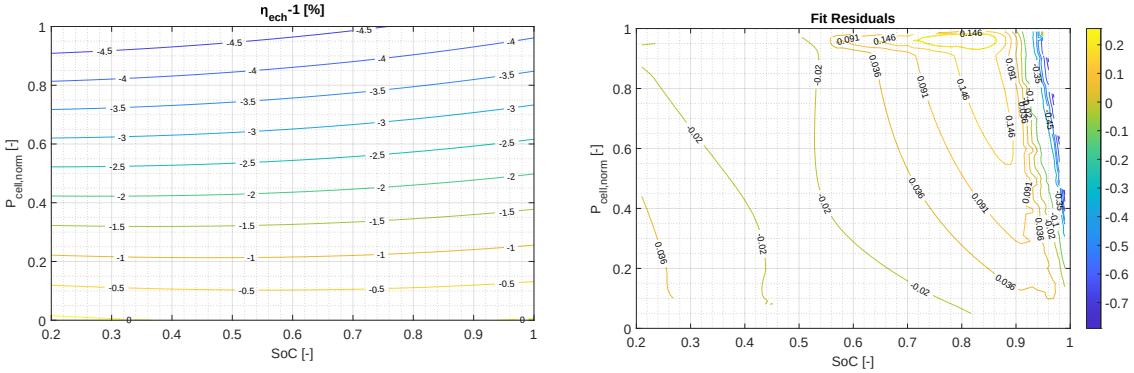


Figure 6.8: Polynomial fit for the electrochemical efficiency when discharging minus one, $\eta_{ech} - 1[\%]$ as a function of the normalised cell power $P_{cell,norm}$ and state of charge $SoC$. R-square: 0.9956. Note that the region close to $SoC = 1$, especially at high power outputs, presents significant residuals, however in the implementation, the agreement is satisfactory. Since negative values stand for underestimation, the residuals are on the safe side, and should steer the controller away from this region.

## 6.2 Verification of the Reduced Component Description

In this section the results of the offline reduced component description, formulated in the previous section, are plotted against the online dynamic model counterparts, in order to demonstrate that the reduced description is indeed sufficient for steady-state use. A variety of setpoints are used for a profile trajectory of 3000 $[s]$. From Figs. 6.9-6.14 it can be concluded that all components are described with satisfactory accuracy.

It is important to note that, between $t = 1500$ $[s]$ and $t = 2300$ $[s]$, the chattering effect noticed in Figs. 6.10-6.11 is created by the offline reduced model, and the corresponding setpoints given to the online model, discussed in Sec. 7.1.2. Even in the chattering region, the offline and online behaviour are very close, which shows that the component reduction demonstrate very good agreement with the dynamic model, even in transient areas (to an extend). In fact, the biggest difference is noticed in 6.11, around 800 $[s]$, and is still low, at approximately 2.7%, and only for a relatively short duration of 200 $[s]$. This is expected as the generator power accumulates all of the residuals, as it is calculated from the electric balance equation in both the online and offline model.

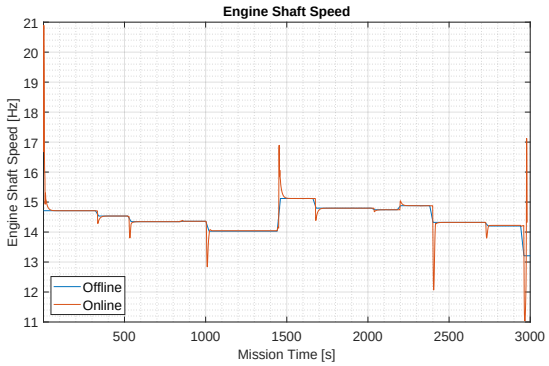


Figure 6.9: Engine Shaft Speed

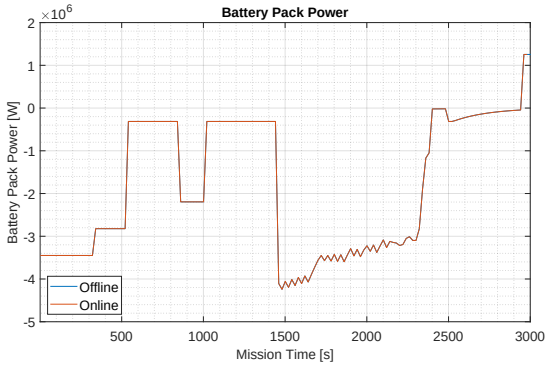


Figure 6.10: Battery Power

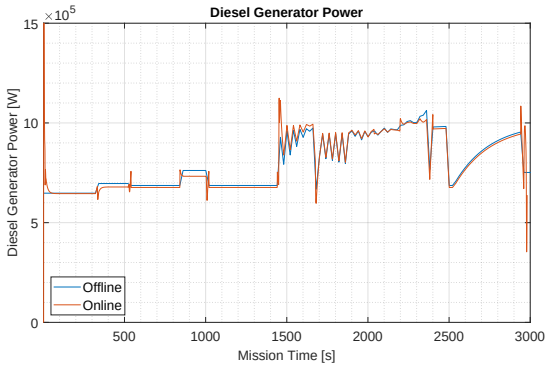


Figure 6.11: Power of Diesel Generator Sets

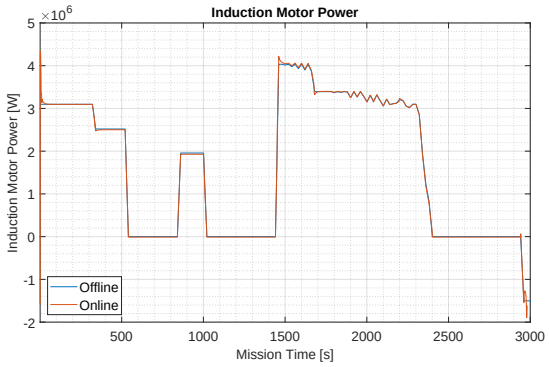


Figure 6.12: Power of induction machine

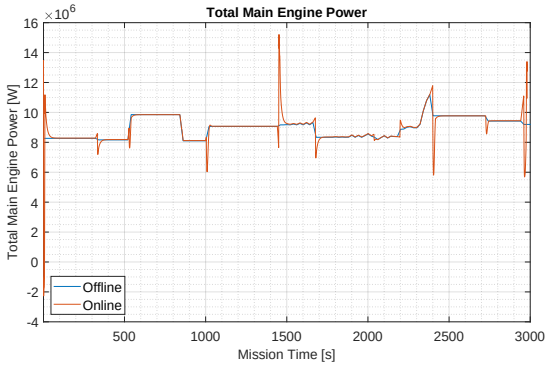


Figure 6.13: Power of Main Engine

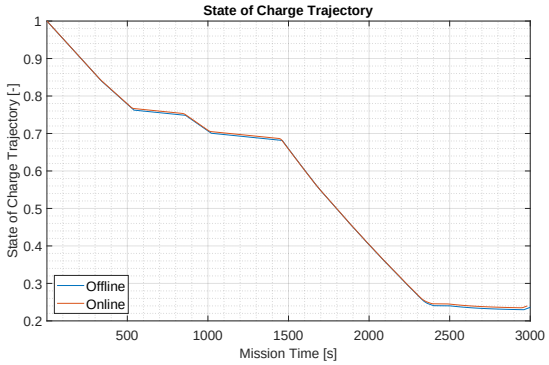


Figure 6.14: State of Charge

# Chapter 7

# Case Study: Framework Verification and Validation

In the following section the proposed EMS strategy implemented on the vessel, is verified and validated. Firstly, the controller framework has to be submitted to a number of verification tests to ensure that it behaves as expected. The second part entails the incorporation of the controller framework in the vessel's powertrain, and its performance in realistic mission scenarios.

## 7.1 Model Verification

The same model description, and the same solver are used twice in the framework:

- in the reference trajectory generation, which is utilising Dynamic Programming to solve the Optimal Control Problem under the assumption of a certain disturbance sequence,
- in the Model Predictive Controller, that is doing the same procedure but for every time step, in a receding horizon fashion

For this reason, in this section the results of the Dynamic Programming coupled with the given model description are assessed in order to ensure they behave as expected, and to identify any potential limitations. Moreover, the receding horizon performance is also verified. At last, in this phase the solver's parameter are decided, taking into account accuracy and computational considerations.

A recap of the model description equations are iterated here for convenience. In parentheses, it

is noted on which input, disturbance, or state, a quantity depends:

$$\begin{aligned}
\mathbf{u} &= [M_{PTO/I,n}\ I_{bat,AC,n}]^T \\
\mathbf{x} &= [SoC\ NoE]^T \\
\mathbf{r} &= [n_P\ P_{prop}\ P_{hotel}]^T \\
\mathbf{y} &= [P_{gen}\ P_B] \\
P_B &= \frac{P_{prop}}{k_p} - P_{IM}(M_{PTO/I,n}) \\
\sum_{i=1}^{NoE} P_{DG} &= P_{hotel} + (P_{IM}(M_{PTO/I,n}) + P_{IM,loss}(M_{PTO/I,n}, n_P) \cdot k_p + P_{bat,AC}(I_{bat,AC,n}) \\
\dot{SoC} &= \frac{I_{cell,bat}(I_{bat,AC,n}, SoC)}{Q_{cell,0}}
\end{aligned} \tag{7.1}$$

while the cost functional, J, is:

$$J = \sum_{t=1}^{t=N\Delta t} \{\dot{m}_{f,B}(P_{prop}, M_{PTO/I,n}) + \sum_{i=1}^{NoE} P_{DG}(P_{hotel}, M_{PTO/i,n}, I_{bat,AC,n}) + \mu \cdot \delta NoE\} \tag{7.2}$$

and the inequality constraints are:

$$\begin{aligned}
0.45 \cdot P_{B,MCR} \leq P_B \leq 0.95 \cdot P_{B,MCR} \wedge P_B \leq 0.95 \cdot P_{B,max,TB}(n_B) \\
SoC_{min} \leq SoC \leq SoC_{max} \\
0.3 \cdot M_{PTO/I,n,max} \leq |M_{PTO/I,n}| \\
0.2 \cdot P_{DG,nom} \leq \sum_{i}^{NoE} P_{DG} \leq \sum_{i}^{k_{DG}} P_{DG,nom}
\end{aligned} \tag{7.3}$$

### 7.1.1 Computational Considerations

It is noted that the term $\mu \cdot \delta NoE$ of the cost functional is optional and, together with the additional state, $NoE$, has not been used due to its computational burden and the limitation of the DP algorithm [98] to only one state variable when the Boundary Line option is chosen (See Sec. 7.2.2). Furthermore, the boundaries regarding the component operating limits are decided after occasional or consistent undesirable behaviour of the components in the online model. The discretisation of the control inputs and state, $N_u$ and $N_x$, correspondingly, where chosen to be 41 as a fair trade-off between computational effort and results. An odd number is important to be able to include exactly the zero setpoints for the induction machine torque and battery output. As demonstrated in [110], the performance of the DP solver is sensitive to these discretisation numbers and a consistent convergent analysis is not possible due to case specific differences observed.

On another note, the combinator curve is considered to be the same throughout the whole mission for the following verification tests, which allows for the calculation of the propulsive load $P_{prop}$ and shaft speed $n_p$ disturbances to be fully defined by the virtual shaft speed $N_{virt}$, and, subsequently, by

the rack position. This also allows for the disturbances to be calculated only once for every Dynamic Programming code run, as opposed to carrying out such a calculation inside the model's description routine, thus, reducing computational costs. Finally, since the end goal of the controller is to utilise human input regarding future load alterations, a single telegraph position input is appropriate.

### 7.1.2 Fuel Consumption Consistency

The first verification test concerns the consistency of the DP and model description results, in terms of yielding the correct fuel consumption, for the case of a baseline load, a 10% increase of the telegraph, and a 10% decrease of the telegraph, with a constant hotel power demand of 1000 $[kW]$. The battery is operating in plug-in mode, while the hotel demand is well below the design point.

Table 7.1: Results of Dynamic Programming for a baseline load $-+10\%$

| **Profile** | **Consumption [kg]** |
|---|---|
| Base | 1974.3 |
| $-10\%$ | 1908.1 |
| $+10\%$ | 2085.5 |

As demonstrated in Table 7.1 and Figs. 7.1, 7.2, 7.3 the results are consistent, and the decreased load case yields a 3.35% reduction in fuel consumption, while the increase yields a 5.63% increase in fuel consumption. The bigger change for load increase with the same rack position difference is expected, as rack position is linked to shaft speed, and the curve in Fig. 6.3 yields increasingly more power demand at consecutive increments.

It can be seen in all cases that the induction machine is active when the battery is active, meaning the the electric pathway from the battery to the propeller shaft via the motor is preferred, over the more inefficient path from the gensets to the motor, as expected.

The fact that the hotel loads are way bellow the design point can be seen by how far the setpoints are from the fuel consumption minimisation area of the main engine at the $6.5 - 8.5$ $[MW]$ region, and by the fact that only one diesel engine is running. At the end of the mission the battery is fully depleted, which means that, even at that low load and the safety requirement for the main engines and one generator engine to be always on, the battery capacity is way too small to not activate the end-state constraint (See discussion in Sec.3.3 for battery sizing).

Finally, at baseline and increased load, a *chattering* behaviour is observed, which should not be acceptable in on board applications, and should be dealt with in order to reduce strain on the various components of the powertrain. It appears that increasing the threshold torque for the PTI helps with this behaviour (indeed, by increasing the minimum allowable torque to 40% of the max eliminates this), although other approaches, such as penalising such variations with the *var* operator

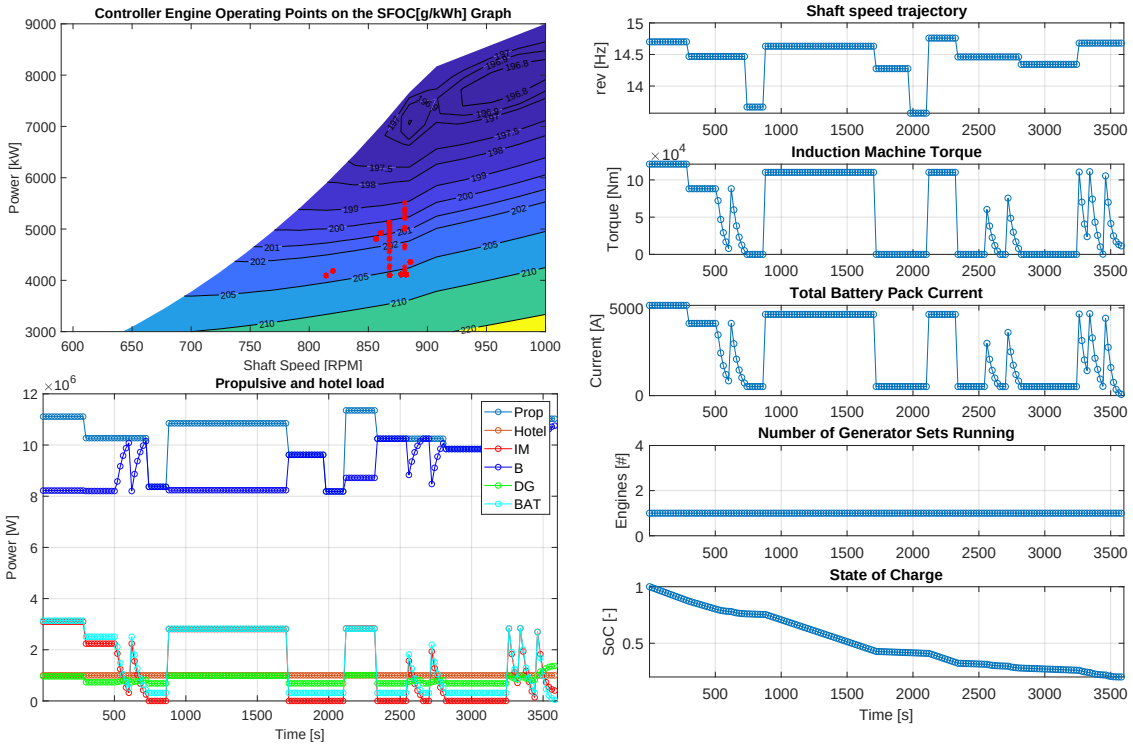


Figure 7.1: Baseline load consumption result details

in the cost functional [124], might also be effective. Nonetheless, since an increase of the minimum torque to 40% was sufficient to eliminate the problem, without affecting the consumption in this specific load profile.

### 7.1.3 Boundary Consistency

Since more stringent boundaries to the problem reduce the search space of the solution paths, introducing more boundaries or smaller operating windows for the components in the powertrain should increase fuel consumption, while relaxing the boundaries should yield a fuel consumption decrease. The same base load of the previous tests has been used.

As expected, an increase in the minimum allowable engine power $P_{B,min}$ from $0.45\%P_{MCR}$ to $0.5\%P_{MCR}$, increases the fuel consumed from 1974.3 $[kg]$ to 2055.1 $[kg]$, an increase of 4.09%. From the results shown in Fig. 7.4, it can be seen that the increase obligates the controller to run the induction motor as a PTO in the lower propulsive demand periods, in order to satisfy the new main engine envelope boundaries.

Increasing the lower limit of the induction machine torque $M_{PTO/I,min}$, from 0.3 to 0.5 of the maximum, yields an increase to 2056.7 $[kg]$ in fuel consumption (4.17%). In Fig. 7.5, the limitation clearly takes effect, with the induction machine online working only at the top torque portions.

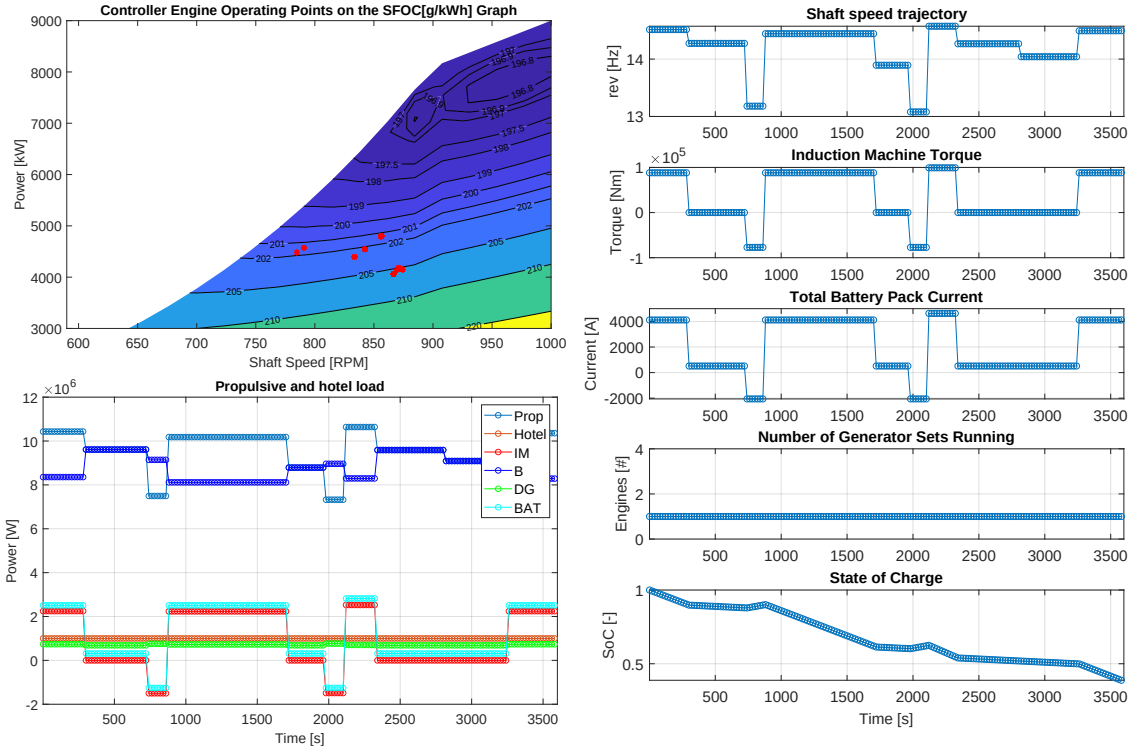


Figure 7.2: Reduced load consumption result details

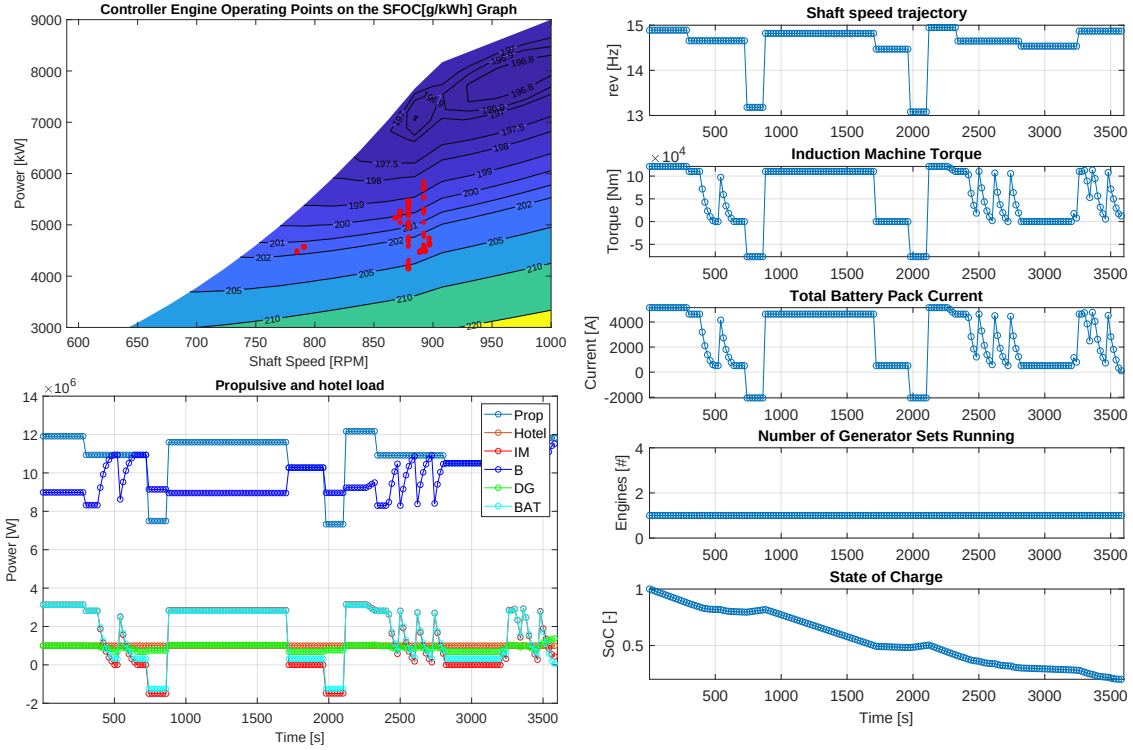


Figure 7.3: Increased load consumption result details

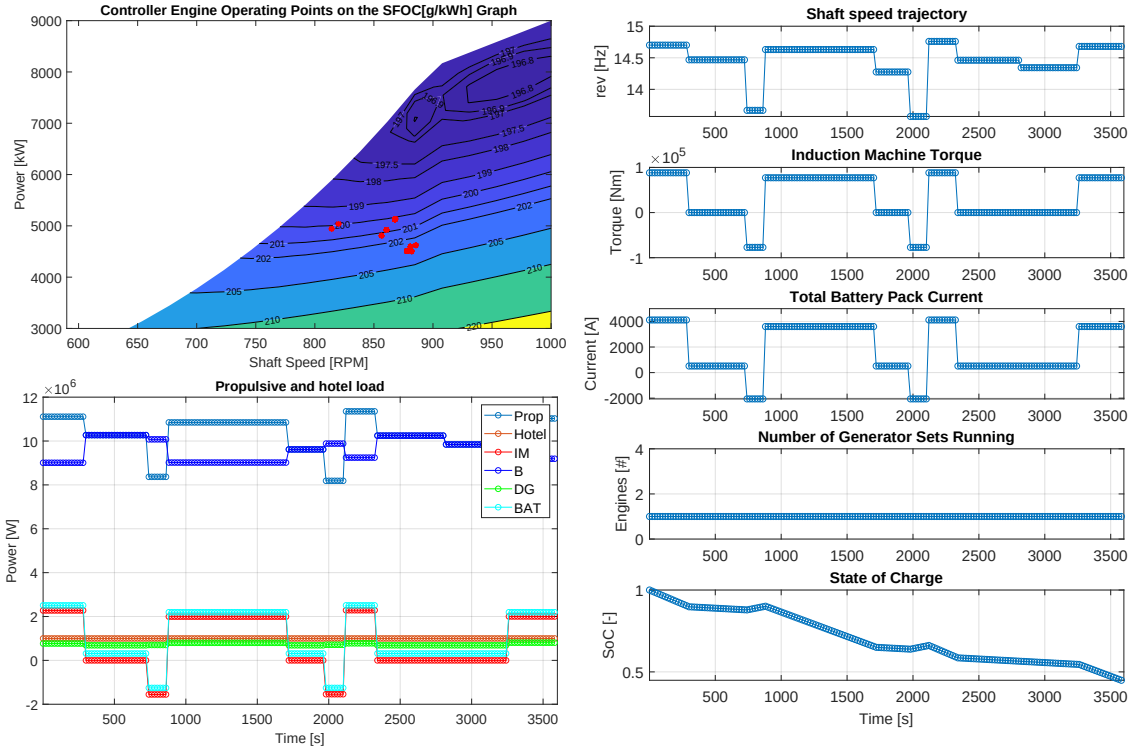


Figure 7.4: Increased $P_{B,min}$ from 0.45%$P_{MCR}$ to 0.5%$P_{MCR}$, result details

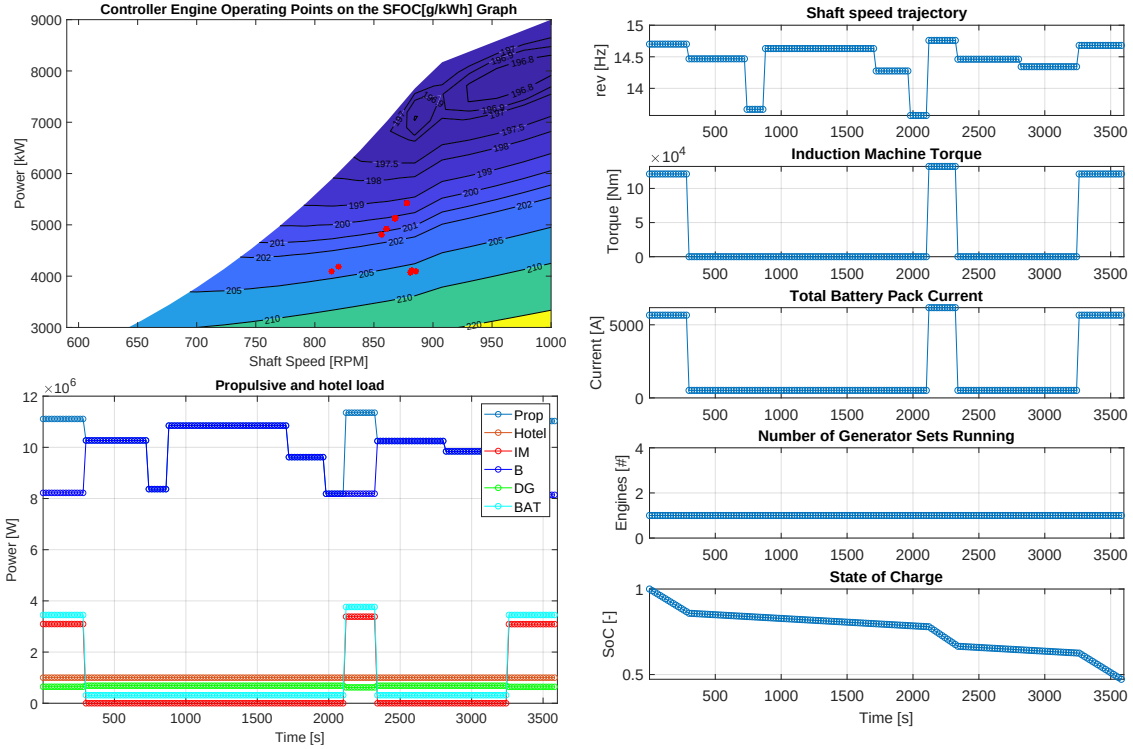


Figure 7.5: Increased $M_{PTO/I,min}$ from 0.3 to 0.5 of maximum torque, result details

### 7.1.4 MPC Framework Verification

The MPC framework is implemented offline here, meaning that the update of its states are essentially sampled from the reduced model description using the MPC control input setpoints, as opposed to an online implementation where the samples are taken from the physical system or dynamic model. Furthermore, the disturbances are kept the same for the long term and the short term solution, as, otherwise, they would add another dimension of complexity that seems to be unnecessary in an offline verification. Since the reduced model is accurate enough, this setup was found to be sufficient to verify the MPC behaviour, and decide on its parameters. The MPC framework algorithm has been explained in detail in Sec. 5.2. Nonetheless, the key points and the corresponding block diagrams (Fig. 7.7,7.6) are also provided here for convenience:

- The full mission solution is generated from a DP solution, using i) a long-term disturbance estimation, $\mathbf{r}_{1...N}$, and ii) the reduced vessel model
- For a set control horizon that is significantly smaller than the full mission length, $N_c << N$, at each time step $k$, using i) a short-term disturbance estimation $\mathbf{r}_{k...Nc}$, ii) the reduced vessel model[1], iii) the current sampled state $\mathbf{x}_k$, and iv) the reference state at the end of the horizon, $x_{ref,Nc+1}$, a DP solution is found, and only the control inputs, $\mathbf{u}_{k+1}$, for the next time step, $k+1$, are fed to the system, while the other generated control inputs $\mathbf{u}_{k+2...Nc}$ are scrapped. The end-state constraint is Eq. (5.22):

$$|SoC(k + N_p \cdot \Delta t) - SoC_{ref}(k + N_p \cdot \Delta t)| \leq E$$

- In the online implementation, the control inputs, $\mathbf{u}_{k+1}$, are fed to the powertrain, and the resulting state, $x_{k+1}$, is sampled from that powertrain, acting as a feedback from the actual system.
- The procedure is iterated, by setting the new time step $k = k+1$. To enable online **long-term feedback**, if there is a new long-term disturbance estimation, a new full mission solution is generated and the procedure starts again, from the first step of this list.

The main parameters, which are to be decided here according to the framework's performance, are the horizon length $N_c$, the discretisation of the grid of the short-term DP solution for every MPC step, and the window parameter, $E$, of the end state constraint Eq. (5.22).

Starting from the same discretisation for the control input and state grids as the one of the long-term DP, $N_u, N_x = 41$, the window parameter, $E$, is decided first. This parameter is very critical, as if it is too small, the DP problem for the MPC step $k$ might not have a feasible solution path, and the controller crashes. After trial and error, a value of $E = 0.01$ was found to be the minimum

[1] that is not necessarily the same as the one used in the long-term DP

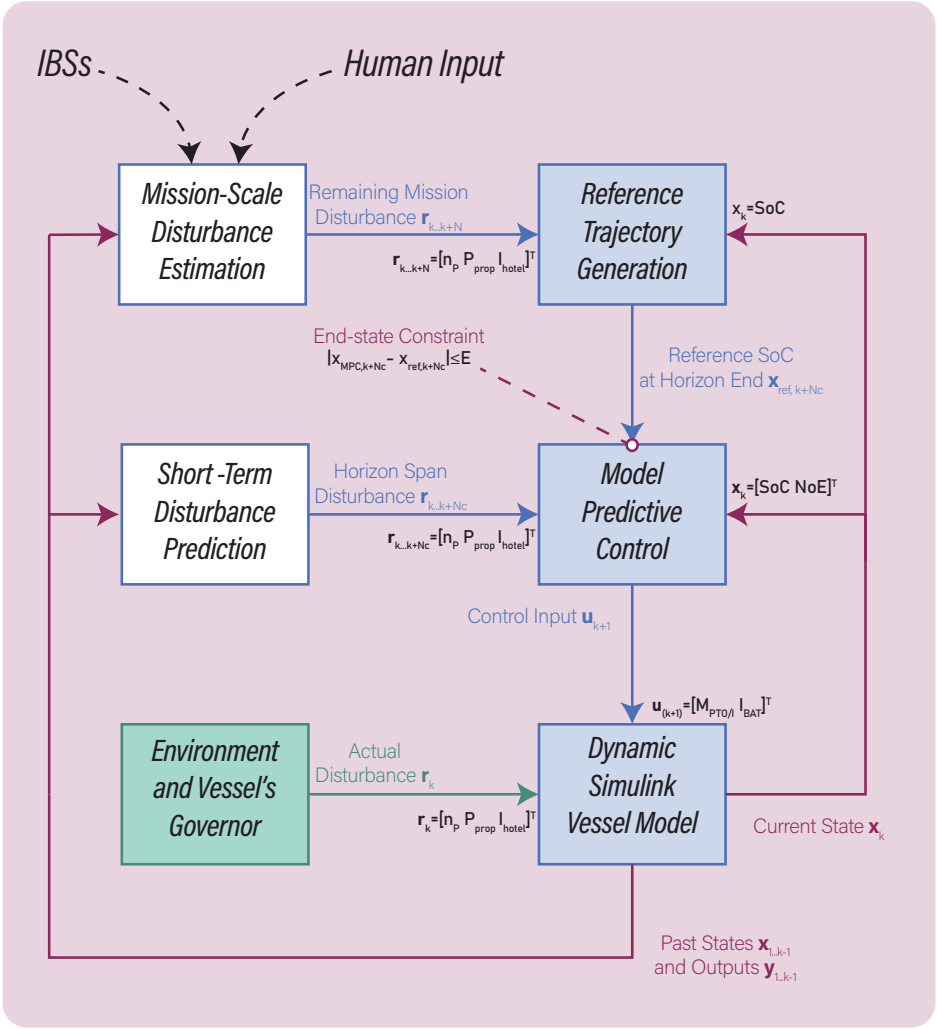


Figure 7.6: The Model Predictive -based, prediction enabled, Energy Management Control framework. In the figure the data routes are depicted for time step $k\Delta t$, adapted from [65]

stable value that still allows for the existence of feasible solutions in a variety of operating loads. It is noted here that, if the grids are denser $N_u, N_x = 61$, the minimum value is found to be $E = 0.007$, which is an expected behaviour as a finer grid would create more possible solution paths, allowing for the end constraint window to be smaller.

## Control Horizon Length

To decide on the appropriate control horizon length, $N_c$, the base load used previously is fed into the full mission DP solver. Then, the MPC controller utilises the results, for an experiment span of 800 $[s]$ with varying control horizon lengths $N_c$.

In Figs. 7.8-7.12, the results of the MPC framework are shown. It is found that for a control

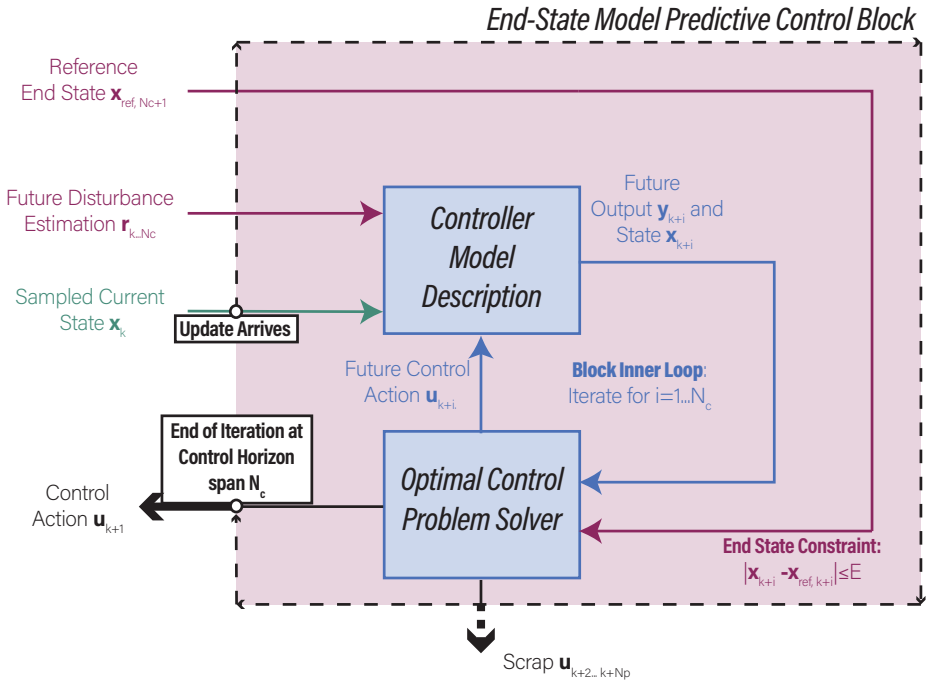


Figure 7.7: End-state constraint approach with a cost functional that includes only the minimisation term. The actions and data flows that are being iterated over the horizons (predictive and control, respectively) are shown in blue. Adapted from [112]

horizon of 600 $[s]$ the MPC framework performs exceptionally, with almost zero deviation from the global solution.

The cyan lines indicate the optimal path trajectories of the DP for every MPC time step. In the $N_c = 600$ $[s]$ case, the cyan lines show that the end portion close to the horizon end, does not necessarily fall close to the optimal solution in order to yield an output for $k+1$ that does agree with the optimal solution. The findings here are a perfect example of the discussion regarding the superior capabilities of an end-constraint tracking MPC, as opposed to a traditional setpoint tracking MPC, in Sec. 5.3.3.

Regarding the various control horizon lengths in more detail:

- $N_c = 40$ $[s]$: The control step is 20 $[s]$ which means that there are only 2 stages for the DP solution. The setpoints fail to follow the optimal path and oscillate, even when no step change is made. There is a noticeable deviation at the end SoC as well.

- $N_c = 100$ $[s]$: While the initial oscillation has stopped, when the step at 300 $[s]$ occurs, the controller not only fails to follow the optimal path, but also begins an unstable behaviour. The SoC discrepancy is even bigger than before.

- $N_c = 200$ $[s]$: The results are very similar to the previous case, with somewhat faster correction of the instabilities.
- $N_c = 400$ $[s]$: The behaviour is noticeably better, however, the battery and genset power after 300 $[s]$ still behave suboptimally.
- $N_c = 600$ $[s]$: The behaviour is optimal, both in the step up and the step down responses, while absolutely no instability is noticed.

It is noted here that sometimes the optimal global solution show regions where chattering occurs, as previously demonstrated in the DP verification tests. Around these regions, MPC has been shown to not follow exactly the global solution, however, when that happened the consumption deviations were measured to be negligible. A conjectured explanation for this phenomenon is that such chattering occurs when two paths are almost equally optimal.

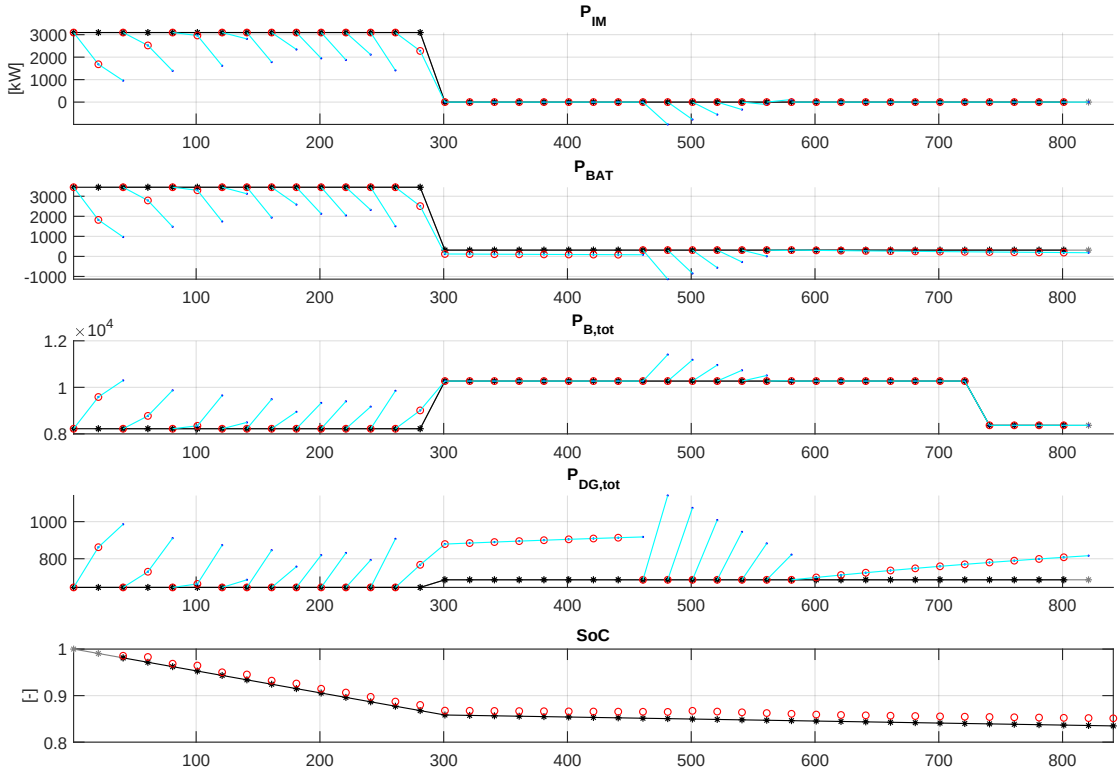


Figure 7.8: MPC with control horizon $N_c = 40$ $[s]$, power distribution (from top to bottom: Induction Motor, Battery Pack, total Main Engine, total Diesel Generator) and SoC (bottom last). The red circles indicate the outputs of the MPC for the next step $k+1$. The cyan lines ending at a blue dot indicate the path of the MPC solution $(k+1...N_c)$ at each time step $k$ that gets discarded. The black stars indicate the optimal output, while grey indicate the future optimal output that is after the experiment end (which is equal to the horizon length). For the SoC graph (bottom) the red circles indicate how close to the reference (black stars) the end state of the MPC solution is, while the gray stars showcase the control horizon span at the beginning.

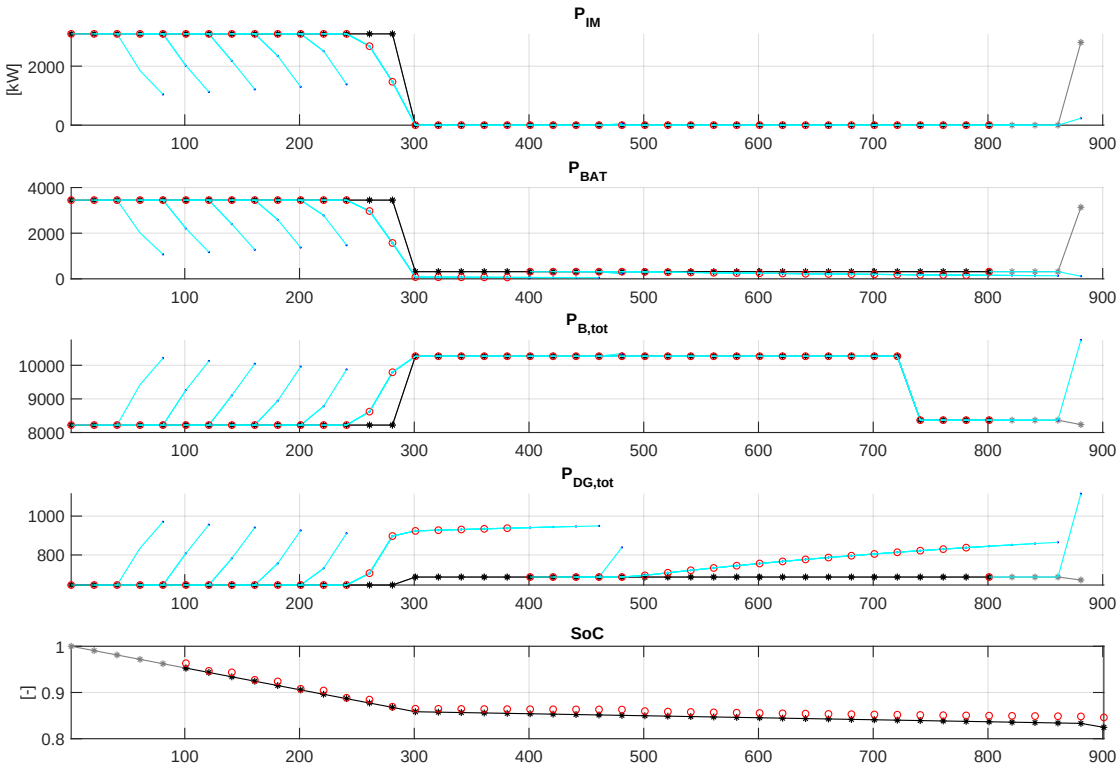


Figure 7.9: MPC with control horizon $N_c = 100$ $[s]$, power distribution (from top to bottom: Induction Motor, Battery Pack, total Main Engine, total Diesel Generator) and SoC (bottom last). The red circles indicate the outputs of the MPC for the next step $k + 1$. The cyan lines ending in a blue dot indicate the path of the MPC solution $(k + 1...N_c)$ at each time step $k$ that gets discarded. The black stars indicate the optimal output, while grey indicate the future optimal output that is after the experiment end (which is equal to the horizon length). For the SoC graph (bottom) the red circles indicate how close to the reference (black stars) the end state of the MPC solution is, while the gray stars showcase the control horizon span at the beginning.

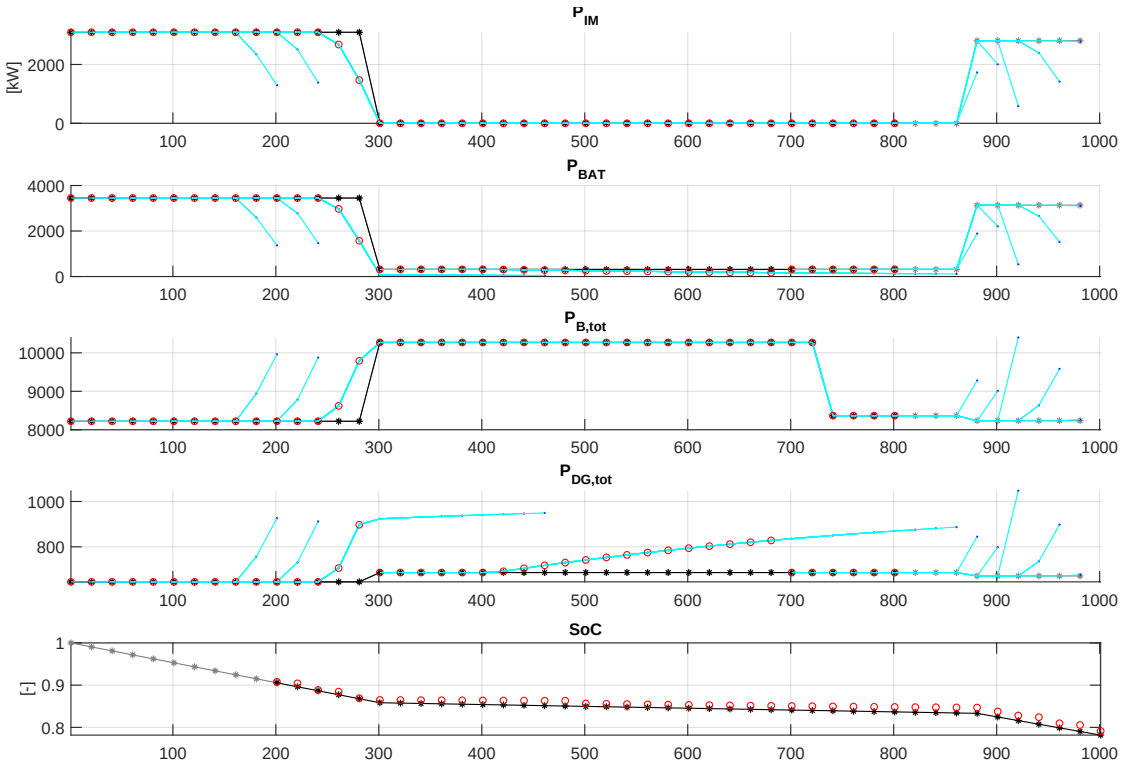


Figure 7.10: MPC with control horizon $N_c = 200$ $[s]$, power distribution (from top to bottom: Induction Motor, Battery Pack, total Main Engine, total Diesel Generator) and SoC (bottom last). The red circles indicate the outputs of the MPC for the next step $k+1$. The cyan lines ending in a blue dot indicate the path of the MPC solution $(k+1...N_c)$ at each time step $k$ that gets discarded. The black stars indicate the optimal output, while grey indicate the future optimal output that is after the experiment end (which is equal to the horizon length). For the SoC graph (bottom) the red circles indicate how close to the reference (black stars) the end state of the MPC solution is, while the gray stars showcase the control horizon span at the beginning.

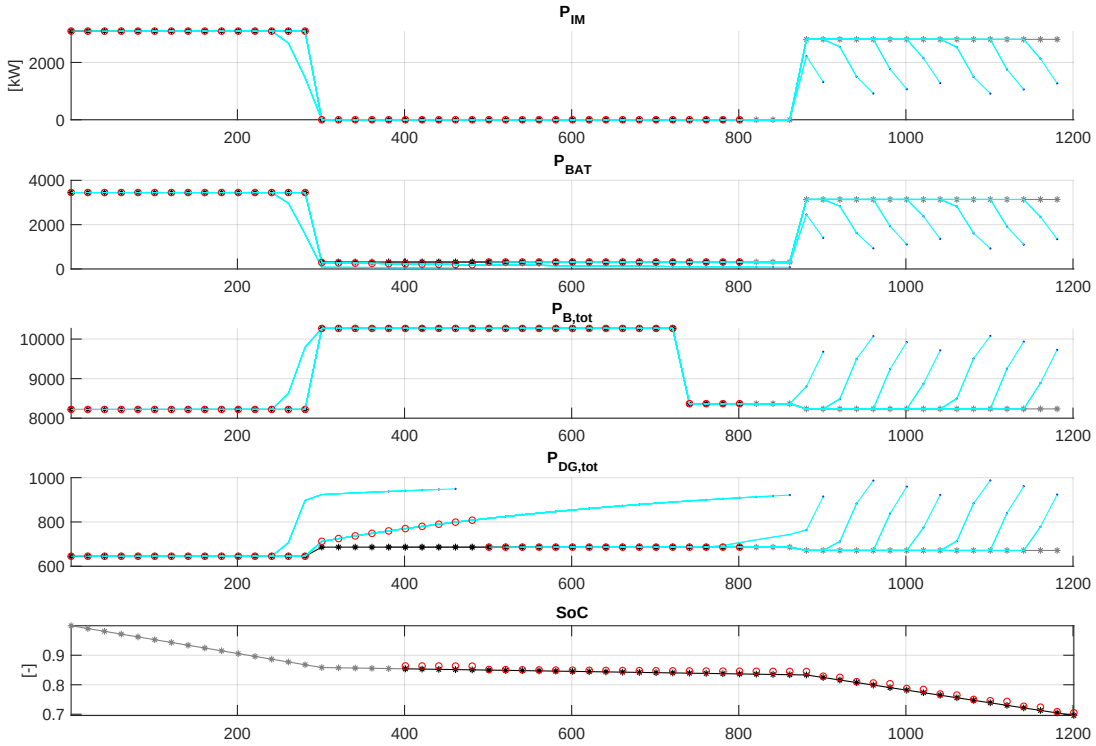


Figure 7.11: MPC with control horizon $N_c = 400$ $[s]$, power distribution (from top to bottom: Induction Motor, Battery Pack, total Main Engine, total Diesel Generator) and SoC (bottom last). The red circles indicate the outputs of the MPC for the next step $k + 1$. The cyan lines ending in a blue dot indicate the path of the MPC solution $(k + 1...N_c)$ at each time step $k$ that gets discarded. The black stars indicate the optimal output, while grey indicate the future optimal output that is after the experiment end (which is equal to the horizon length). For the SoC graph (bottom) the red circles indicate how close to the reference (black stars) the end state of the MPC solution is, while the gray stars showcase the control horizon span at the beginning.

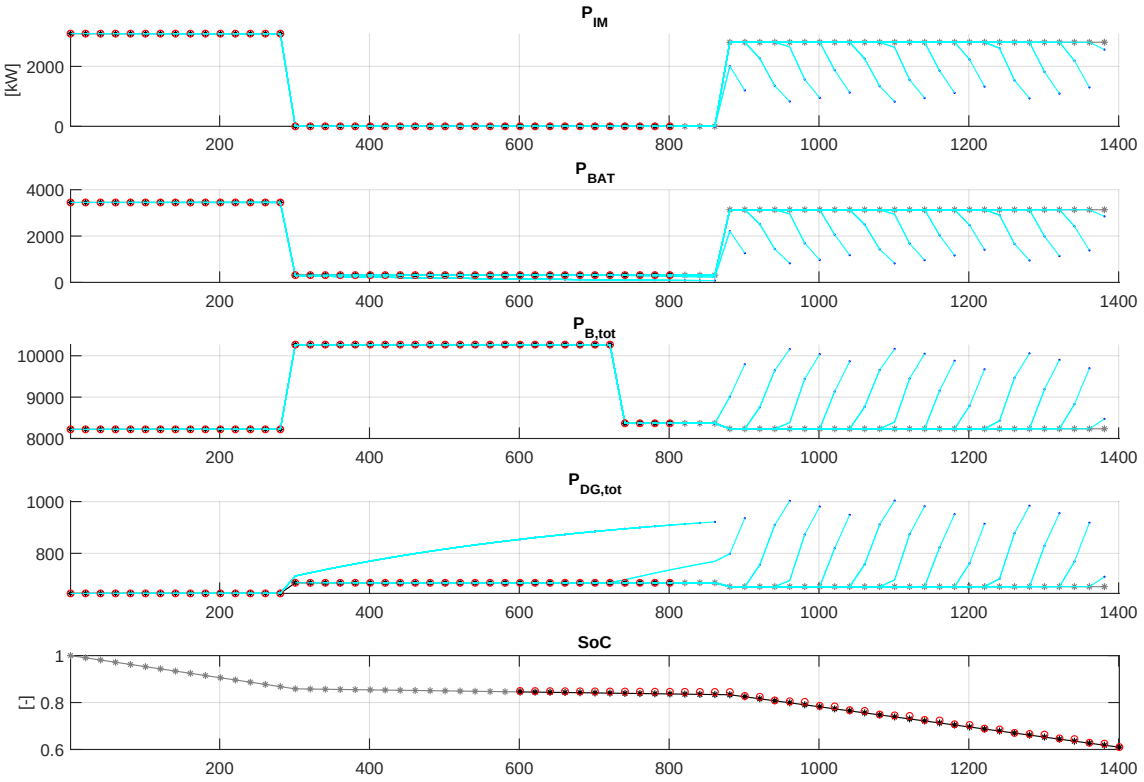


Figure 7.12: MPC with control horizon $N_c = 600$ $[s]$, power distribution (from top to bottom: Induction Motor, Battery Pack, total Main Engine, total Diesel Generator) and SoC (bottom last). The red circles indicate the outputs of the MPC for the next step $k+1$. The cyan lines ending in a blue dot indicate the path of the MPC solution $(k+1...N_c)$ at each time step $k$ that gets discarded. The black stars indicate the optimal output, while grey indicate the future optimal output that is after the experiment end (which is equal to the horizon length). For the SoC graph (bottom) the red circles indicate how close to the reference (black stars) the end state of the MPC solution is, while the gray stars showcase the control horizon span at the beginning.

## 7.2 Validation

In this section the EMS control framework is integrated in the Simulink® model of the vessel, provided by DAMEN® in order to validate its performance. As discussed in Sec. 5.3.3, the disturbance estimators are not the focus of the present study, however, realistic load conditions have been utilised, and the performance has been benchmarked against exhaustive solutions, and has proven its strict superiority over any other EMS that does not have a pathway to utilise online long-term information regarding the future disturbances.

### 7.2.1 Realistic Vessel Operating Profiles

From provided historical data of the vessel's missions, a probability density function has been made for the telegraph position. The distribution is shown in Fig. 1 of the Confidential Appendix.

This distribution is used to create realistic mission profiles, by randomly creating a sequence for the rack position, for mission lengths of 3600 $[s]$. These profiles are used throughout the verification and validation section to ensure that the loads on the vessel's powertrain are realistic.

With a constant combinator curve and propeller curve (See Sec. 6.1.1), the propulsive power load demand and the shaft speed can be found just from the telegraph position. If not stated otherwise, a hotel power load of 1000 $[kW]$ is used. From all the above, a realistic disturbance vector for an 1 $[hr]$ long mission, $r_{1...N} = [n_P \ P_{prop} \ P_{hotel}]^T$ is generated, in order for the controller to be benchmarked.

### 7.2.2 Information Barrier Validation

As it has been previously discussed in 5.3.3, in order for the framework's performance to be validated, an exhaustive optimal solution without online update capabilities is used as a benchmark solution, from now on referred to as *information barrier optimal* (or barrier) controller solution. Such a benchmark solution is better than any other causal controller, including ECMS, A-ECMS, or other, as it assumes that for each portion of the mission, perfect information is available, and the solution is acausal and exhaustive, found via DP.

This approach is essentially giving the barrier controller, which has no available information pathway for long-term disturbance updates, its "best chance". The benchmark barrier controller has perfect information and acausal optimality (DP solution), up until an information barrier, and after that information barrier, again, perfect information and acausal optimality until the end of the mission.

For the suggested MPC framework each control horizon length is assumed to have perfect information. However, such an assumption would still allow the MPC framework to prove its strictly superior performance if the following are true:

- the MPC framework performs better than the barrier controller
- the short-term predictor is strictly more accurate than the long-term prediction, which should, of course, be true

The online implementation of the MPC framework consists of a long-term SoC trajectory generator, which solves the long-term disturbance and provides the reference state of charge throughout the mission, $SoC_{ref,1...N}$, and the MPC, which, at time $k$, samples the $SoC_k$ from the dynamic model and solves for the control horizon $N_c$, using the $SoC_{ref,k+N_c+1}$ to constrain its end-state $SoC_{k+N_c+1}$. The MPC controller yields the control inputs $\mathbf{u} = [M_{PTO/I} \ I_{bat,AC}]^T$ for the next time step $k+1$, and feeds it to the dynamic model.

The long-term SoC is yielding a new reference trajectory, $SoC_{ref,k...N}$, every time step $k$, when new information for the long-term disturbances $\mathbf{r}_{k...N}$ is available. The MPC controller is then utilising this update via its end-state constraint.

The experiments have a final horizon zone that is not taken into account. Although an implementation where the MPC yields its results for the remaining setpoints is possible, extending the experiment to include this final horizon is of little use. With that being said, the offline trajectories for the full mission are also given, in order to show potential high activity in that region.

Finally, the second benchmark controller utilised is an optimal DP controller with full information about the actual mission load, and which is expected to yield better results than both the MPC framework controller and the barrier controller.

In more detail regarding the Simulink® implementation, the DP algorithm in the MPC controller is being solved with a *Boundary Line* method [109], in order to effectively enforce the end-state constraint. However, the algortihm does not allow for the Boundary Line option if there are more than one state variables. For that reason, the "number of active diesel engines" variable, $NoE$, was excluded. Nonetheless, this does not affect the results for most realistic load cases, as the hotel load data given for the test cases are low enough that can be covered entirely by one diesel generator set. Thus, no frequent turning on/off effect is observed anyways.

The MPC framework is validated below, utilising realistic operating profiles generated with the procedure described above, in Sec. 7.2.1. An information barrier is present at time $t_{bar} = 2400$ $[s]$, where a considerable change in propulsive load takes place, compared to the initial estimation. A feedback update regarding the barrier becomes available to the MPC framework at time $t_{upd} = 600$ $[s]$. The experiment is terminated at the final horizon time, $t_{fh} = 2980$ $[s]$.

### 7.2.3 Plug-in Mode

The MPC framework functions in charge-depleting mode, starting at a state of charge, $SoC = 1$, and allowing for any end-state, $SoC \in [0.2\ 1]$.

#### Profile 1

For the first validation case the resulting SoC trajectories are given in Fig. 7.15. The MPC is following a trajectory between the the DP and barrier controller results, while the update point at 600 $[s]$ clearly affects the optimal path. More importantly, the fuel consumption reduction with the MPC framework is 3.56%, compared to the barrier controller, and very close to the optimal value, as it can be demonstrated on Table 7.2[2][3].

[2] In parenthesis, the offline consumption for the full mission, evaluated only with the offline implementation, is given, to showcase the available margin for improvement

[3] The difference in online and offline consumption is attributed to a number of factors, including the dynamic behaviour and, more importantly, the exclusion of the shaft losses (See Sec. 6.1.3)

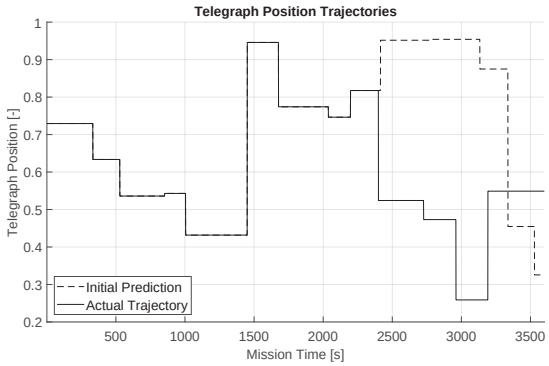


Figure 7.13: (Profile 1) Telegraph position

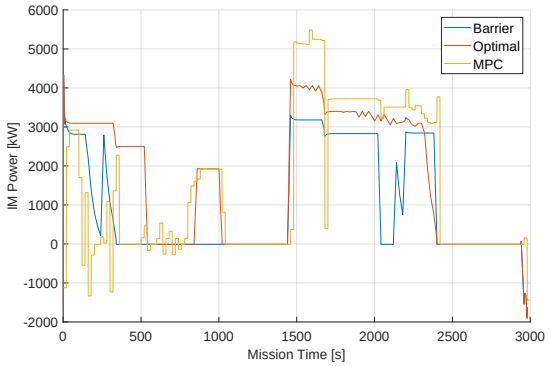


Figure 7.14: (Profile 1)Power of the induction machine

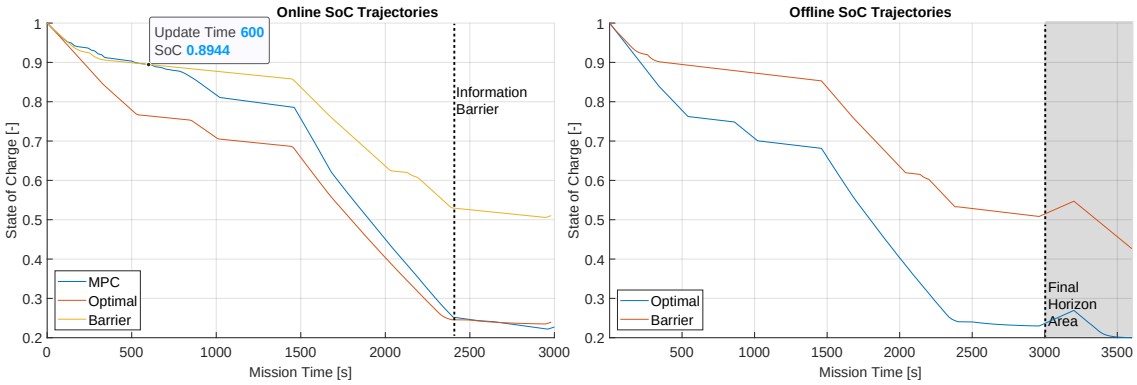


Figure 7.15: (Profile 1) Online SoC for barrier, optimal and MPC (left), Offline SoC for the information barrier at $t_{bar} = 2400$ $[s]$ and optimal (right)

Table 7.2: Fuel Consumption Results For Profile 1

| **Controller** | **Consumption [kg]** | |
|---|---|---|
| | **Online** | **Offline** |
| **Optimal** | 1787.1 | 1632.5 (1961.3) |
| **Barrier** | 1878.3 | 1720.1 (2030.6) |
| **MPC** | 1811.3 | |

The results show that the barrier controller does not get informed in time for the significantly lower propulsive load after the information barrier, and discharges the battery pack more slowly. When the change occurs, the barrier controller is no longer able to utilise its battery, mainly due to the engine lower limit providing adequate power, while, simultaneously, the IM torque limit does not allow for very low torque operation. This is a case of a specific mechanism for suboptimality, that from now on will be referred to as *"trapped charge"*.

On the other hand, the same limitation applies also for the case of the optimal and the MPC

framework controllers, as, in Fig. 7.14, it can be seen that actually none of the three controllers are utilising the induction machine after $t_{bar} = 2400$ $[s]$. However, the optimal controller, being aware of this limitation, cares to discharge its battery pack earlier, by utilising the induction motor more.

With all of the above taken into consideration, the behaviour of the MPC framework controller can be demonstrated: Initially, the MPC framework has a similar reference SoC trajectory, as the first portion of the SoC trajectory of the barrier controller (before the barrier). However, at $t_{upd} = 600$ $[s]$, the controller is updated regarding the long-term load alteration, and starts using the induction machine more, in order to gradually reach an almost depleted SoC, before the barrier, thus, avoiding the "trapped charge" effect.

### Profile 2

The second tested profile concerns a load update that is marginally different. This case demonstrates some nuances and limitations involved in the benchmarking procedure, namely the consumption of the end horizon and the setpoint chattering. In more detail, since the final horizon is not included in the expreriment, it can happen that, although the optimal controller remains optimal compared to the barrier controller when the full experiment is concerned (see 7.3, in parentheses are the full experiment horizons), at the final horizon time, $t_{fh} = 2980$ $[s]$, the barrier controller might be at a marginally lower fuel consumption level. This is because the barrier controller has used the battery charge sooner than the optimal controller. This can yield an consumption increase for the case of the MPC controller, even though it would probably still end with lower consumption if the full experiment would have been considered.

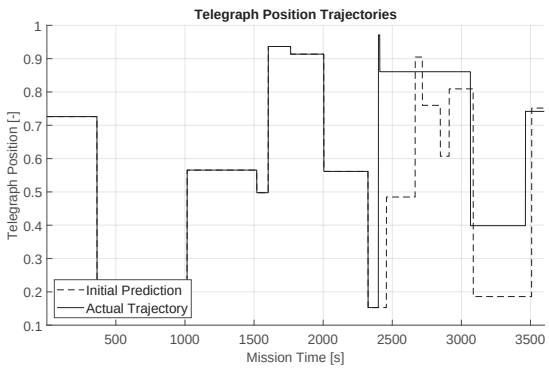


Figure 7.16: (Profile 2) Telegraph position

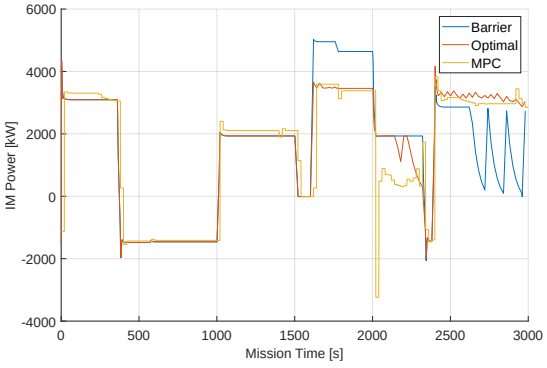


Figure 7.17: (Profile 2)Power of the induction machine

However, these results are found due to the small difference between the predicted and actual load, together with the particularities involved to generate the behaviour above.

Nonetheless, the MPC framework behaviour manages to remain close to the optimal controller, as it can be seen from the SoC trajectories in Fig. 7.18.

Another positive behaviour regarding the MPC framework controller is that, probably due to the

dynamic model feedback, it generates setpoints that do not seem to contain the negative chattering effect found in the optimal and barrier controllers. This can be seen in Fig. 7.17, in the region between $t = 2100$ $[s]$ and $t = 2300$ $[s]$.

These results show satisfactory behaviour for the controller framework, but simultaneously indicate that, when there is no mechanism of "trapped charge" (explained in the discussion for Profile 1), the fuel consumption decrease margin is limited.

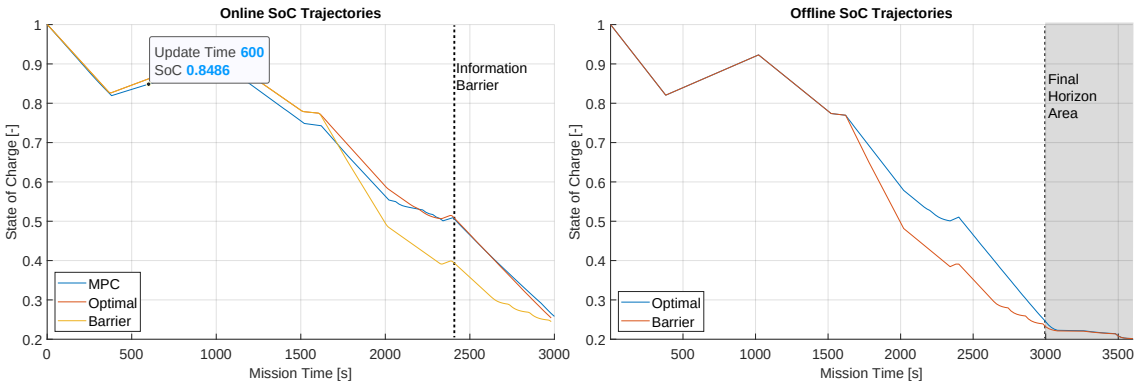


Figure 7.18: (Profile 2) Online SoC for barrier, optimal and MPC (left), Offline SoC for the information barrier at $t_{bar} = 2400$ $[s]$ and optimal (right)

Table 7.3: Fuel Consumption Results For Profile 2, (in parentheses the full experiment consumption)

| **Controller** | **Consumption [kg]** | |
|---|---|---|
| | **Online** | **Offline** |
| **Optimal** | 1758.1 | 1608.2 (1948.9) |
| **Barrier** | 1757.9 | 1607.5 (1952.5) |
| **MPC** | 1797.9 | |

### Profile 3

In profile 3 a lower starting SOC has been selected, in order to ensure that the low load region between $t = 400$ $[s]$ and $t = 800$ $[s]$, does not restrict the possible paths, or overcharges the batteries. However, even when infeasible paths are present, the DP algorithm [98] will violate the operating limits instead of exiting with an error, a useful behaviour that can be handled by the batteries' low-level controller, which could, for example, protect against overcharging, until the EMS control yields a state of charge lower than $SoC = 1$ again. Such considerations are also discussed for profile 4, and, in general, it can be concluded that implementation would probably be more robust if $SoC_{start} = 0.9$.

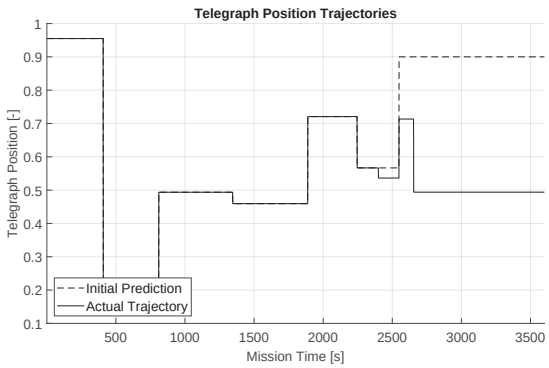


Figure 7.19: (Profile 3) Telegraph position

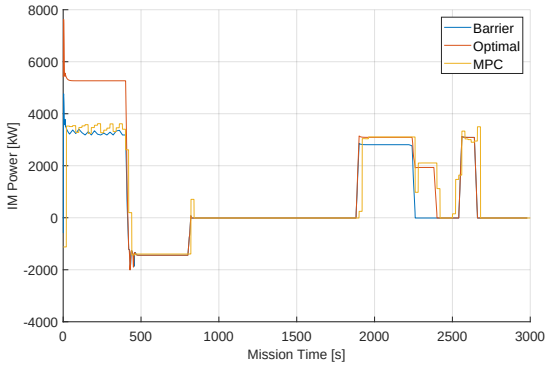


Figure 7.20: (Profile 3)Power of the induction machine

It can be seen from Fig. 7.20 that the MPC framework follows the barrier controller up until the update point, however, after the update point, the induction machine load is the same for both the barrier and the optimal controller until around the information barrier point, $t_{bar} = 2400\ [s]$. After the barrier point, it can be clearly seen that the MPC framework follows the optimal controller.

Finally, it is noticed that, in this particular profile, the long periods of non utilisation of the induction machines result in even the optimal controller not fully depleting the battery, even for the full one-hour mission.

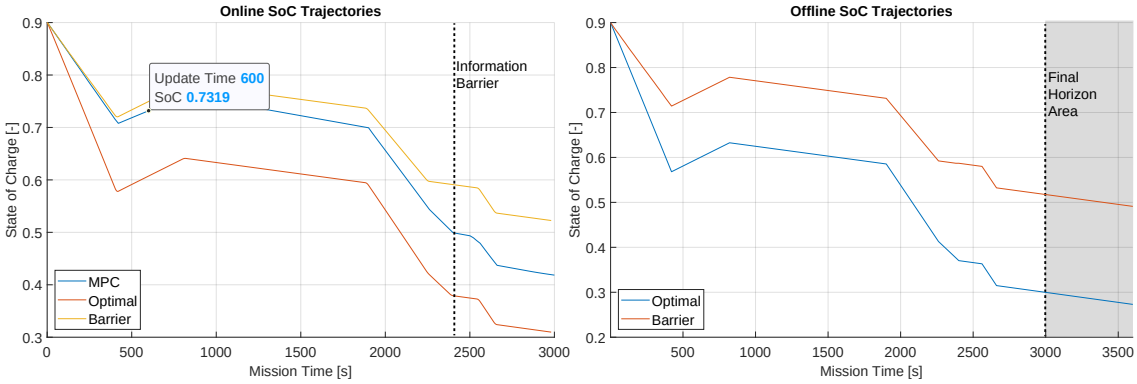


Figure 7.21: (Profile 3) Online SoC for barrier, optimal and MPC (left), Offline SoC for the information barrier at $t_{bar} = 2400\ [s]$ and optimal (right)

### Profile 4

An important note is that for profile 2, up until around $t = 1650\ [s]$, the barrier and optimal control trajectories coincide. This is an indication that the DP results are heavily **boundary driven**, which means that, in order to satisfy all boundaries set to the problem, there is little room for difference due to the late information, and only a few optimal paths which still satisfy all operating boundaries remain. In fact, for profile 4, in Fig. 7.24 it can be seen that the barrier and optimal controls coincide entirely.

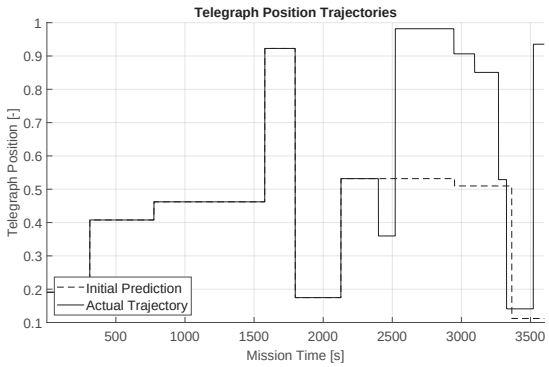


Figure 7.22: (Profile 4) Telegraph position

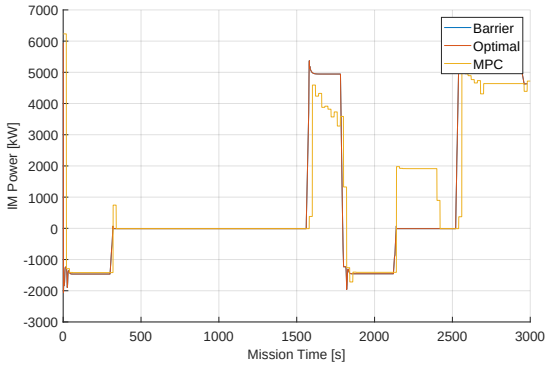


Figure 7.23: (Profile 4 overbounded) Power of the induction machine

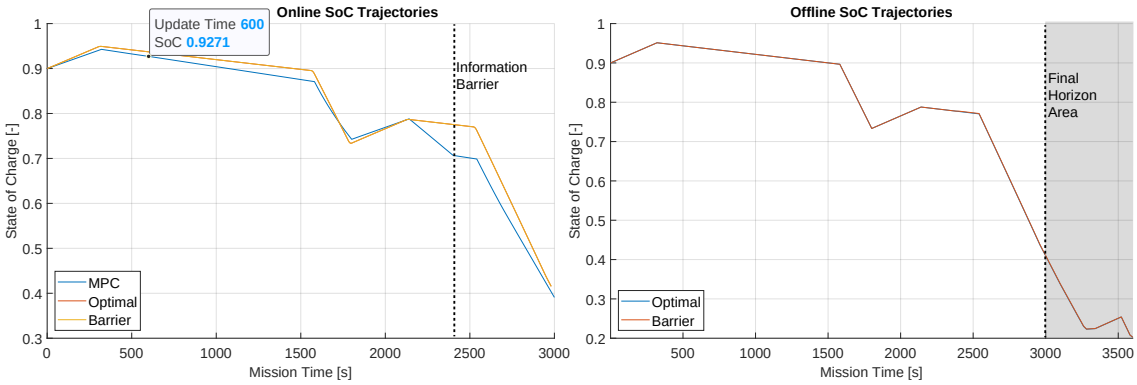


Figure 7.24: (Profile 4 overbounded) Online SoC for barrier, optimal and MPC (left), Offline SoC for the information barrier at $t_{bar} = 2400$ $[s]$ and optimal (right)

This is taken into consideration, and the experiment for profile 4 is repeated, but with the operating boundaries relaxed, not because these boundaries are not realistic, but more for demonstration purposes. In fact, being able to yield solutions in a heavily bounded system means that the controller is robust.

In this profile, the lower main engine power was reduced to $30\%P_{MCR}$ and the minimum torque to $10\%M_{PTO/I,max}$. It is also important to note for this profile that, due to the minimum engine power limit, $P_{B,min}$, the upper bound for the SoC would deem the profile infeasible, because a lower than $P_{B,min}$ propulsive load happens right at the start. For that reason, the initial SoC level has been changed to 0.9. The same SoC level will be adopted also for the charge sustaining experiments to follow.

Although the difference between the two results at the end of the whole experiment are again marginal ( 0.1%), since no "trapped charge" mechanism occurs, the significantly higher charge of the MPC framework solution at the point of the final horizon would deem meaningless any comparison anyway. It is reminded to the reader that this was not the case in profile 1, where the SoC of the

barrier controller never reaches the 0.2 value. It is fair to conclude from the offline trajectories that if the horizon would continue the MPC framework would hit the 0.2 mark, as it is already following the optimal path closely.

Nevertheless, it is important to notice that if no "trapped charge" mechanism is present, and if enough charge is in the battery pack, the DP controller can utilise the batteries to move the operating points of the main components in the powertrain, regardless of the long-term future information. This conjecture is validated in the profiles tested, as it is noticed that when the end SoC is between the barrier and the optimal controller, the fuel consumption of the barrier controller converges to the optimal.

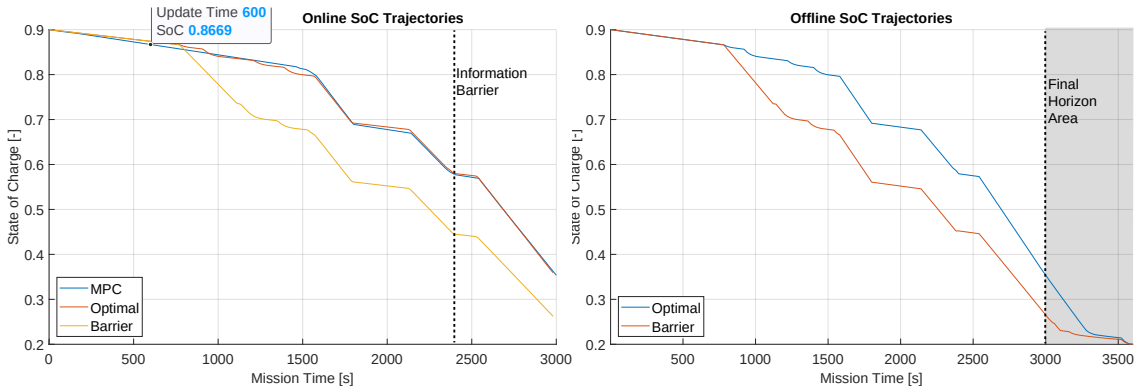


Figure 7.25: (Profile 4) Online SoC for barrier, optimal and MPC (left), Offline SoC for the information barrier at $t_{bar} = 2400$ $[s]$ and optimal (right)

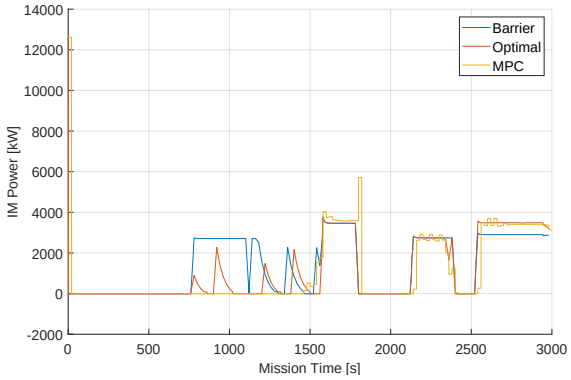


Figure 7.26: (Profile 4) Power of Induction Machine

### Plug-in Mode Conclusions

The following points may be concluded from the results above:

- The MPC framework closely follows the optimal controller consistently, utilising the information update effectively

- Under certain conditions, an effect identified as *"trapped charge"* can occur in the case of the barrier controller, which acts as a mechanism that prevents optimality due to the information barrier. It has been showcased that the MPC framework is capable of utilising online long-term feedback effectively, and eliminate such an effect, yielding in some case even above 3.5% fuel consumpiton reduction.

- The boundaries of the system under certain load sequences can result into a significant portion of the control path of the optimal and the barrier control case coinciding

- If no "trapped charged" effect is present, the barrier controller is able to utilise the battery charge as effectively as the optimal controller, yielding no considerable difference in fuel consumption compared to the optimal controller

- Even if there is no considerable fuel consumption reduction in utilising long term information, the MPC framework proves to be a robust controller that closely follows the optimal path.

- It should also be considered that the difference in a predictor's performance for long-term predictions ($> 1000$ $[s]$), and a predictor's performance for short term predictions equal to the horizon length (600 $[s]$), is, of course, expected to be in favour of the MPC framework. Thus, it is expected that, in full implementations that include the predictors, the MPC framework will result in lower fuel consumption than any other EMS with no long-term feedback.

- Every experiment simulation of 2980 $[s]$ was run on MATLAB® R2019b in under than 1000 $[s]$, suggesting that the MPC framework is computationally light enough to be implemented on board. The code has not been optimised to be embedded on a controller (e.g. with C-MEX), and the laptop used has a low end i3-3217U mobile processor unit and 8GB of RAM.

### 7.2.4 Charge Sustaining Mode

After examining the behaviour of the charge depleting, or plug-in case, the experiments for the same profiles have been iterated for the charge sustaining mode. In this mode the end-state charge is bounded, $SoC_{N+1} = [0.89\ 0.91]$. The consumption differences in this section are negligible, which is consistent with the findings in [1], where it is demonstrated that a rule-based controller performs very close to the optimal solution in charge-sustaining scenarios.

#### Profile 1

It can be seen that this particular profile with normal operating boundaries does not utilise the induction motor at all, as demonstrated on Fig. 7.41. The battery energy is used only to cover hotel loads, while no more than 0.3% of the battery charge is used (Fig. 7.43).

This is **not** due to the induction motor tight operating limits, but due to the low hotel demand. To examine this, the experiment is iterated, but this time the induction motor torque is reduced from 0.3 to $0.1 \cdot M_{PTO/I,max}$. As it can be seen on Figs. 7.32, 7.33, the induction motor still remains non utilised, while the looser IM boundaries allow for the late informed barrier controller to follow the same path as the optimal control.

The experiment is iterated once again, this time with design hotel demand, which corresponds to 3 of the 4 installed generator sets running at $0.9 \cdot P_{DG,max}$, which is equal to $P_{hotel} = 7269\ [kW]$, and the same relaxed operating boundaries. The design hotel load has not been used up until this point because it does not correspond to the usual vessel loads. It can be clearly seen that now the induction motor is utilised and that the MPC controller follows the optimal controller path, however, a discrepancy is found around mission time $t = 1500\ [s]$. The cause of that discrepancy seems to be connected with the high propulsive load and jump at the corresponding time and the relaxed operating boundaries.

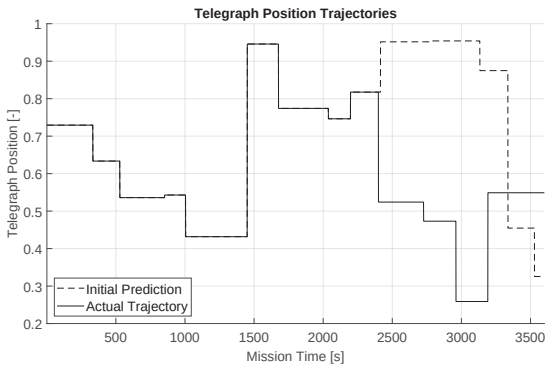


Figure 7.27: (Profile 1) Telegraph position

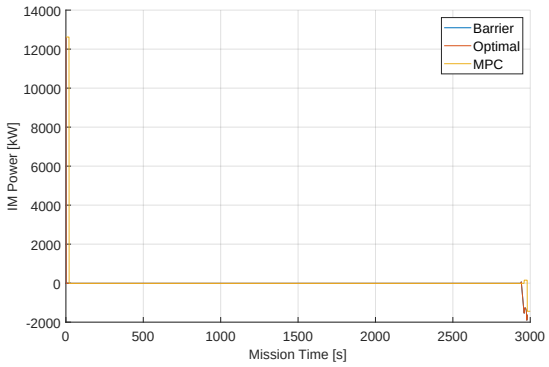


Figure 7.28: (Profile 1 CS Normal)Power of the induction machine

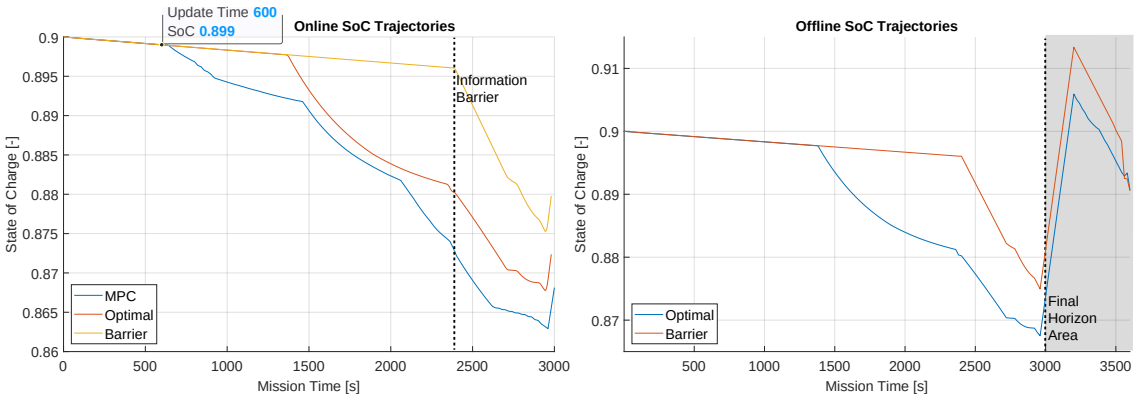


Figure 7.29: (Profile 1 CS Normal) Online SoC for barrier, optimal and MPC (left), Offline SoC for the information barrier at $t_{bar} = 2400\ [s]$ and optimal (right)

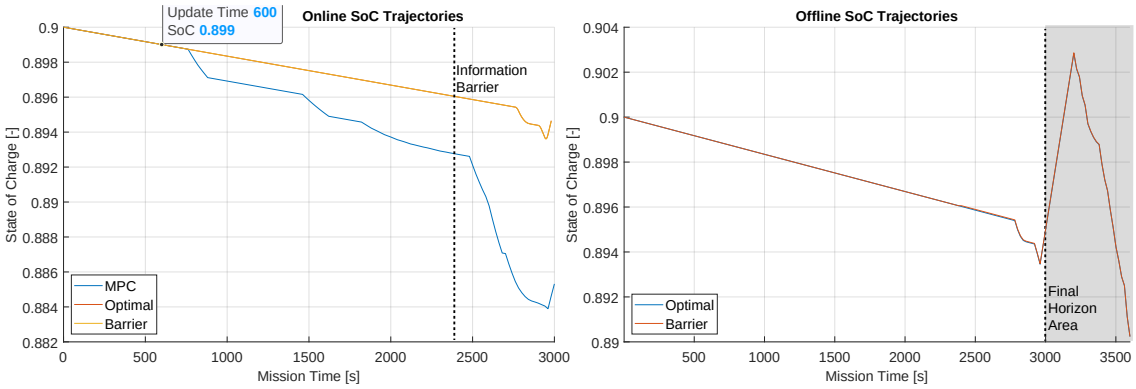


Figure 7.30: (Profile 1 CS Reduced IM threshold) Online SoC for barrier, optimal and MPC (left), Offline SoC for the information barrier at $t_{bar} = 2400$ $[s]$ and optimal (right)

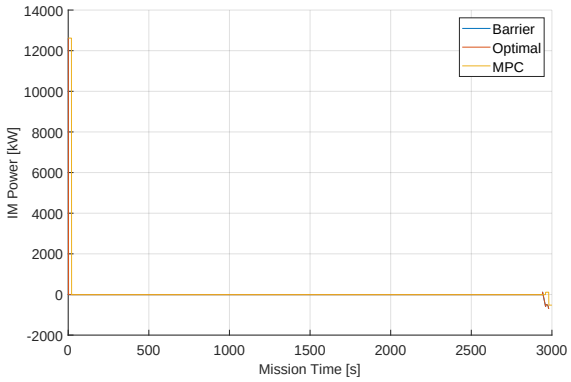


Figure 7.31: (Profile 1 CS Reduced IM threshold) Power of the induction machine

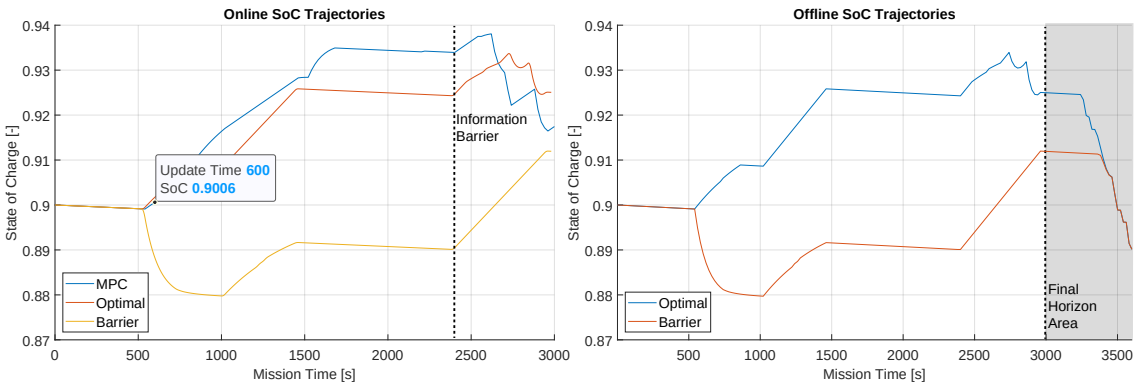


Figure 7.32: (Profile 1, CS Reduced IM threshold, design hotel loads) Online SoC for barrier, optimal and MPC (left), Offline SoC for the information barrier at $t_{bar} = 2400$ $[s]$ and optimal (right)

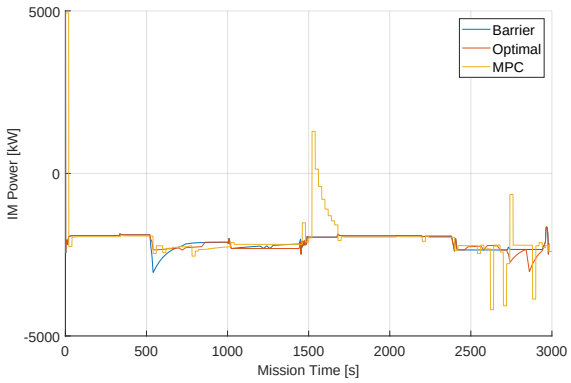


Figure 7.33: (Profile 1, CS Reduced IM threshold, design hotel loads) Power of the induction machine

### Profile 2

Using again normal operating boundaries and loads, an experiment for profile 2 has been carried out. It can be seen that, although the battery utilisation is low, the induction motor is used in the low propulsive load region in order to push the main engine operating points inside its operating envelope. The MPC framework controller still seems to be following the optimal controller path, and does not utilise the induction motor at around 1700 $[s]$, where a spike for the barrier controller is noticed.

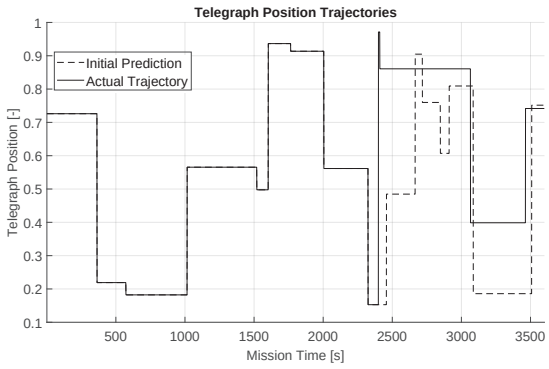


Figure 7.34: (Profile 2 CS) Telegraph position

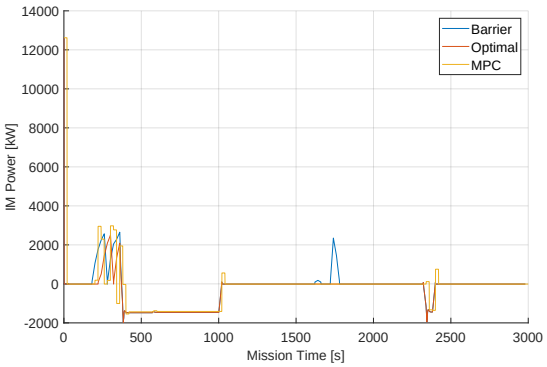


Figure 7.35: (Profile 2 CS) Power of the induction machine

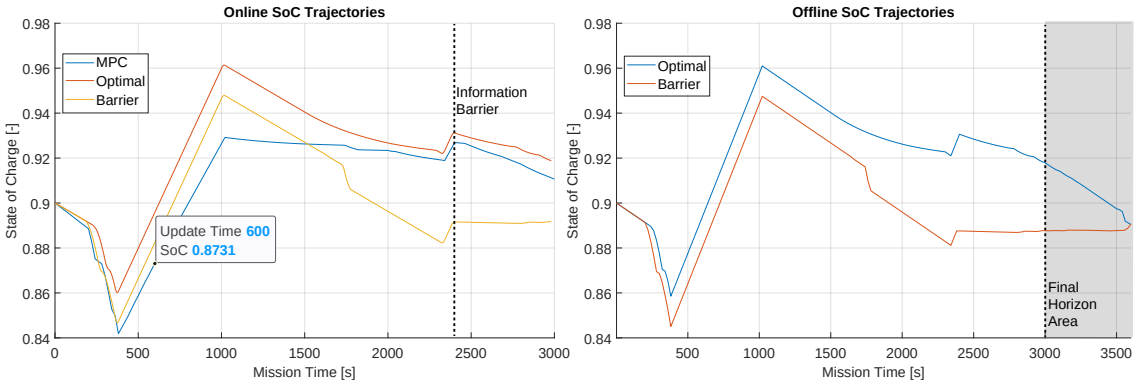


Figure 7.36: (Profile 2 CS) Online SoC for barrier, optimal and MPC (left), Offline SoC for the information barrier at $t_{bar} = 2400$ $[s]$ and optimal (right)

### Profile 3

Profile 3 yields similar results to profile 2, with the difference that the barrier controller seems to not utilise the battery to cover hotel demands, up until the point where the information barrier is located. After the barrier, it quickly discharges the battery pack, in order to return to the *SoC* terminal window.

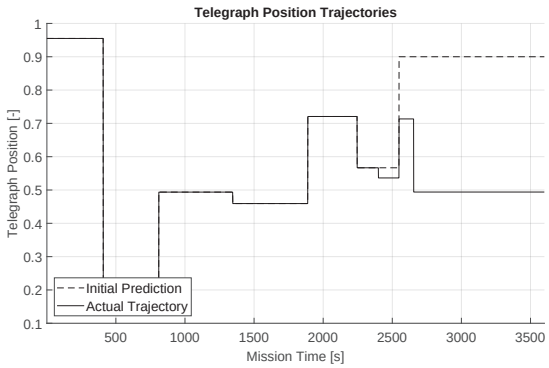


Figure 7.37: (Profile 3 CS) Telegraph position

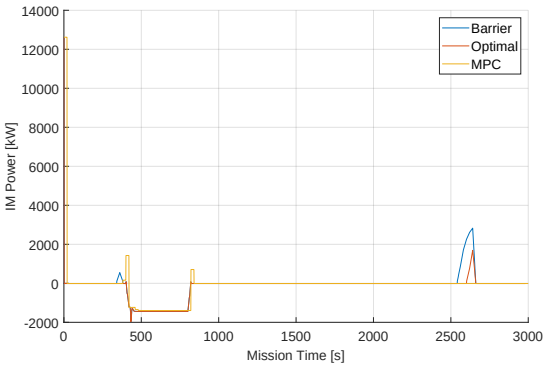


Figure 7.38: (Profile 3 CS) Power of the induction machine

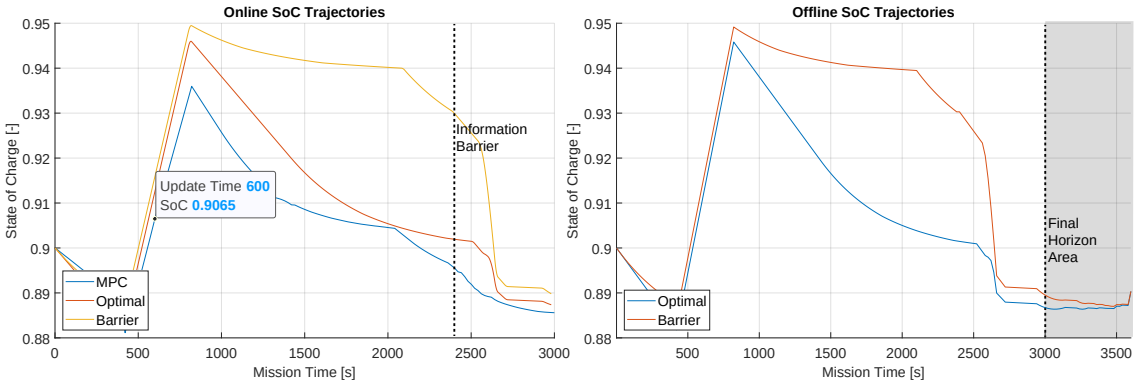


Figure 7.39: (Profile 3 CS) Online SoC for barrier, optimal and MPC (left), Offline SoC for the information barrier at $t_{bar} = 2400$ $[s]$ and optimal (right)

### Profile 4

In profile 4 the behaviour is similar, with the particularity that the barrier controller seems to utilise the induction machine for a small period as a PTI. However, the MPC framework follows the optimal controller and does not opt for that utilisation.

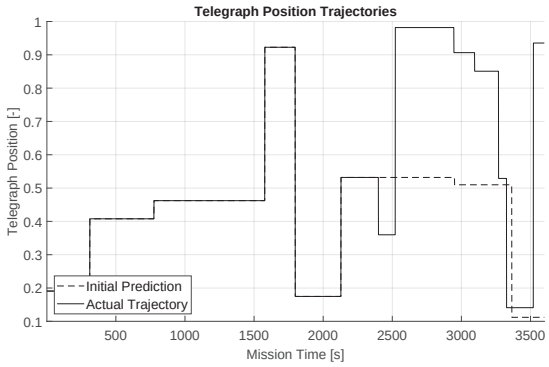


Figure 7.40: (Profile 3 CS) Telegraph position

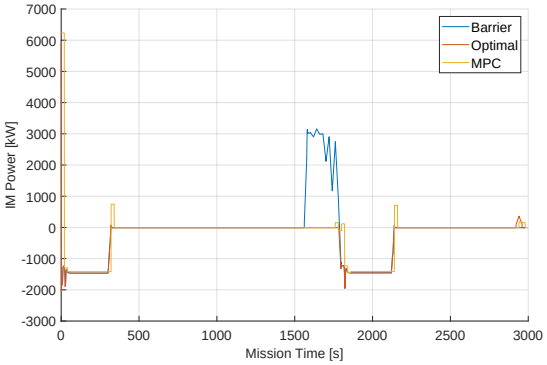


Figure 7.41: (Profile 3 CS) Power of the induction machine

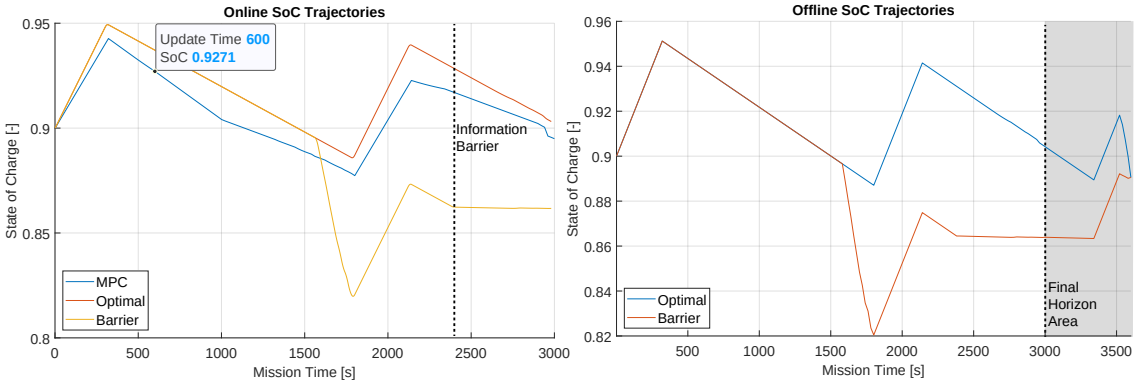


Figure 7.42: (Profile 3 CS) Online SoC for barrier, optimal and MPC (left), Offline SoC for the information barrier at $t_{bar} = 2400$ $[s]$ and optimal (right)

### Charge-Sustaining Mode Conclusions

As it is expected, the MPC framework only shows small deviations from the optimal controller, while the barrier controller, although it behaves differently, generates alternate path trajectories which does not seem to affect significantly the power consumption.

Furthermore, apart from the case of design hotel load, the only reason why the induction motor is utilised is to keep the main engine point inside the operating envelope, in a PTO mode. However, in the design hotel load case, since the induction motor is already being used, slight alteration can be noticed, which correspond to moving the operating point of the engine to lower SFOC levels. This is a potential mechanism for further consumption reduction, further discussed in Sec. 7.3.2. Nonetheless, as far as fuel consumption is concerned, and in accordance with the findings in [1], there is not considerable difference between the optimal and barrier in this case.

## 7.3 Parametric Study

Here a parametric study is carried out to examine the behaviour of the MPC framework controller in alterations of the update point position and the hotel demand. Profile 1 has been used for these experiments, while the controller operates in plug-in (charge-depleting) mode. The fuel consumption differences are also demonstrated.

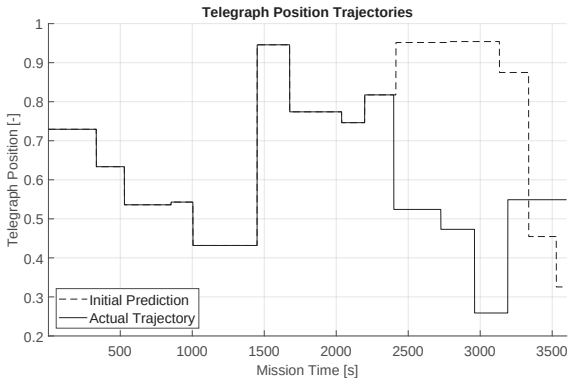


Figure 7.43: (Profile 1) Telegraph trajectory

### 7.3.1 Update Point Position

A full mission DP solution generates an SoC reference trajectory every $t_{interval} = 600$ $[s]$. Here, the update point $t_{upd}$, at which the DP solution is fed with the profile update, is moved from $t_{upd} = 600$ $[s]$ to $t_{upd} = 1200$ $[s]$, and then to $t_{upd} = 1800$ $[s]$. The information barrier is kept constant at $t_{bar} = 2400$ $[s]$. The goal is to examine:

- if the MPC framework follows consistently the optimal solution when the update is later than the previous experiments and
- how the update position affects fuel consumption.

The results are the expected, with the consumption decrease showing smaller values, from $-3.56\%$ to $-3.44\%$, and then to $-1.92\%$, for the corresponding update positions at 600 $[s]$, 1200 $[s]$, and 1800 $[s]$ in mission time, as it is shown on Table 7.4. While for the first two cases the SoC trajectories in Fig. 7.44 reach an end-state close to the one of the optimal controller, the third case ($t_{upd} =$ 1800 $[s]$) has an end-state that is significantly higher, thus, it yields smaller fuel reduction. This indicates that, for the MPC framewrok controller, whenever there is a "trapped charge" mechanism present, there is a relatively **wide time window** for the long-term feedback update to occur and still yield fuel consumption reduction.

A consistent behaviour for the induction motor power is shown in Fig 7.45, with the MPC framework controller following the optimal controller where the update has reached the MPC, and the barrier controller where it has not. The bifurcations in the MPC framework SoC trajectories for the different update time positions, which can be seen in Fig. 7.44, also occur when expected, as their positions are after the different MPC frameworks receive the update about the mission load (the updates are shown with the white dots).

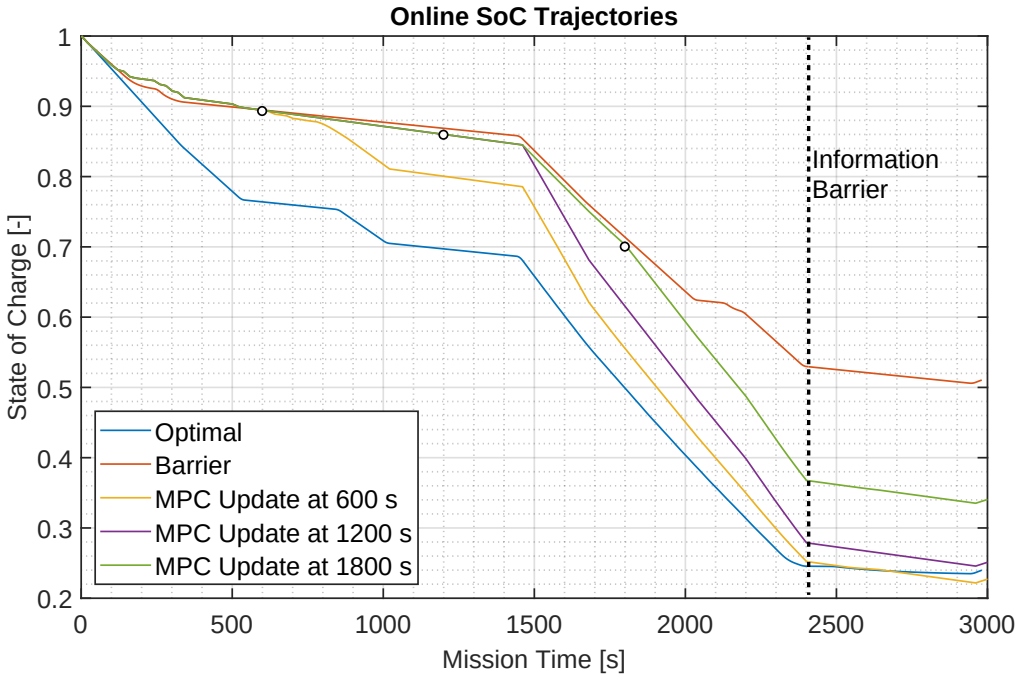


Figure 7.44: (Profile 1) Different trajectories of the state of charge of the battery pack for different update points

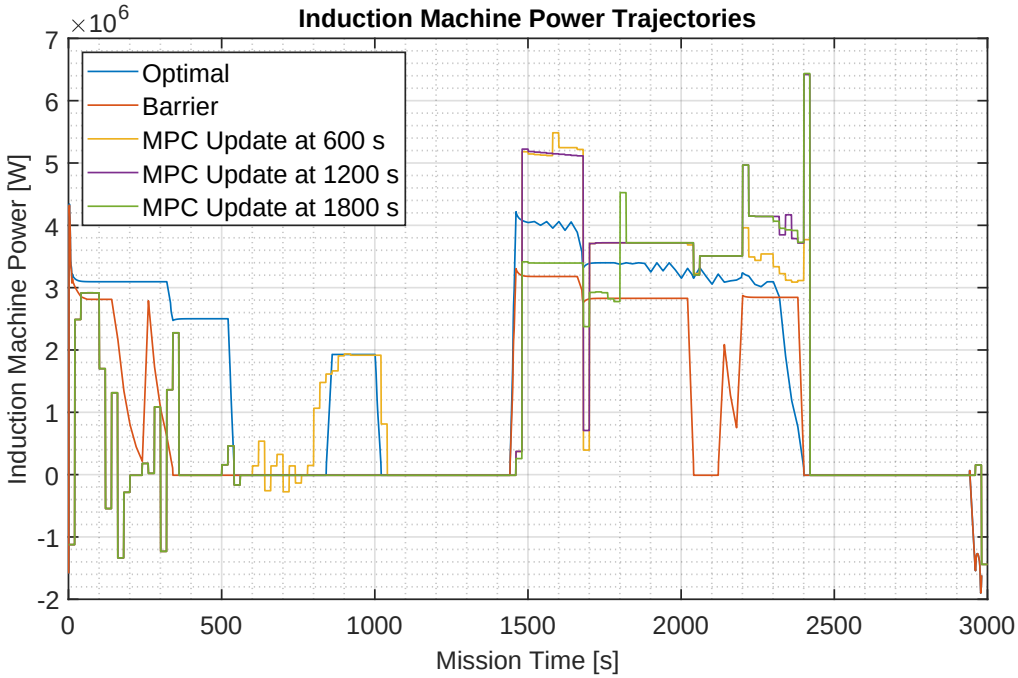


Figure 7.45: (Profile 1) Different trajectories of the power of the induction motor for different update points

Table 7.4: Total Fuel Consumption for Different Update Positions $t_{upd}$

| **Controller** | **Consumption [kg]** | | | |
|---|---|---|---|---|
| | **Online** ($t_{upd} = 600$ [$s$]) | **Online** ($t_{upd} = 1200$ [$s$]) | **Online** ($t_{upd} = 1800$ [$s$]) | **Offline** |
| **Optimal** | 1787.1 | 1787.1 | 1787.1 | 1632.5(1961.3) |
| **Barrier** | 1878.1 | 1878.1 | 1878.1 | 1720.1(2030.6) |
| **MPC** | 1811.3 (-3.56%) | 1813.4 (-3.44%) | 1842.0 (-1.92%) | - |

### 7.3.2 Hotel Demand Alterations

A parametric study which shows the behaviour of the MPC framework controller has been carried out, for the case of an intermediate and a design constant hotel demand, $P_{hot} = 5$ [$MW$] and $P_{hot} = 7.3$ [$MW$]. The goal of the study is, again, to check the controller's consistency and the implications of higher hotel demands for the fuel consumption reduction, which has previously been noticed for profile 1.

From the SoC trajectories, shown on Fig. 7.50, it can be concluded that the effect of the information barrier mainly affects low and intermediate loads, with the high design loads showing a stable and aggressive charge depletion, as it can be also undestood from the small difference in the optimal and barrier consumption in Table 7.5. All cases are closely following the optimal SOC trajectory, although it is not shown here, however, this behaviour has been validated numerous times in the present study and here is omitted.

The effect of the higher hotel demand is shown in Table 7.5, where the MPC framework reduction becomes negligible for the intermediate and the design load. However, it can be seen that there is still a reduction for the design load. This is because, while in the intermediate load the propulsive demand is well within the engine operating limits and the induction machine is way less active due to the IM torque threshold, in design load the induction machine is constantly operating in PTO conditions, and the controller is capable of better manipulating the control inputs to focus the main engine load at the minimal fuel consumption regions (Fig. 7.48). The PTO functionality, together with the aggressive charge depletion, is apparent in the number of active generator sets (See Fig. 7.47), where only for short time periods the second engine is needed to operate.

Due to the low hotel demand compared to the design demand in usual conditions, the case study up until now has not included the engine envelope graphs due to the low engine operating points, way lower than the specific fuel consumption minimisation points for the main engines. This can be demonstrated in Fig. 7.48, where the area for the operating setpoints in the case of $P_{hot} = 1000$ [$kW$] is in the lower region of the graph[4]. However, with higher hotel loads it is apparent that the design

[4] See dense cyan circles - it is reminded that $P_{B,min} = 4$ [$MW$], while the graph includes lower regions because of transitional trajectories

operating point, which should be at the consumption minimisation point, is reached (red stars). As expected, the 5 $[MW]$ hotel load corresponds to an intermediate main engine load.

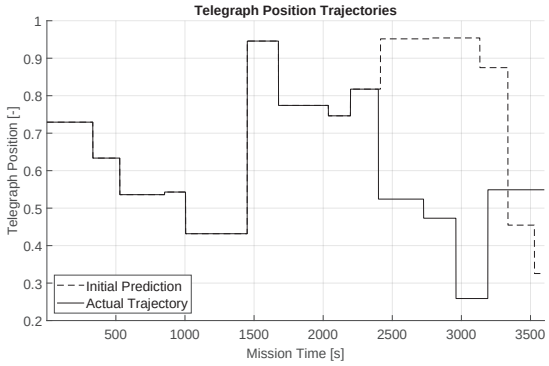


Figure 7.46: (Profile 1) Telegraph position

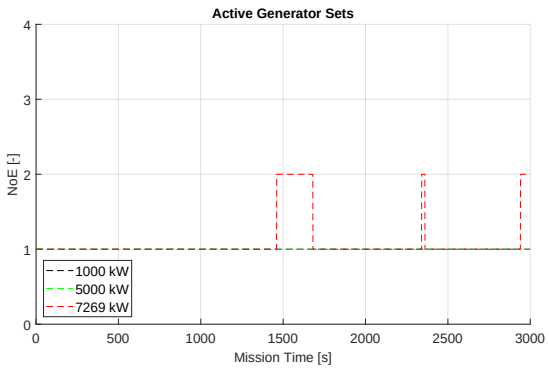


Figure 7.47: Active Generator Sets

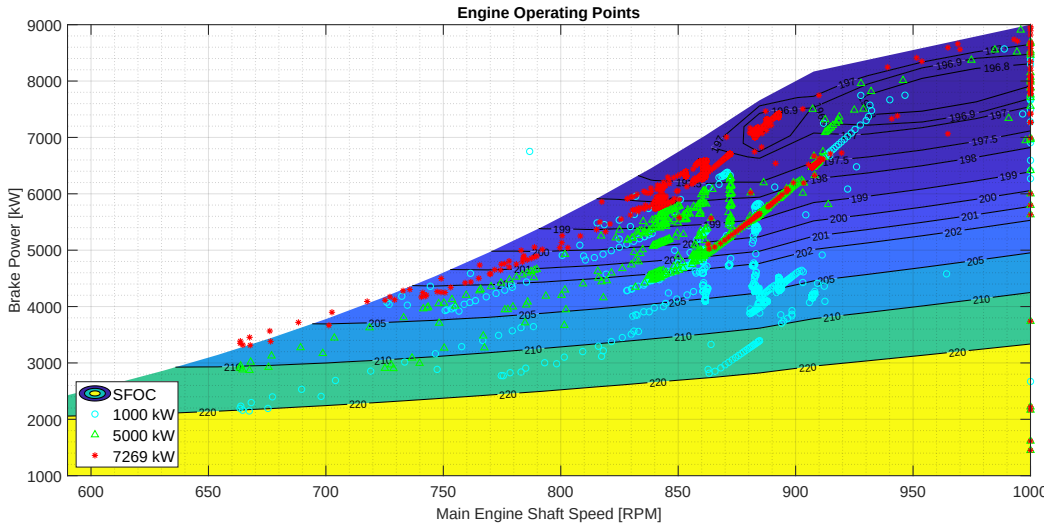


Figure 7.48: Online operating points (including transitions) plotted on the consumption envelope of the main engine

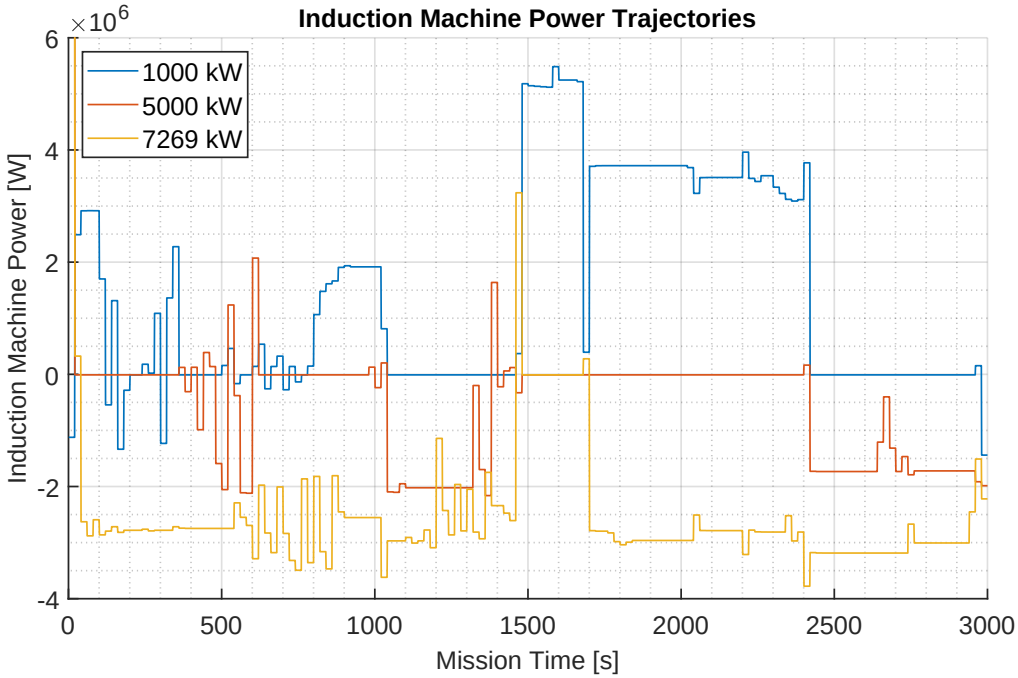


Figure 7.49: Trajectories of the power of the induction machine for different hotel demands

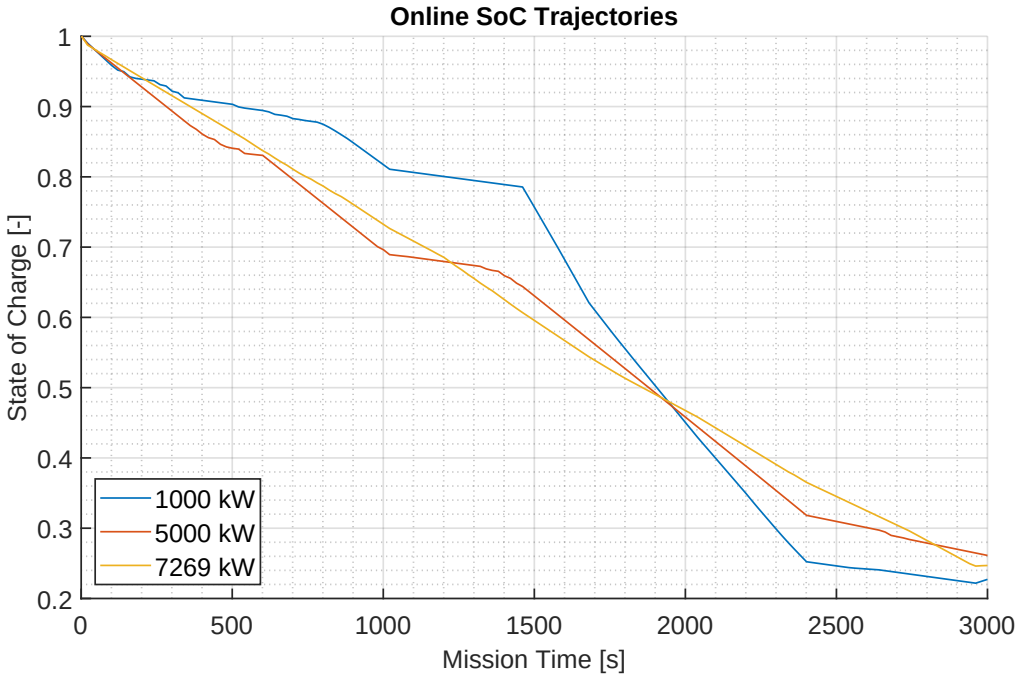


Figure 7.50: Trajectories of SoC for different hotel demands

Table 7.5: Total Fuel Consumption for Different Hotel Power Demand $P_{hot}$

| **Controller** | **Consumption [kg]** | | |
|---|---|---|---|
| | Online ($P_{hot} = 1$ $[MW]$) | Online ($P_{hot} = 5$ $[MW]$) | Online ($P_{hot} = 7.3$ $[MW]$) |
| **Optimal** | 1787.1 | 2442.2 | 2824.6 |
| **Barrier** | 1878.1 | 2446.7 | 2838.5 |
| **MPC** | 1811.3 (-3.56%) | 2447.7 (+0.04%) | 2826.1 (-0.44%) |

### 7.3.3 Extended Main Engine Envelope

All previous cases concerned conventional operating envelope boundaries, according to typical project guides provided by engine manufacturers, with conventional turbochargers; however, the operating envelope in specialised propulsive plants as in naval applications, with technologies such as sequential turbocharging (STC), allow for extended low-load operation without negative effects on emissions and engine wear [125]. Controllable pitch propellers allow for effective utilisation of such low-load main engine capabilities.

The Mean Value First Principle (MVFP) Simulink® model used in the present case study has the capability of modelling sequential turbocharging (STC) by changing the effective turbocharger area [122], as an extension to the initial model, proposed in [126].

To demonstrate the versatility of the proposed EMS framework, by using the STC modelling capabilities of the dynamic (MVFP) model, an extended operating profile case has been tested. The virtual shaft speed boundaries have been extended to $N_{virt} \in [20\ 120]$ $[rpm]$, and by using Eq. (6.1) and profile 1, a totally different trajectory of virtual shaft speed has been generated with the same telegraph position sequence. Profile 1 has been used again as a general profile case, however, **no comparison** should be made with the previous cases, as the new virtual shaft speed $N_{virt}$ boundaries map the telegraph positions to completely different $N_{virt}$ shaft speed levels.

The hybrid diesel-electric propulsive model is used in transit mode, where the minimum fuel consumed is prioritised, as opposed to manoeuvring and fast manoeuvre mode where fast acceleration and transient behaviour are the focus of the non-EMS control [122]. Thus, in manoeuvring mode the EMS strategy, which focuses on fuel minimisation, is not used, due to the control objective conflict between the different controller levels; the combinator curve which includes the electric drive in [122] should be used instead, in order to minimise acceleration times and thermal loading.

The new extended transit mode combinator curve correlates the virtual $N_{virt}$, to the engine shaft speed, $n_e$, and the propulsive power $P_{prop}$, with the interpolated fits, created from the high-end model measurements, shown in Figs. 7.51, 7.52, correspondingly.

Finally, the minimum allowable PTO/I torque has been set to 10% $M_{PTO/I}$, the minimum main engine power has been set to 6% $P_B$, while the maximum engine power has been set to 98% of the

torque and power limits of the envelope.

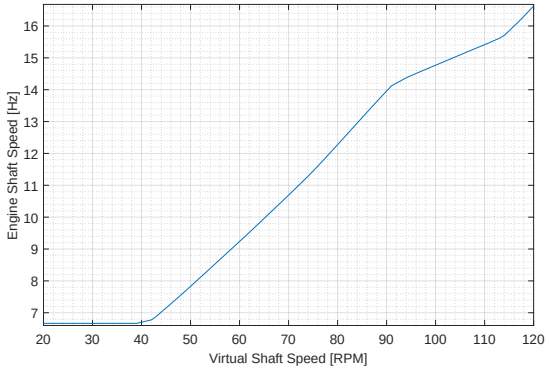


Figure 7.51: Virtual and engine speed

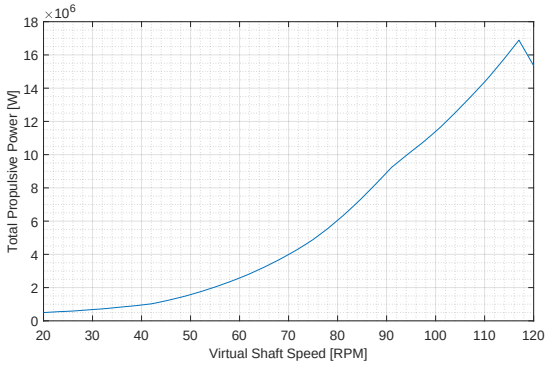


Figure 7.52: Virtual Shaft speed and propulsive demand

## Charge Depleting

From Figs. 7.54 and 7.55 it can be seen that the MPC framework controller is following closely the optimal controller's PTO/I power output, and SOC trajectory, after the update point at 600 $[s]$. The fuel consumption reduction might seem substantial in Table 7.6, at 3.07%. However, by noticing the small headroom between the optimal and barrier controller solutions at the end of the offline full mission (shown in parentheses), it should be expected that if the final horizon would have been taken into account, a smaller reduction would have been shown. This is expected as there is no trapped charge at the end of the mission for the barrier case, which is the primary mechanism for significant reduction due to long-term information utilisation, as it has been established in the previous cases. The reduction of fuel consumption seems to be greater when the operating boundaries of the powertrain components are narrower.

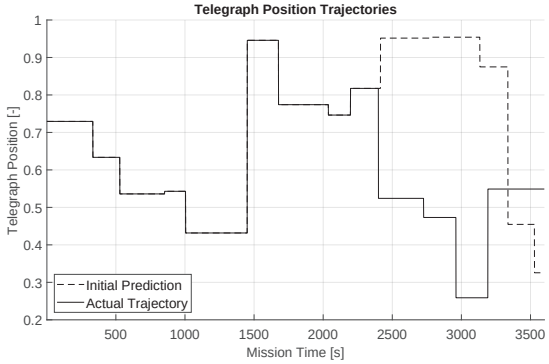


Figure 7.53: (Profile 1) Telegraph position

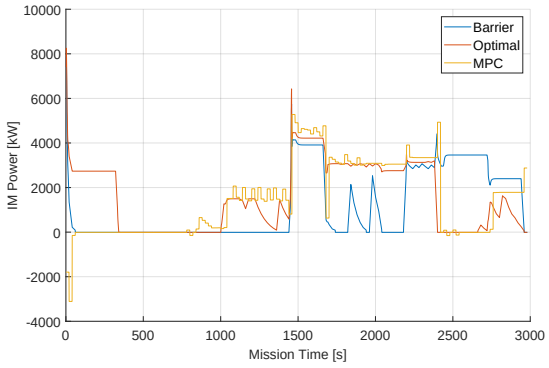


Figure 7.54: Power of Induction Machine

Nevertheless, the MPC framework controller solution behaviour is again consistent with the update point and the optimal trajectory. This indicates that the MPC framework is close to optimal,

Table 7.6: Total Fuel Consumption for the Extended Envelope Case, Profile 1

| **Controller** | **Consumption [kg]** | |
|---|---|---|
| | **Online** | **Offline** |
| **Optimal** | 1281.1 | 1161.6 (1314.8) |
| **Barrier** | 1333.4 | 1212.2 (1315.5) |
| **MPC** | 1292.4 (-3.07%) | |

robust, and effective in a wide variety of powertrains with conventional or specialised operating boundaries. The controller is using the PTI when it provides the most benefits in terms of main engine fuel oil consumption reduction. The low-power main engine set-points are shown in Figs. 7.56 and 7.57. The points plotted are chosen so that transient behaviour is not shown, as operation here is way within the operating envelope at this hotel load, thus, including transient set-points would clutter the plot without contributing much [5]. This means that transition effects such as inertia, pressure and thermal effects have settled, and the points are in agreement with the reduced steady state model.

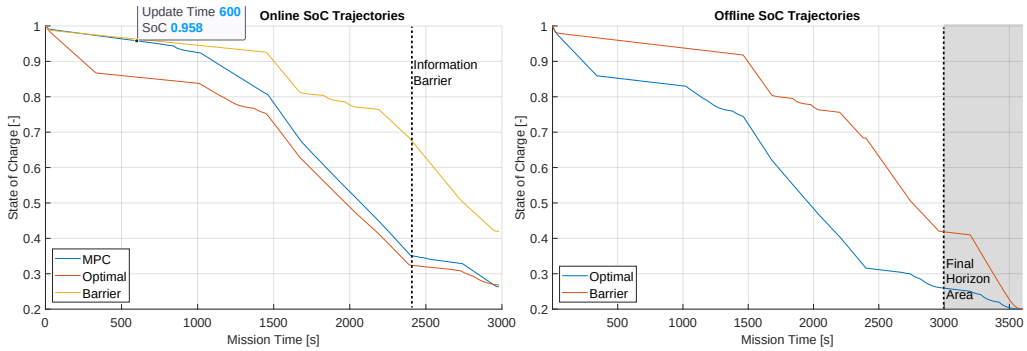


Figure 7.55: (Profile 1 Extended Envelope) Online SoC for barrier, optimal and MPC (left), Offline SoC for the information barrier at $t_{bar} = 2400$ $[s]$ and optimal (right)

[5] Previously, in Fig. 7.48, for the case of design hotel demand, the operating points during transitions were close to the operating limits, so they were plotted to demonstrate that the controller does not yield transitions outside the operating envelope

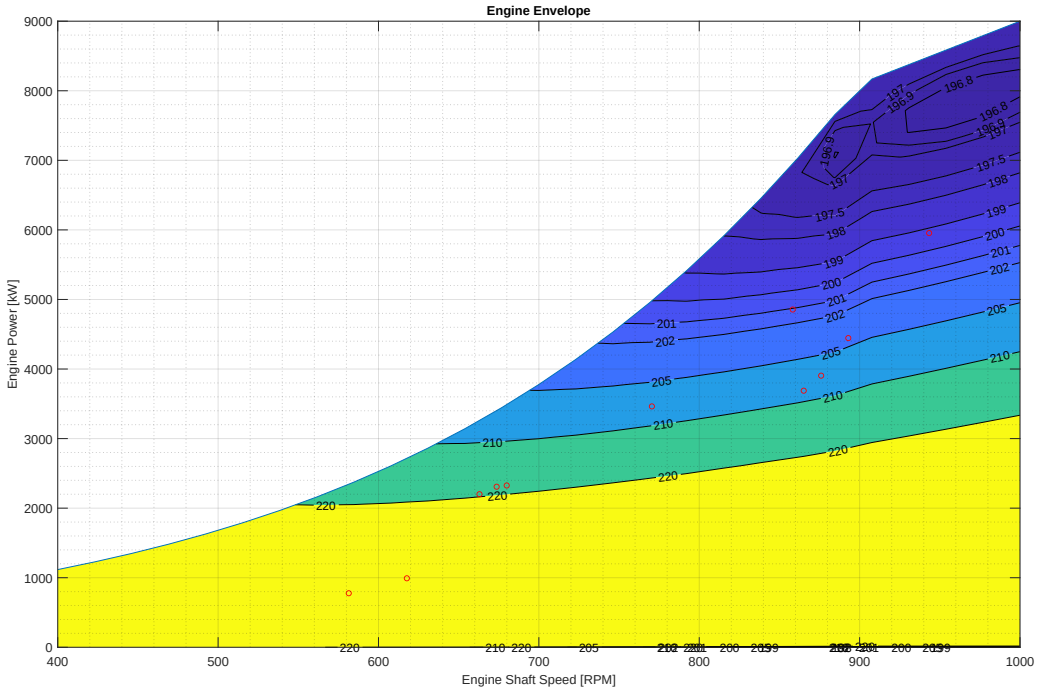


Figure 7.56: Online operating points (excluding transitions) plotted on the specific fuel oil consumption envelope of the main engine. It should be reminded that the fuel consumption of the main engine within the MPC reduced model is a fitted function, thus, it does not coincide exactly with the SFOC figure shown here.

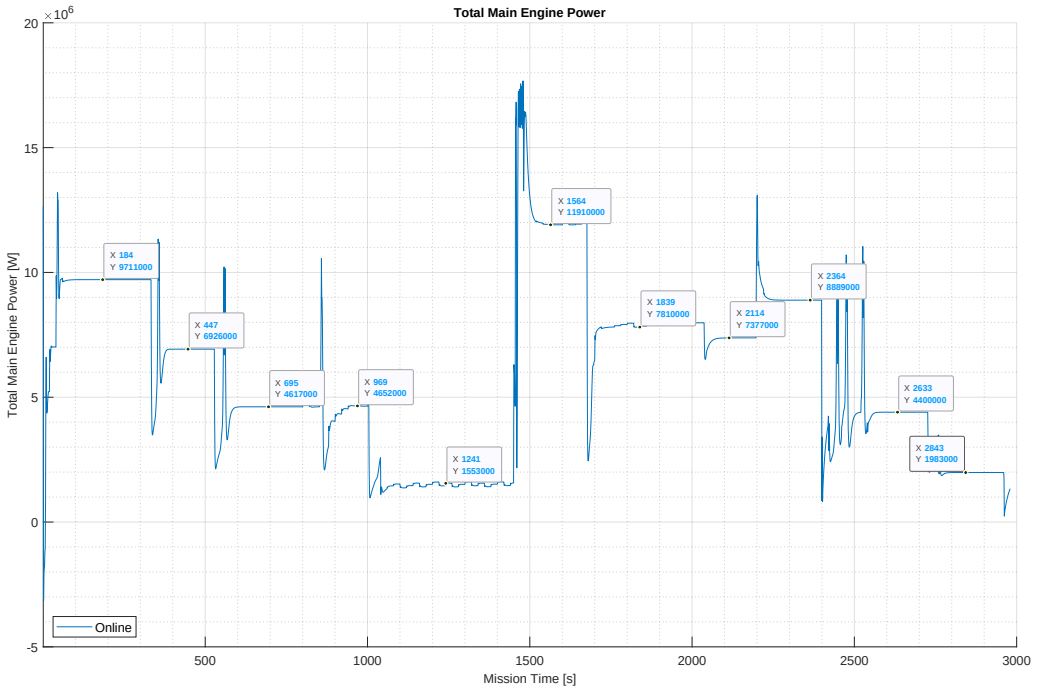


Figure 7.57: Online operating trajectory and the online (equilibrium) operating points plotted on the fuel consumption diagram above

## Charge Sustaining and End State Parametric Study

Previously, the end state was free to terminate in the full state of charge window, $SoC_{N+1} = [0.2\ 1]$. For the charge sustaining case, the terminal state is bounded within a small window $SoC_{N+1} = [0.89\ 0.91]$, while the initial state starts at $SoC_1 = 0.9$, so that it is also possible to initiate the mission with battery charging.

As shown before for profile 1 in Sec. 7.2.4, it can again be seen, even just from the offline SoC trajectories on Fig. 7.58, that the battery utilisation is minimal, and the new extended operating boundaries, again, do not result in more battery activity. This also means that there is no noticable difference between the optimal and barrier controllers. The induction motor is not utilised, and the battery energy is used only to cover hotel loads. From the profiles 2-4 run in Sec. 7.2.4 it seems that this behaviour is only particular to profile 1, as there is some degree of PTI activity in the other scenarios[6].

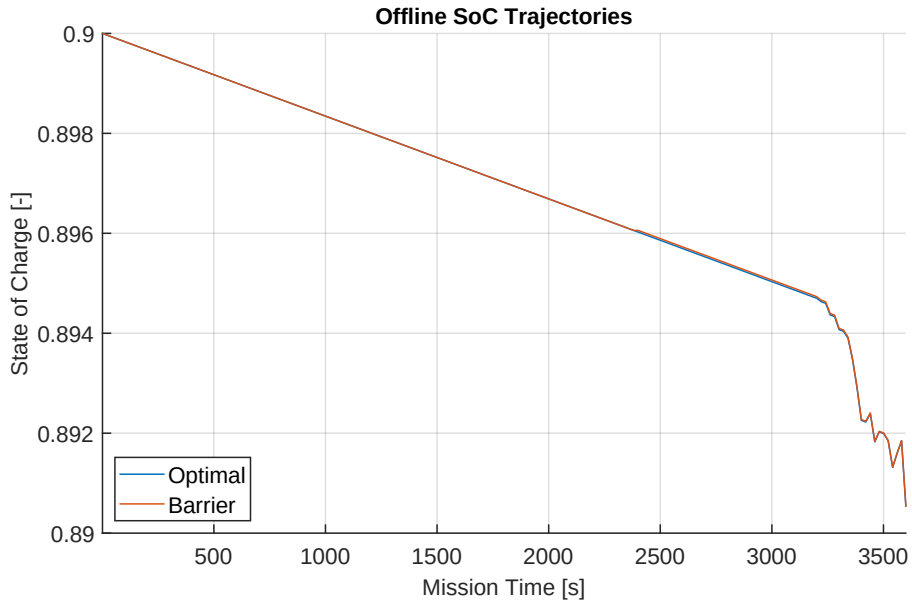


Figure 7.58: (Profile 1 Extended Envelope) Offline Trajectories of SoC in Charge Sustaining Mode

To demonstrate how the MPC framework behaves in such a scenario, a parametric study has been carried out, with the end state lower limit taking the values $SoC_{N+1,min} = 0.89$ (charge sustaining), $SoC_{N+1,min} = 0.79$ and $SoC_{N+1,min} = 0.69$. The goal of this study is to examine at what level of **depth of discharge** of the batteries the framework starts yielding fuel reduction. This may be important as, although this scenario strictly speaking deviates from the charge sustaining mode, in real world cases there might be occasions where a small battery depletion window is allowed.

[6] Note: PTO activity in profiles 2-4 in Sec. 7.2.4 was because of the narrow operating boundaries of the main engine so it is irrelevant for now

Table 7.7: Total Fuel Consumption for the Extended Envelope Case, Profile 1, Different Minimum End SoC

| **Controller** | **Consumption [kg]** | | |
|---|---|---|---|
| $SoC_{min}$ | **0.69** | **0.79** | **0.89** |
| **Optimal** | 1469.8 | 1505.7 | 1531.6 |
| **Barrier** | 1490.1 | 1521.5 | 1531.6 |
| **MPC** | 1481.8 (-0.55 %) | 1504.7 (-1.10%) | 1539.5 (+0.52%) |

As expected, once there is a depletion possibility, the MPC framework optimally depletes the battery, by appropriately utilising the induction machine as a motor (PTI). This can be seen in Fig. 7.60, where the induction machine activity is shown. With the depletion possibility, the optimal and barrier difference also grows, as shown in Table 7.7, allowing for the MPC framework to utilise the difference via the update point at $t = 600$ $[s]$, and follow the optimal controller yielding consumption reduction. This means that the benefits of future information utilisation can have an impact on fuel reduction, even if partial depletion is possible. The reduction is not consistent due to the end horizon, however, it is noticeable, indicating that whenever there might be a possibility for *trapped charge*, the MPC framework would be able to timely avoid it. Furthermore, the fuel reduction for the optimal controller at the mission end, including the end horizon, is at 3.29 $[kg]$ for the $SoC_{N+1,min} = 0.69$ case, and at 1.42 $[kg]$ for the $SoC_{N+1,min} = 0.79$ case. This means that, through correct use of the battery there is a consistent reduction in fuel consumed, which the MPC framework controller is able to consistently utilise.

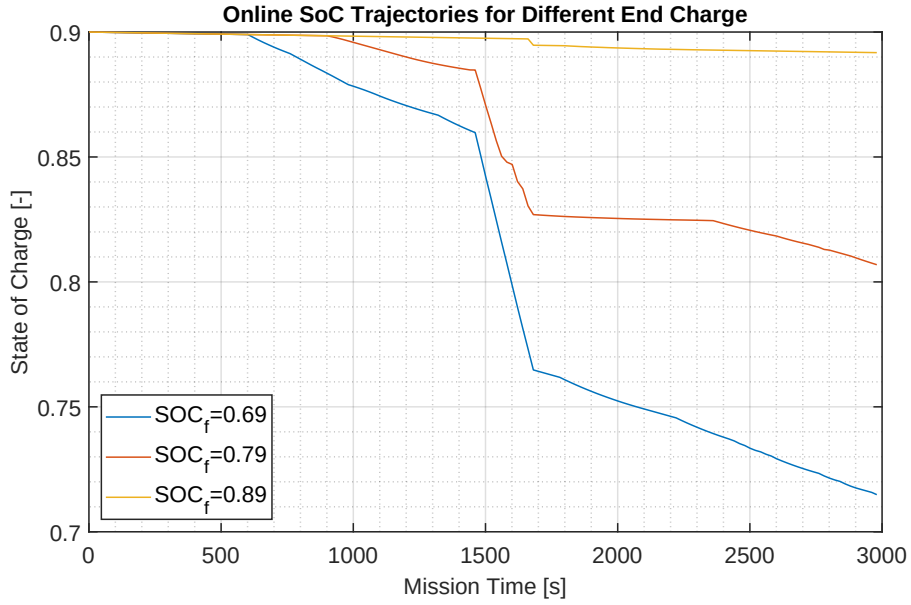


Figure 7.59: (Profile 1 Extended Envelope) Different trajectories of the state of charge of the battery pack for different end SoC

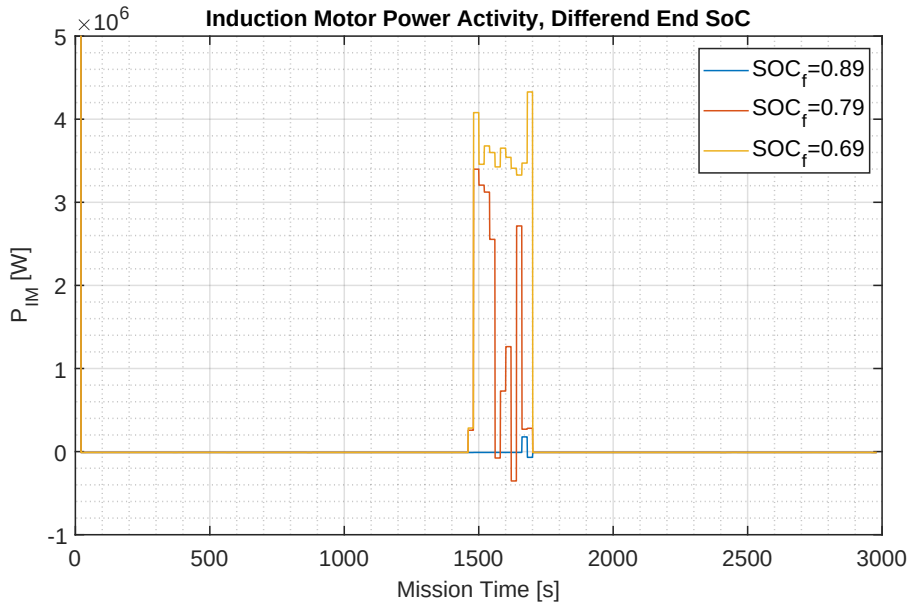


Figure 7.60: (Profile 1 Extended Envelope) Trajectories of the power of the induction machine for different end SoC

# Chapter 8

# Conclusions

A Model Predictive Control framework Energy Management Strategy based on [65] has been devised and implemented in naval powertrains. The approach is motivated by the conclusive remarks in [1], where an ECMS strategy used in tugboats did not show robust behaviour when load changes or heavy loadings were present. The framework has been verified and validated by using a dynamic Simulink® model, provided by DAMEN® SNS.

In more detail, the research goals of the present study were:

1. to successfully utilise real-time, long-term future information, provided by Integrated Bridge Systems or as human input, to better plan the battery discharge trajectory in order to minimise fuel consumption
2. to examine to what extent such long-term information is useful regarding fuel consumption minimisation
3. to implement the controller in a case study for a naval vessel
4. to correctly provide sufficient modelling detail so that it can adequately describe the powertrain, while still managing to keep the computational load of the EMS controller low enough to allow for implementation on board
5. to benchmark the performance against optimal and sub-optimal controllers

Addressing the above research goals one by one, the following remarks are made for the present report, correspondingly:

1. The long-term information has been successfully utilised with the formulation of a Model Predictive Control Framework. The framework includes a long-term state of charge trajectory end-constraint as a feedback pathway (Chapter 5). The formulations have been coded into both offline and online (Simulink) MATLAB® scripts (Chapter 7).

2. The fuel consumption minimisation for the suggested framework is part of the cost function of the optimal control problem (See Section 5.3.3). The main mechanisms for fuel consumption minimisation due to use of long-term information ("trapped charge" and main engine operating point manipulation) have been identified and demonstrated in Chapter 7, and mainly concern the charge-sustaining mode. Fuel consumption reduction capabilities in the charge-sustaining mode are small. The limits of such mechanisms are explored in three parametric studies in Sec. 7.3. The consumption reduction is situational and more prominent for systems with limited operating envelopes for the components of the powertrain.

3. The MPC framework controller has been successfully implemented inside the given dynamic model, utilising S-Function Blocks in Simulink® (Chapter 7), while the profiles used for the case study are generated from realistic historical data, provided by DAMEN® SNS (See Sec.7.2.1). A case with an extended, due to sequential turbocharging, main engine envelope has also been studied in Sec. 7.3.3.

4. The reduced component description has been formulated, and its level of detail has been verified in Chapter 6. The reduced model description inside the MPC framework has been verified and validated in Chapter 7. An example of the satisfactory level of detail is the ability of the controller to identify offline the SFOC low point of the main engine and provide the correct setpoints to the dynamic (MVFP) model to guide its operation to that area, demonstrated in Fig. 7.48. The implementation capabilities can be showcased by the significantly lower running time of the algorithm compared to the total mission time (See Sec. 7.2.3).

5. The performance of the online EMS framework controller has been verified and validated in four realistic profiles for both charge-sustaining and charge-depleting modes in Chapter 7, and follows closely the optimal controller behaviour, while it is also reasonably robust. The only significant discrepancy has been noticed in profile 1 for charge-sustaining mode and design hotel demand in Sec. 7.2.4. The suggested framework is capable of yielding fuel consumption reduction of up to approximately 3.5%, under certain load sequences, when compared to any other present EMS solution with no long-term feedback, with the barrier controller validation scheme (See Sec. 7.2.2). In Sec. 7.3, three parametric studies have been carried out to examine the extent of the possibility for fuel reduction, by varying the update point position, the hotel power demand, and the operating boundaries of the engine, when sequential turbocharging is used. The first studies showed considerable opportunities in a wide range of update positions. However, the fuel reduction is smaller for the cases of increased hotel demand and wider operating boundaries.

Concluding the study, all of the above goals have successfully been addressed, yielding an MPC framework solution for EMS of naval powertrains that proves to be robust, while it also performs

very close to an optimal controller. It is noted that an undesirable behaviour, which can be described as *chattering*, has been found, with possible solutions discussed in Chapter 7. Furthermore, in the present study the limits of the long-term information utilisation for fuel consumption minimisation have been examined, and the key mechanisms for fuel reduction utilising realistic information availability, concerning the particularities of hybrid power-supply ships, have been identified.

In more detail, the mechanism of "trapped charge" has been identified to be the most crucial for fuel consumption reduction, which concerns the charge-depleting EMS control mode, and which, under certain load sequences, allows for utilisation of long-term information to yield a reduction above 3.5% when compared to the optimal controller with no long-term feedback pathway. It is reminded to the reader that all previous control strategies, including ECMS, A-ECMS and RB can, at best, perform as well as the barrier controller, or optimal controller with no long-term feedback (See Sec. 7.2.2).

Moreover, a parametric study has been carried out to examine different update points and their effects on the suggested framework. It is concluded that, when there is headroom for reduced fuel consumption, there is a considerably large time window for the information update to occur, and still yield such reduction. However, the "trapped charge" mechanism seems to be less prominent in cases of design hotel demand and sequential turbocharging.

The controller has been tested for both plug-in and charge-depleting modes, demonstrating that future information is of less importance for the latter, a result that is consistent with the findings in [1]. Nevertheless, the robustness of the controller has been demonstrated in both modes, yielding close-to-optimal results for four different realistic loading profiles, with a discrepancy noted only for the case of Profile 1 in design hotel demand.

A second parametric study has been carried out to examine the effects of added electric load on fuel consumption and robustness. The controller behaviour remains close to optimal, after the update point. A potential second mechanism for fuel consumption reduction has been identified for the design load case, where the aggressive PTO function of the induction motor contributes in better control of the operating points of the main engine, keeping them in the most fuel-efficient region, resulting in a fuel consumption reduction of approximately 0.4%. This difference is observed solely due to the optimal discharge of the battery through future information utilisation.

Finally, an extended main engine envelope study has been carried out, with an appropriately extended combinator curve and a wider operating range for the main engine and the induction motor. This study has been carried to examine the controller's behaviour in the full capability of the propulsive train, achieved via Sequential Turbocharging (STC) of the main engines. In charge-depleting mode, the MPC framework demonstrated consistent behaviour, indicating that it can readily be implemented in powertrains with different operating boundaries and still be robust, effective and close to optimal. However, it has been found that the wider operating range of the engine and the

induction machine reduced the trapped charge effect that has been previously observed, suggesting that future information utilisation yields less fuel reduction for propulsive trains with relaxed operating boundaries. For the charge-sustaining mode, a parametric study has been carried out, by varying the end state of charge lower limit, demonstrating that, if a relatively small battery depletion is allowed, fuel reduction is possible and future information utilisation becomes important. When that happens, the MPC framework is also able to closely follow the optimal controller and yield a reduction in fuel consumed, although the results should be carefully interpreted, due to the end horizon, which has not been taken into account.

## Future Research

Following the contribution of the present study, research can be made in the direction of implementing the suggested MPC framework, together with a short-term disturbance predictor. Such an approach should yield a pronounced fuel reduction, due to short-term predictors performing better with MPC, compared to adaptive ECMS, used in [1]. Several choices for possible short-term predictors have been discussed in Sec. 5.3.3, which include, namely, ARMA models, Markov Chain Monte Carlo methods, and neural networks.

Extension of the cost function of the optimal control problem to include criteria such as emissions, component wear, and chattering minimisation is also possible, as the formulations in Sec. 5.3.3 are flexible to include such terms. However, since the controller is relying on a quasi-static internal model, transient noise emission extensions of the objective function are not readily implementable. Furthermore, model reduction formulations that include several combinator curves for a variety of operating modes can also be implemented.

The MPC framework controller suggested can be used in powertrain design, to examine the size of the batteries and the corresponding fuel consumption reduction with given operating profiles (Also See Sec.3.3).

Another possible research direction is further validation of the suggested framework in a physical system, or in detailed dynamic models, against existing EMS controllers.

Finally, developing an interface to utilise the long-term prediction capabilities, by introducing outputs from the Integrated Bridge Systems or Human Input to the feedback pathway of the present framework is also possible and a key step for real-world implementation of the strategy, and realisation of its full potential.

# Bibliography


[1] M Kalikatzarakis, RD Geertsma, EJ Boonen, K Visser, and RR Negenborn. Ship energy management for hybrid propulsion and power supply with shore charging. *Control Engineering Practice*, 76:133–154, 2018.

[2] RD Geertsma, RR Negenborn, K Visser, and JJ Hopman. Design and control of hybrid power and propulsion systems for smart ships: A review of developments. *Applied Energy*, 194:30–54, 2017.

[3] Lorenzo Serrao, Simona Onori, and Giorgio Rizzoni. A comparative analysis of energy management strategies for hybrid electric vehicles. *Journal of Dynamic Systems, Measurement, and Control*, 133(3):031012, 2011.

[4] Gudmundur Gunnarsson, Jón Skúlason, Árni Sigurbjarnarson, and Sigurd Enge. Regenerative electric/hybrid drive train for ships rensea ii, 01 2016.

[5] Regenerative Hybrid-Electric Propulsion - RENSEA REPORT, Phase 1. `https://bellona.no/assets/Hybrid-report_2013_v4_web.pdf`. Accessed: 2019-11-25.

[6] E. Ovrum and T. F. Bergh. Modelling lithium-ion battery hybrid ship crane operation. *Applied Energy*, 2015.

[7] Eleftherios K. Dedes, Dominic A. Hudson, and Stephen R. Turnock. Assessing the potential of hybrid energy technology to reduce exhaust emissions from global shipping. *Energy Policy*, 40(1):204–218, 2012.

[8] Hans Klein Woud and Douwe Stapersma. *Design of propulsion and electric power generation systems*, volume 1902536479. IMarEST, 2002.

[9] DS de Waard. Parameterization of ship propulsion drives and their fuel efficiency under different operatiobal modes and configurations. In *Proceedings of the engine as a weapon VI conference. Bath, UK*, pages 44–57, 2015.

[10] Ioana Georgescu, Milinko Godjevac, and Klaas Visser. Efficiency constraints of energy storage for on-board power systems. *Ocean Engineering*, 162(November 2017):239–247, 2018.

[11] S Topaloglou, G Paplambrou, and N Kyrtatos. Energy management controller design for hybrid ship propulsion during transient operation. In *Proceedings of 28th CIMAC congress*, volume 50, pages 1–9, 2016.

[12] Bijan Zahedi, Lars E. Norum, and Kristine B. Ludvigsen. Optimized efficiency of all-electric ships by dc hybrid power systems. *Journal of Power Sources*, 255:341–354, 2014.

[13] Damen Launches Two Road Ferries for Canadian Operator BC Ferries. `https://www.damen.com/en/news/2019/04/damen_launches_two_road_ferries_for_canadian_operator_bc_ferries`. Accessed: 2019-11-25.

[14] Damen Secures Repeat Order from BC Ferry Services. `https://www.damen.com/en/news/2019/11/damen_secures_repeat_order_from_bc_ferry_services`. Accessed: 2019-11-25.

[15] Implementing the Paris agreement. `https://op.europa.eu/en/publication-detail/-/publication/b38840b2-4b2a-11e7-aea8-01aa75ed71a1/language-en`. Accessed: 2020-04-07.

[16] Joeri Rogelj, Michel Den Elzen, Niklas Höhne, Taryn Fransen, Hanna Fekete, Harald Winkler, Roberto Schaeffer, Fu Sha, Keywan Riahi, and Malte Meinshausen. Paris agreement climate proposals need a boost to keep warming well below 2 c. *Nature*, 534(7609):631–639, 2016.

[17] UN body adopts climate change strategy forshipping. `http://www.imo.org/en/MediaCentre/PressBriefings/Pages/06GHGinitialstrategy.aspx`. Accessed: 2020-04-07.

[18] Third IMO GHG Study 2014. `http://www.imo.org/en/OurWork/Environment/PollutionPrevention/AirPollution/Pages/Greenhouse-Gas-Studies-2014.aspx`. Accessed: 2020-04-07.

[19] International Maritime Organization - Energy Efficiency Measures. `www.imo.org/en/OurWork/Environment/PollutionPrevention/AirPollution/Pages/Technical-and-Operational-Measures.aspx`. Accessed: 2019-10-18.

[20] International Maritime Organization - SEB Report, IMO 2020 Comment #2: MFO Price Dynamics - Navigating 2019 and 2020, 12th March 2019. `https://webapp.sebgroup.com/mbs/research.nsf/alldocsbyunid/BA30E75B70065883C12583BB0031DC34/$FILE/2019_03_12_IMO_2020_Comment_02_MFO_05_Trading_dynamics.pdf`. Accessed: 2019-10-21.

[21] Congbiao Sui, Douwe Stapersma, Klaas Visser, Peter de Vos, and Yu Ding. Energy effectiveness of ocean-going cargo ship under various operating conditions. *Ocean Engineering*, 2019.

[22] Apostolos Papanikolaou, George Zaraphonitis, Elzbieta Bitner-Gregersen, Vladimir Shigunov, Ould El Moctar, Carlos Guedes Soares, Devalapalli N. Reddy, and Florian Sprenger. Energy efficient safe ship operation (SHOPERA). In *Transactions - Society of Naval Architects and Marine Engineers*, 2016.

[23] H Yasukawa, M Zaky, I Yonemasu, and R Miyake. Effect of engine output on maneuverability of a vlcc in still water and adverse weather conditions. *Journal of Marine Science and Technology*, 22(3):574–586, 2017.

[24] Fig.3 Share of trasport greenhouse gas emissions, EU Convention. `https://www.eea.europa.eu/data-and-maps/indicators/transport-emissions-of-greenhouse-gases/transport-emissions-of-greenhouse-gases-12`. Accessed: 2020-04-07.

[25] Effort sharing: Member States' emission targets. `https://ec.europa.eu/clima/policies/effort_en`. Accessed: 2020-04-07.

[26] Reducing emissions from the shipping sector. `https://ec.europa.eu/clima/policies/transport/shipping_en`. Accessed: 2020-04-07.

[27] Víctor Manuel Moreno Sáiz and Alberto Pigazo López. Future trends in electric propulsion systems for commercial vessels. *Journal of Maritime Research*, 4(2):81–100, 2007.

[28] Clemente Capasso and Ottorino Veneri. Experimental analysis on the performance of lithium based batteries for road full electric and hybrid vehicles. *Applied Energy*, 2014.

[29] Gene Castles, Greg Reed, Ashish Bendre, and Robert Pitsch. Economic benefits of hybrid drive propulsion for naval ships. *IEEE Electric Ship Technologies Symposium, ESTS 2009*, pages 515–520, 2009.

[30] M Wijsmuller and T Hasselaar. Optimisation of the propulsion arrangement in emergency towing vessels. *Ship and boat international*, pages 34–7, 2007.

[31] Renato Barcellos et al. The hybrid propulsion system as an alternative for offshore vessels servicing and supporting remote oil field operations. In *OTC Brasil*. Offshore Technology Conference, 2013.

[32] A. Sciarretta and L. Guzzela. Control of hybrid - Electric vehicles. *IEEE Control Systems Magazine*, 4(April):60–70, 2007.

[33] A. Sciarretta, L. Serrao, P. C. Dewangan, P. Tona, E. N.D. Bergshoeff, C. Bordons, L. Charmpa, Ph Elbert, L. Eriksson, T. Hofman, M. Hubacher, P. Isenegger, F. Lacandia, A. Laveau, H. Li, D. Marcos, T. Nüesch, S. Onori, P. Pisu, J. Rios, E. Silvas, M. Sivertsson,

L. Tribioli, A. J. van der Hoeven, and M. Wu. A control benchmark on the energy management of a plug-in hybrid electric vehicle. *Control Engineering Practice*, 29:287–298, 2014.

[34] Thanh Long Vu, Aaron Alexander Ayu, Jaspreet Singh Dhupia, Louis Kennedy, and Alf Kare Adnanes. Power Management for Electric Tugboats Through Operating Load Estimation. *IEEE Transactions on Control Systems Technology*, 23(6):2375–2382, 2015.

[35] Liza Chua Wan Yuan, Tegoeh Tjahjowidodo, Gerald Seet Gim Lee, Ricky Chan, and Alf Kare Adnanes. Equivalent Consumption Minimization Strategy for hybrid all-electric tugboats to optimize fuel savings. *Proceedings of the American Control Conference*, 2016-July:6803–6808, 2016.

[36] Clara Marina Martinez, Xiaosong Hu, Dongpu Cao, Efstathios Velenis, Bo Gao, and Matthias Wellers. Energy Management in Plug-in Hybrid Electric Vehicles: Recent Progress and a Connected Vehicles Perspective. *IEEE Transactions on Vehicular Technology*, 66(6):4534–4549, 2017.

[37] Pierluigi Pisu and Giorgio Rizzoni. A comparative study of supervisory control strategies for hybrid electric vehicles. *IEEE Transactions on Control Systems Technology*, 15(3):506–518, 2007.

[38] Eneko Unamuno and Jon Andoni Barrena. Hybrid ac/dc microgrids - Part II: Review and classification of control strategies. *Renewable and Sustainable Energy Reviews*, 52(October 2018):1123–1134, 2015.

[39] Josep M Guerrero, Juan C Vasquez, José Matas, Luis García De Vicuña, and Miguel Castilla. Hierarchical control of droop-controlled ac and dc microgrids—a general approach toward standardization. *IEEE Transactions on industrial electronics*, 58(1):158–172, 2010.

[40] C Guardiola, B Pla, S Onori, and G Rizzoni. Insight into the hev/phev optimal control solution based on a new tuning method. *Control Engineering Practice*, 29:247–256, 2014.

[41] Mahyar Vajedi, Amir Taghavipour, Nasser L. Azad, and John McPhee. A comparative analysis of route-based power management strategies for real-time application in plug-in hybrid electric vehicles. *Proceedings of the American Control Conference*, pages 2612–2617, 2014.

[42] Yong Tang, Wei Yuan, Minqiang Pan, and Zhenping Wan. Experimental investigation on the dynamic performance of a hybrid pem fuel cell/battery system for lightweight electric vehicle application. *Applied Energy*, 88(1):68–76, 2011.

[43] Sten Karlsson. Optimal size of PHEV batteries from a consumer perspective - Estimation using car movement data and implications for data harvesting. *World Electric Vehicle Journal*, 3(2):387–395, 2009.

[44] V. Larsson, L. Johannesson, and B. Egardt. Impact of trip length uncertainty on optimal discharging strategies for PHEVs. *IFAC Proceedings Volumes (IFAC-PapersOnline)*, 43(7):55–60, 2010.

[45] Alireza Khaligh and Zhihao Li. Battery, ultracapacitor, fuel cell, and hybrid energy storage systems for electric, hybrid electric, fuel cell, and plug-in hybrid electric vehicles: State of the art. *IEEE Transactions on Vehicular Technology*, 59(6):2806–2814, 2010.

[46] Council directive 70/220/eec of 20 march 1970 on the approximation of the laws of the member states relating to measures to be taken against air pollution by gases from positive-ignition engines of motor vehicles official journal l 76, 6 april 1970, pp. 1-22. *Official Journal L*, 76:1–22, 1970.

[47] US EPA approves California auto emissions standard. `https://www.reuters.com/article/autos-epa-california/update-2-us-epa-approves-california-auto-emissions-standard-idUSN3044688920090630`. Accessed: 2019-10-21.

[48] Lars Henrik Björnsson and Sten Karlsson. Plug-in hybrid electric vehicles: How individual movement patterns affect battery requirements, the potential to replace conventional fuels, and economic viability. *Applied Energy*, 143:336–347, 2015.

[49] Lina Fu, Ümit Özguner, Pinak Tulpule, and Vincenzo Marano. Real-time energy management and sensitivity study for hybrid electric vehicles. *Proceedings of the American Control Conference*, pages 2113–2118, 2011.

[50] Joanne T Woestman, Prabhakar B Patil, Ross M Stunz, and Thomas E Pilutti. Strategy to use an on-board navigation system for electric and hybrid electric vehicle energy management, November 26 2002. US Patent 6,487,477.

[51] Antonio Sciarretta, Lino Guzzella, and Michael Back. A Real-Time Optimal Control Strategy for Parallel Hybrid Vehicles with On-Board Estimation of the Control Parameters. *IFAC Proceedings Volumes*, 37(22):489–494, 2004.

[52] Eva Finkeldei and Michael Back. Implementing an MPC Algorithm in a Vehicle with a Hybrid Powertrain using Telematics as a Sensor for Powertrain Control. *IFAC Proceedings Volumes*, 37(22):433–438, 2004.

[53] Lars Johannesson, Mattias Asbogard, and Bo Egardt. Assessing the potential of predictive control for hybrid vehicle powertrains using stochastic dynamic programming. *IEEE Transactions on Intelligent Transportation Systems*, 8(1):71–83, 2007.

[54] Chan Chiao Lin, Huei Peng, and J. W. Grizzle. A stochastic control strategy for hybrid electric vehicles. *Proceedings of the American Control Conference*, 5:4710–4715, 2004.

[55] G Paganelli. General supervisory control policy for the energy optimization of charge-sustaining hybrid electric vehicles. *JSAE Review*, 22(4):511–518, 2001.

[56] Cristian Musardo, Giorgio Rizzoni, Yann Guezennec, and Benedetto Staccia. A-ECMS : An Adaptive Algorithm for Hybrid Electric Vehicle Energy Management A-ECMS : An Adaptive Algorithm for Hybrid Electric Vehicle. *European Journal of Control*, 11(December 2005):509–524, 2005.

[57] Bo Gu and Giorgio Rizzoni. An adaptive algorithm for hybrid electric vehicle energy management based on driving pattern recognition. In *ASME 2006 International Mechanical Engineering Congress and Exposition*, pages 249–258. American Society of Mechanical Engineers, 2006.

[58] Soon Il Jeon, Sung Tae Jo, Yeong Il Park, and Jang Moo Lee. Multi-mode driving control of a parallel hybrid electric vehicle using driving pattern recognition. *Journal of Dynamic Systems, Measurement and Control, Transactions of the ASME*, 124(1):141–149, 2002.

[59] EHJA Nuijten, M Koot, JTBA Kessels, B De Jager, M Heemels, W Hendrix, and P van den Bosch. Advanced energy management strategies for vehicle power nets. In *Proc. EAEC 9th Int. Congress: European Automotive Industry Driving Global Changes*, 2003.

[60] Fengjun Yan, Junmin Wang, and Kaisheng Huang. Hybrid electric vehicle model predictive control torque-split strategy incorporating engine transient characteristics. *IEEE Transactions on Vehicular Technology*, 61(6):2458–2467, 2012.

[61] Avra Brahma, Yann Guezennec, and Giorgio Rizzoni. Optimal energy management in series hybrid electric vehicles. In *Proceedings of the 2000 American Control Conference. ACC (IEEE Cat. No. 00CH36334)*, volume 1, pages 60–64. IEEE, 2000.

[62] A R Salisa, N Zhang, and J G Zhu. A Comparative Analysis of Fuel Economy and Emissions Between a Conventional HEV and the UTS PHEV. *IEEE Transactions on Vehicular Technology*, 60(1):44–54, 2011.

[63] Michael Patrick O'Keefe and Tony Markel. Dynamic programming applied to investigate energy management strategies for a plug-in hev. Technical report, National Renewable Energy Lab.(NREL), Golden, CO (United States), 2006.

[64] P. Tulpule, V. Marano, and G. Rizzoni. Effects of different PHEV control strategies on vehicle performance. *Proceedings of the American Control Conference*, pages 3950–3955, 2009.

[65] Chao Sun, Scott Jason Moura, Xiaosong Hu, J. Karl Hedrick, and Fengchun Sun. Dynamic Traffic Feedback Data Enabled Energy Management in Plug-in Hybrid Electric Vehicles. *IEEE Transactions on Control Systems Technology*, 23(3):1075–1086, 2015.

[66] Thillainathan Logenthiran and Dipti Srinivasan. Short term generation scheduling of a microgrid. In *TENCON 2009-2009 IEEE Region 10 Conference*, pages 1–6. IEEE, 2009.

[67] Petr Stluka, Datta Godbole, and Tariq Samad. Energy management for buildings and microgrids. In *2011 50th IEEE Conference on Decision and Control and European Control Conference*, pages 5150–5157. IEEE, 2011.

[68] Farid Katiraei, Reza Iravani, Nikos Hatziargyriou, and Aris Dimeas. Microgrids management. *IEEE power and energy magazine*, 6(3):54–65, 2008.

[69] Yu Zhang, Nikolaos Gatsis, and Georgios B Giannakis. Robust energy management for microgrids with high-penetration renewables. *IEEE Transactions on Sustainable Energy*, 4(4):944–953, 2013.

[70] Soojeong Choi, Sunju Park, Dong-Joo Kang, Seung-jae Han, and Hak-Man Kim. A microgrid energy management system for inducing optimal demand response. In *2011 IEEE International Conference on Smart Grid Communications (SmartGridComm)*, pages 19–24. IEEE, 2011.

[71] Aris L Dimeas and Nikos D Hatziargyriou. Operation of a multiagent system for microgrid control. *IEEE Transactions on Power systems*, 20(3):1447–1455, 2005.

[72] Wenbo Shi, Xiaorong Xie, Chi-Cheng Chu, and Rajit Gadh. Distributed optimal energy management in microgrids. *IEEE Transactions on Smart Grid*, 6(3):1137–1146, 2014.

[73] Z Ouyang and SM Shahidehpour. An intelligent dynamic programming for unit commitment application. *IEEE Transactions on Power Systems*, 6(3):1203–1209, 1991.

[74] Weerakorn Ongsakul and Nit Petcharaks. Unit commitment by enhanced adaptive lagrangian relaxation. *IEEE Transactions on Power Systems*, 19(1):620–628, 2004.

[75] Emanuele Crisostomi, Mingming Liu, Marco Raugi, and Robert Shorten. Plug-and-play distributed algorithms for optimized power generation in a microgrid. *IEEE transactions on Smart grid*, 5(4):2145–2154, 2014.

[76] Carlo Cecati, Costantino Citro, and Pierluigi Siano. Combined operations of renewable energy systems and responsive demand in a smart grid. *IEEE transactions on sustainable energy*, 2(4):468–476, 2011.

[77] Pierluigi Siano, Carlo Cecati, Hao Yu, and Janusz Kolbusz. Real time operation of smart grids via fcn networks and optimal power flow. *IEEE Transactions on Industrial Informatics*, 8(4):944–952, 2012.

[78] S Ali Pourmousavi, M Hashem Nehrir, Christopher M Colson, and Caisheng Wang. Real-time energy management of a stand-alone hybrid wind-microturbine energy system using particle swarm optimization. *IEEE Transactions on Sustainable Energy*, 1(3):193–201, 2010.

[79] Alejandro D Dominguez-Garcia and Christoforos N Hadjicostis. Distributed algorithms for control of demand response and distributed energy resources. In *2011 50th IEEE Conference on Decision and Control and European Control Conference*, pages 27–32. IEEE, 2011.

[80] Zhe Wang, Kai Yang, and Xiaodong Wang. Privacy-preserving energy scheduling in microgrid systems. *IEEE transactions on Smart Grid*, 4(4):1810–1820, 2013.

[81] Jun Hou, Jing Sun, and Heath Hofmann. Mitigating power fluctuations in electrical ship propulsion using model predictive control with hybrid energy storage system. *Proceedings of the American Control Conference*, pages 4366–4371, 2014.

[82] Ali Haseltalab, Rudy R. Negenborn, and Gabriel Lodewijks. Multi-Level Predictive Control for Energy Management of Hybrid Ships in the Presence of Uncertainty and Environmental Disturbances. *IFAC-PapersOnLine*, 49(3):90–95, 2016.

[83] Georgios Papalambrou, Sergey Samokhin, Sotirios Topaloglou, Nikolaos Planakis, Nikolaos Kyrtatos, and Kai Zenger. Model Predictive Control for Hybrid Diesel-Electric Marine Propulsion. *IFAC-PapersOnLine*, 50(1):11064–11069, 2017.

[84] Hyeongjun Park, Jing Sun, Steven Pekarek, Philip Stone, Daniel Opila, Richard Meyer, Ilya Kolmanovsky, and Raymond Decarlo. Real-Time Model Predictive Control for Shipboard Power Management Using the IPA-SQP Approach. *IEEE Transactions on Control Systems Technology*, 23(6):2129–2143, 2015.

[85] Jun Hou, Jing Sun, and Heath Hofmann. Adaptive model predictive control with propulsion load estimation and prediction for all-electric ship energy management. *Energy*, 150:877–889, 2018.

[86] E. A. Sciberras and R. A. Norman. Multi-objective design of a hybrid propulsion system for marine vessels. *IET Electrical Systems in Transportation*, 2(3):148–157, 2012.

[87] Thanh Long Vu, Jaspreet Singh Dhupia, Aaron Alexander Ayu, Louis Kennedy, and Alf Kare Adnanes. Optimal power management for electric tugboats with unknown load demand. *Proceedings of the American Control Conference*, pages 1578–1583, 2014.

[88] International Maritime Organization - Integrated Bridge System. `http://www.imo.org/en/OurWork/Safety/SafetyTopics/Pages/IntegratedBridgeSystems.aspx`. Accessed: 2019-11-11.

[89] Blagovest Chanev Belev. Information capabilities of integrated bridge systems. *Journal of Navigation*, 57(1):145–151, 2004.

[90] Lokukaluge P. Perera and C. Guedes Soares. Weather routing and safe ship handling in the future of shipping. *Ocean Engineering*, 130(August 2016):684–695, 2017.

[91] Lokukaluge P. Perera and C. Guedes Soares. Collision risk detection and quantification in ship navigation with integrated bridge systems. *Ocean Engineering*, 109:344–354, 2015.

[92] Keh Sik Min. Automation and control systems technology in Korean shipbuilding industry: The state of the art. *IFAC Proceedings Volumes (IFAC-PapersOnline)*, 17(1 PART 1):7185–7190, 2008.

[93] Ali Emadi, Kaushik Rajashekara, Sheldon S Williamson, and Srdjan M Lukic. Topological overview of hybrid electric and fuel cell vehicular power system architectures and configurations. *IEEE Transactions on vehicular technology*, 54(3):763–770, 2005.

[94] D. Stapersma. *Diesel Engines Volume 4: Emissions and Heat transfer (Reader WB4408B)*, volume 4. Faculty of Mechanical, Maritime and Mechanical Engineering, 2010.

[95] Congbiao Sui, Douwe Stapersma, Klaas Visser, Peter de Vos, and Yu Ding. Energy effectiveness of ocean-going cargo ship under various operating conditions. *Ocean Engineering*, 190:106473, 2019.

[96] Gunter Sattler. Fuel cells going on-board. *Journal of power sources*, 86(1-2):61–67, 2000.

[97] Ampere Electric-Powered Ferry. `https://www.ship-technology.com/projects/norled-zerocat-electric-powered-ferry/`. Accessed: 2020-4-22.

[98] Olle Sundström and Lino Guzzella. A generic dynamic programming Matlab function. *Proceedings of the IEEE International Conference on Control Applications*, (7):1625–1630, 2009.

[99] DNVGL-RP-0043 Safety, operation and performance of grid-connected energy storage systems. `https://rules.dnvgl.com/docs/pdf/DNVGL/RP/2015-12/DNVGL-RP-0043.pdf`. Accessed: 2020-5-14.

[100] Lino Guzzella, Antonio Sciarretta, et al. *Vehicle propulsion systems*, volume 1. Springer, 2007.

[101] Rinze Geertsma. *Autonomous Control for Adaptive Ships with Hybrid Propulsion and Power Generation*. PhD thesis, 2019.

[102] Milinko Godjevac, Joost Drijver, Leo de Vries, and Douwe Stapersma. Evaluation of losses in maritime gearboxes. *Proceedings of the Institution of Mechanical Engineers, part M: Journal of Engineering for the Maritime Environment*, 230(4):623–638, 2016.

[103] Richard Bellman. Dynamic programming. Technical report, RAND CORP SANTA MONICA CA, 1956.

[104] Dimitri P Bertsekas, Dimitri P Bertsekas, Dimitri P Bertsekas, and Dimitri P Bertsekas. *Dynamic programming and optimal control*, volume 1. Athena scientific Belmont, MA, 1995.

[105] Theo Hofman, Maarten Steinbuch, Roell Van Druten, and Alex Serrarens. Rule-based energy management strategies for hybrid vehicles. *International Journal of Electric and Hybrid Vehicles*, 1(1):71–94, 2007.

[106] Michael Back, Matthias Simons, Frank Kirschaum, and Volker Krebs. Predictive control of drivetrains. *IFAC Proceedings Volumes*, 35(1):241–246, 2002.

[107] Daniele De Vito. Power flow management with predictive capabilities for a hybrid fuel cell vehicle. *IFAC Proceedings Volumes*, 40(10):9–16, 2007.

[108] Jonathan How. Lecture Notes for *16.323: Principles of Optimal Control*. Spring 2008. Massachusetts Institute of Technology: MIT OpenCourseWare . `https://ocw.mit.edu/courses/aeronautics-and-astronautics/16-323-principles-of-optimal-control-spring-2008/index.htm`. Accessed: 2020-05-16.

[109] Olle Sundström, Daniel Ambühl, and Lino Guzzella. On implementation of dynamic programming for optimal control problems with final state constraints. *Oil & Gas Science and Technology–Revue de l'Institut Français du Pétrole*, 65(1):91–102, 2010.

[110] Philipp Elbert, Soren Ebbesen, and Lino Guzzella. Implementation of dynamic programming for $n$-dimensional optimal control problems with final state constraints. *IEEE Transactions on Control Systems Technology*, 21(3):924–931, 2012.

[111] Nikolce Murgovski, Lars Johannesson, Jonas Sjöberg, and Bo Egardt. Component sizing of a plug-in hybrid electric powertrain via convex optimization. *Mechatronics*, 22(1):106–120, 2012.

[112] Carlos Bordons, Félix Garcia-Torres, and Miguel A Ridao. *Model Predictive Control of Microgrids*. Springer, 2020.

[113] Lorenzo Serrao. A comparative analysis of energy management strategies for hybrid electric vehicles [ph. d. thesis]. *Columbus (Ohio, United States): The Ohio State University*, 2009.

[114] Yutao Chen, Mattia Bruschetta, Enrico Picotti, and Alessandro Beghi. Matmpc-a matlab based toolbox for real-time nonlinear model predictive control. In *2019 18th European Control Conference (ECC)*, pages 3365–3370. IEEE, 2019.

[115] Vatche Donikian. *Model predictive control of advanced hybrid powertrain systems*. PhD thesis, UC Irvine, 2016.

[116] RD Geertsma, RR Negenborn, K Visser, and JJ Hopman. Torque control for diesel mechanical and hybrid propulsion for naval vessels. In *Proceedings of the 13th international naval engineering conference. Bristol, UK*, pages 476–92, 2016.

[117] RD Geertsma, K Visser, and RR Negenborn. Adaptive pitch control for ships with diesel mechanical and hybrid propulsion. *Applied Energy*, 228:2490–2509, 2018.

[118] Daniel Ambuhl and Lino Guzzella. Predictive reference signal generator for hybrid electric vehicles. *IEEE transactions on vehicular technology*, 58(9):4730–4740, 2009.

[119] Stephen Boyd, Stephen P Boyd, and Lieven Vandenberghe. *Convex optimization*. Cambridge university press, 2004.

[120] Simona Onori, Lorenzo Serrao, and Giorgio Rizzoni. *Hybrid electric vehicles: Energy management strategies*. Springer, 2016.

[121] M Nijhuis, M Gibescu, and JFG Cobben. Bottom-up markov chain monte carlo approach for scenario based residential load modelling with publicly available data. *Energy and Buildings*, 112:121–129, 2016.

[122] Rinze Geertsma, Jasper Vollbrandt, Rudy Negenborn, Klaas Visser, and Hans Hopman. A quantitative comparison of hybrid diesel-electric and gas-turbine-electric propulsion for future frigates. In *2017 IEEE Electric Ship Technologies Symposium (ESTS)*, pages 451–458. IEEE, 2017.

[123] R. D. Geertsma, R. R. Negenborn, K. Visser, M. A. Loonstijn, and J. J. Hopman. Pitch control for ships with diesel mechanical and hybrid propulsion: Modelling, validation and performance quantification. *Applied Energy*, 206:1609–1631, 2017.

[124] A. Haseltalab. *Control for Autonomous All-Electric Ships*. PhD thesis, 2019.

[125] MAN® V28-33D STC Project Guide. `https://marine.man-es.com/docs/librariesprovider6/4-stroke-project-guides/man-v28-33d-stc-imo-tier-iii-marine.pdf?sfvrsn=f6cb9178_7`. Accessed: 2020-6-20.

[126] RD Geertsma, RR Negenborn, K Visser, MA Loonstijn, and JJ Hopman. Pitch control for ships with diesel mechanical and hybrid propulsion: Modelling, validation and performance quantification. *Applied Energy*, 206:1609–1631, 2017.